An Initial Guess Generator for Launch and Reentry Vehicle Trajectory Optimization

Von der Fakultät Luft- und Raumfahrttechnik der Universität Stuttgart zur Erlangung der Würde eines Doktor-Ingenieurs (Dr.-Ing.) genehmigte Abhandlung

vorgelegt von

Albert Walter Markl

aus München

Hauptberichter:	Prof. K.-H. Well, Ph. D.
Mitberichter:	Prof. Dr.-Ing. G. Sachs
Tag der mündlichen Prüfung	11. Juni 2001

Institut für Flugmechanik und Flugregelung
der Universität Stuttgart
2001

 Albert Markl
Institut für Flugmechanik und Flugregelung
Universität Stuttgart
Pfaffenwaldring 7a
70550 Stuttgart
Deutschland

Printed in Germany

Acknowledgements

Tell my wife, I love her very much. She knows.
David Bowie – Space Oddity

Foremost I would like to express my thankfulness to my advisor, Professor Well, for giving me the opportunity to perform the studies which lead to this thesis. His many insightful inputs were invaluable to my work.

My deeply felt appreciation extends to Prof. Dr. Sachs, for taking the task of co-referent and for teaching me the basics of flight mechanics and optimization, long time ago.

Dr. Mehlem, Director of the Mathematical Studies Office of the European Space Agency, deserves my special thanks, since his unwavering support of the ASTOS program was and is one of the foundations of this project.

To all my present and former colleagues, notably to Dr. Grimm and to Mr. Jänsch, I would like to express my gratitude for their stimulations and for the productive atmosphere, in which this work could grow.

Finally I would like to thank my wife Darlina for all her love and for her understanding when I spent my time working on this thesis. I appreciate her support very much.

Table of Contents

List of Figures

List of Tables

Notation

Symbols in Formulas

Symbol	Description	Unit
α	angle of attack	radian
α_t	total angle of attack	radian
β	side slip angle	radian
χ	flight-path azimuth	radian
δ	geocentric latitude	radian
δ_C	cross range	radian
$\Delta\Theta$	amount of pitch over	radian
ε	vertical thrust incidence angle	radian
ε	singular perturbation parameter	–
ϕ	Mayer cost term	
Φ	roll angle	radian
Φ’	aeroballistic roll angle	radian
γ	flight-path angle	radian
λ	longitude	radian
μ_E	gravitational constant of the central body	m^3/s^2
μ_a	air-path bank angle	radian
μ_t	bank angle in total force system	radian

Symbol	Description	Unit
ν	horizontal thrust incidence angle	radian
Θ	pitch angle	radian
ρ	air density	kg/m³
ρ_0	reference air density	kg/m³
ω_0	natural frequency	1/s
ω_E	angular velocity of the central body	radian/s
ξ	curvature parameter	–
ψ	vector of boundary conditions	
Ψ	yaw angle	radian
ζ	damping factor	–
t	time	s
a_T	thrust acceleration	m/s²
c_D	drag coefficient	–
c_L	lift coefficient	–
c_L^*	lift coefficient for best glide slope	–
c_Y	side force coefficient	–
D	drag	N
d	drag acceleration	m/s²
e	specific energy	J/kg
f	right hand side of a ordinary differential equation	
F	vector of external forces	N
g	path constraints	
g	gravitational acceleration	m/s²
g_δ	meridional component of gravitational acceleration	m/s²
g_n	effective gravity (local gravity less centrifugal effects)	m/s²
h	altitude	m
h_S	scale height of the atmosphere	m
I	scalar cost functional	
i	orbit inclination	radian
i_t	target orbit inclination	radian
K_q	amplification factor on the dynamic pressure error	m³/Ns²
$K_{\dot{h}}$	amplification factor on the error of the altitude rate	s

Symbol	Description	Unit
L	Lagrange cost term	
L	lift	N
m	number of phases	–
m	mass	kg
M	Mach number	–
n	dimension of the state vector	–
n	total aerodynamic load factor	–
n_h	horizontal load factor	–
n_p	dimension of the parameter vector	–
n_u	dimension of the control vector	–
n_v	vertical load factor	–
$\dot{Q}$	heat flux	W/m²
q	dynamic pressure	Pa
r	radius	m
S	aerodynamic reference area	m²
T	thrust	N
$T_{\dot{h}}$	time constant of altitude rate loop	s
t_{acc}	acceleration time	s
t_c	time constant for pitch over maneuver	s
T_h	time constant of altitude rate loop	s
t_{po}	final time of pitch over maneuver	s
u	control vector	
V	flight-path velocity	m/s
V_{curr}	current velocity	m/s
V_d	velocity difference	m/s
V_δ	velocity in north direction	m/s
V_λ	inertial velocity in east direction	m/s
V_r	radial velocity	m/s
V_{req}	required velocity	m/s
V_W	wind velocity	m/s
Δv_D	drag loss	m/s
Δv_g	gravity loss	m/s
Δv_T	thrust alignment loss	m/s

Symbol	Description	Unit
w	pure parameter constraints	
x	state vector	
x_F	fast manifold of state vector	
x_S	slow manifold of state vector	
Y_a	lateral force	N

Indices and Superscripts

Symbol	Description
0	initial (at start of first phase)
B	body-fixed system
0	reference value (input to controller)
a	relating to the air-path axis system
A	air-path system
AV	air-path vertical system
C	commanded value (output of controller)
δ	in direction of the geocentric latitude
f	final
j	phase index
λ	in direction of the longitude
L	local horizontal frame
PL	payload
r	in radial direction
T	trajectory system
TA	total angle of attack system
TF	total force system
V	local vertical system
$\dot{x}$	first derivative of x with respect to time
x'	first derivative of x with respect to velocity

Abbreviations

Abbreviation	Description
ASTOS	Aerospace trajectory optimization software
DOF	Degrees of Freedom
ESA	Energy State Approximation
ESA	also: European Space Agency
IFR	Institute of Flight Mechanics and Control, University of Stuttgart
IGG	Initial Guess Generator
MPOCP	Multi-phase optimal control problem
Promis	Parameterized optimal control using multiple shooting
SLLSQP	Sequential linear least squares quadratic programming
SNOPT	Sparse nonlinear optimization
SSTO	Single Stage to Orbit
Tropic	Trajectory optimization by direct collocation
TSTO	Two Stage to Orbit

Zusammenfassung

In der Raumfahrt bewegt sich der Mensch fast immer an der Grenze des technisch machbaren. Auf Grund des hohen Energiebedarfs ist der Aufwand, einen Satelliten ins All zu befördern, enorm. Meist ist der Anteil der Nutzlast an der Startmasse fast verschwindend gering, schon eine kleine Verschlechterung stellt den Erfolg einer Mission in Frage. Aus diesem Grund ist der Einsatz von Werkzeugen zur Bahnoptimierung in der Raumfahrt weit verbreitet. Am IFR wurde seit acht Jahren ein solches Programmpaket entwikkelt: ASTOS®.

ASTOS benötigt, wie fast alle Optimierungsprogramme, eine Startschätzung der optimalen Flugbahn. Obwohl eine Flugbahn durch ihre Anfangswerte und den Steuerungsverlauf eindeutig beschrieben werden kann, ist es mühsam so vorzugehen. Viel einfacher ist es, ein Programm zur Startwertschätzung zu verwenden. Eine Möglichkeit dafür besteht darin, ein Lenkgesetz zu definieren, bei dem der Flugzustand an einem Punkt der Bahn benutzt wird, um einen passenden Steuerungsverlauf auszurechnen.

Diese Arbeit präsentiert solche Lenkgesetze für drei verschieden Arten von Raumfahrzeugen: konventionelle Raketenträger, luftatmende Aufstiegsfahrzeuge und Wiedereintrittsfahrzeuge. Diese Lenkgesetze werden durch eine kleine Anzahl freier Parameter definiert, die sich direkt aus dem Bahnproblem ableiten lassen und deshalb sehr einfach vom Benutzer bestimmbar sind. Außerdem können diese Parameter noch durch Optimierung angepasst werden. Die kleine Anzahl Steuerungsparameter und die Robustheit der Lenkgesetze beschleunigen die Optimierung erheblich.

Welche Raumfahrzeuge werden unterstützt?

Da ASTOS sehr viele verschiedene Konfiguration von Raumfahrzeugen unterstützt, ist es sinnvoll, zuerst die drei Haupttypen zu definieren und die speziellen Problempunkte anzusprechen.

Der derzeit sicher am meisten benutzte Träger ist die klassische Rakete, die senkrecht von einem festen Startplatz startet. Dieses Konzept wurde mittlerweile allerdings erweitert. Die Pegasus Rakete, beispielsweise, wird von einem Flugzeug in große Höhe gebracht. Nach dem Ablösen vom Trägerfahrzeug benutzt die Rakete eigene Tragflächen, um hochzuziehen. Bei dem Konzept von Sea-Launch Ltd. wird die Rakete von einer schwimmenden Plattform gestartet. Dadurch kann ein Startort gewählt werden, der für de jeweilige Mission ideal ist.

Eines haben aber alle unter dem Begriff “konventionelle Träger” zusammengefassten Fahrzeuge gemeinsam: die Verwendung eines Raketenantriebs. Nicht nur der Treibstoff für diesen Antrieb, sondern auch das Oxydationsmittel für diesen Antrieb werden an Bord mitgenommen.

Nur in den wenigen Fällen, in denen aerodynamischer Auftrieb aktiv genutzt wird, ist die Atmosphäre von Vorteil. Meist bedeutet sie nur eine Quelle von Widerstand und verringerter Effektivität des Antriebs. Deshalb verlassen Raketen meist schon kurz nach dem Start die dichte Atmosphäre. Andererseits bedeutet es auch einen Verlust an Effektivität, wenn Treibstoff erst in großer Höhe verbrannt wird. Deshalb schwenken Raketenflugbahnen oft auf fast horizontale Bahnteile ein, manchen nähern sich sogar wieder der dichten Atmosphäre vor der Zündung der Oberstufe.

Diese Beispiel zeigen, dass das größte Problem bei der Bahnoptimierung konventioneller Träger wohl in der Vielfalt der Konfigurationen und Aufgaben liegt. Ein Lenkgesetz muss also besonders vielseitig sein.

Luftatmende Träger hingegen benötigen, zumindest während eines Teils der Flugbahn, dem Sauerstoff der Umgebungsluft für den Antrieb. Da der Oxydator normaler Raketen den größten Teil der Treibstoffmasse ausmacht, kann auf diese Weise ein große Menge des Startgewichts eingespart werden.

Um luftatmende Triebwerke längere Zeit betreiben zu können, muss das Vehikel fast horizontal fliegen. Da die Fluggeschwindigkeit stets weit unterhalb der Kreisbahngeschwindigkeit liegt, muss das vertikale Kräftegleichgewicht z. B. durch aerodynamischen Auftrieb hergestellt werden.

Deshalb haben die meisten vorgeschlagenen Träger Auftriebshilfen in Form von Tragflächen. Bei manchen Projekten wird die atmosphärische Flugphase auch dazu genutzt, um einen günstigen Startpunkt für die Oberstufe zu erzielen. Diese ist für den Betrieb in Vakuum mit einem Raketentriebwerk ausgestattet.

In der derzeitigen Version kann ASTOS für Wiedereintrittsfahrzeuge mit mittlerem oder hohem Auftrieb (mit einem Verhältnis von Auftrieb zu Widerstand von ca. 0.8 bis 2.0 im Hyperschallbereich) benutzt werden. Diese Vehikel habe typischerweise kleine Tragflächen oder eine besondere Formgebung, um Auftrieb zu erzeugen. Raketenteile mit Auftriebshilfen (z. B. ausgebrannte, wiederverwendbare Unterstufen) können auch behandelt werde, während Kapseln normalerweise zuwenig Auftrieb erzeugen können, um die Flugbahn im nötigen Maße kontrollieren zu können.

Allen Wiedereintrittsfahrzeugen ist gemeinsam, dass ihre sehr hohe kinetisch Energie durch Luftwiderstand abgebaut werden muss. Dies resultiert in spezifischen Beschränkungen. Meist ist der zulässige Flugbereich nur sehr schmal. Bei europäischen Projekten muss zusätzlich ein Bedarf nach hoher seitlicher Reichweite berücksichtigt werden.

Die Rolle des Startwertschätzers

Neben der Modellspezifikation und der Phasenstruktur muss ein Benutzer von ASTOS auch eine Startschätzung der Steuerungen vorgeben. Eine gute Schätzung kann die Optimierung erheblich beschleunigen, ja manchmal sogar erst ermöglichen. Bei Optimierungsproblemen mit mehreren lokalen Optima kann die Wahl der Startschätzung das Ergebnis der Optimierung beeinflußen. Aus diesen Gründen ist es sinnvoll, eine Startschätzung anzugeben, die bereits möglichst nahe am Optimum liegt.

Da ASTOS eine große Anzahl an Optionen bietet, die es erlauben, eine Vielzahl von Fahrzeugen und Missionen zu modellieren, muss auch der Startwertschätzer besonders flexibel sein.

Da die Optimierungssoftware von ASTOS auf einer Diskretisierung der Steuerungen und des Zustandsverlaufs beruht, liegt es nahe, eine Startschätzung einfach in Form einer Tabelle zu spezifizieren. Ein solcher Zeitverlauf kann z. B. von einem ähnlich gelagerten Bahnproblem stammen, von einem externen Programm berechnet werden oder einfach durch Versuche erzeugt werden.

Aus einleuchtenden Gründen ist keine dieser Vorgehensweisen befriedigend, da zu mindest die Grundforderung nach Flexibilität nicht erfüllt werden kann. Aus diesem Grund wurde ein Startwertschätzer implementiert, der auf Lenkgesetzen beruht. Diese können Steuerungen abhängig vom Zustand des Fahrzeugs zu jedem Zeitpunkt berechnen.

Zielsetzung bei der Auswahl fortschrittlicher Lenkgesetze

Da sich nur wenig Literatur mit Lenkgesetzen für einen Startwertschätzer befasst, wurden Lenkgesetze studiert, die zur Lenkung von Luft- und Raumfahrt-Vehikeln konzipiert wurden. Das Ziel dieser Lenkgesetze ist es, ein Fahrzeug in Echtzeit zu bestimmten Zielbedingungen zu lenken, oft jedoch ohne dabei etwaige Zwischenbedingungen einzuhalten.

Der Anwendung solcher Lenkgesetze in der Optimierung sind allerdings enge Grenzen gesetzt. Oft erfüllt ein solcher Algorithmus nur eine einzige Mission, da hierfür umfangreiche Vorrechnungen ausgeführt werden müssen. Ein Startwertschätzer muss aber nicht nur viele verschiedene Missionen berechnen können, sondern auch für eine große Anzahl möglicher Fahrzeugkonfigurationen und Phasenstrukturen tauglich sein.

Die Diskretisierung der Steuerungen kann nicht beliebig fein sein, da sonst die Anzahl der Optimierungsparameter zu groß würde. Deshalb soll auch ein Lenkgesetz nur möglichst glatte Verläufe erzeugen. Sollte es zudem noch die wesentlichen Zustandsbeschränkungen erfüllen und außerdem auch nahe der optimalen Lösung liegen, kann man gute und schnelle Konvergenz erwarten.

Die bisher verwendeten Lenkansätze lagen zwar im Konvergenzbereich der optimalen Lösung, aber es wurde erwartet, dass mit verbesseren Lenkgesetzen eine schnellere Optimierung erzielt werden könne. Insbesonders luftatmenden Träger und Wiedereintrittsfahrzeuge erforderten in den vorherigen Softwareversionen erhebliche Rechenzeiten. Dies ist bedingt durch Flugzeiten, die wesentlich länger sind als relevante Manöverzeiten.

Aus den genannten Gründen wurde ein Startwertschätzer mit neuen Lenkgesetzen implementiert. Diese Lenkgesetze erlauben es, schon mit wenigen Parametern Steuerverläufe zu beschreiben, die sehr nahe an den optimalen Verläufen liegen. Deshalb können diese Lenkgesetze sogar bei der Optimierung selbst benutzt werden. Durch die Einsparung einer großen

Anzahl von Parametern zur Steuerungsdiskretisierung kann die Optimierungszeit drastisch verkürzt werden.

Lenkgesetze für Raketenträger

Die Lenkgesetze für Raketenträger wurden als Steuerungen für den Gierwinkel und den Nickwinkel implementiert. Der dritte Euler-Winkel, das Rollen, spielt für die vorhandenen Aerodynamikmodelle keine Rolle.

Der Gierwinkel wird für die horizontale Steuerung verwendet. Hierfür stehen zwei Optionen zur Verfügung: der Azimut-Winkel kann direkt als Gierwinkel benutzt werden – dann ist die Ausrichtung der Rakete immer tangential an der jeweiligen Bodenspur. Der Azimut kann entweder im erdfesten System gemessen werden (dies bietet sich für die atmosphärischen Teile der Flugbahn an) oder im inertialen System. Alternativ kann die Inklination eines Zielorbits optimiert werden. Der Gierwinkel ergibt sich dann aus dem Azimut der Bodenspur des Orbits, bezogen auf die jeweilige geographische Breite.

Für die vertikale Steuerung wird der Nickwinkel benutzt. Für die erste Flugphase ist ein Schwenkmanöver vorgesehen. Nach dem Start der Rakete, der typischerweise vertikal erfolgt, wird der Nickwinkel aus der Vertikalen bewegt. Der Flugbahnneigungswinkel folgt dieser Bewegung mit Zeitverzögerung. Wenn er sich ausreichend von der Vertikale weg bewegt hat, wird der Nickwinkel wider zurückgefahren, bis er identisch zum Flugbahnneigungswinkel ist. An diesem Punkt wird ein Gravity-Turn Manöver begonnen, bei dem sich die Rakete tangential zur jeweiligen Flugbahn bewegt.

Außerhalb der dichten Atmosphäre kann die Oberstufenlenkung angewendet werden. Zwei Optionen sind programmiert: das Required-Velocity Konzept von Battin und das Bi-Lineare-Tangens Gesetz, das aus der Optimalsteuerungstheorie abgeleitete werden kann. Es besagt, dass – bei Vernachlässigung der Erdkrümmung – der Nickwinkel einer Funktion folgen muss, so dass sein Tangens dem Quotienten zweier linearer Funktionen der Zeit entspricht. Die freien Parameter der lineare Funktionen sowie die Endzeit sind optimierbar.

Lenkgesetze für luftatmende Träger und Wiedereintrittsfahrzeuge

Speziell auf Fahrzeuge, die längere Zeit in der dichten Atmosphäre verbringen, ist ein Lenkgesetz zugeschnitten, das den Staudruckverlauf in eine

Steuerung umwandelt. Dadurch kann die schnelle Vertikalbewegung von der langsameren Horizontalbewegung entkoppelt werden. Durch Anwendung von Differentialgleichungen, in denen die Vertikalbewegung durch die neue Steuerung ersetzt wurde, kann erheblich Rechenzeit eingespart werden.

Der Staudruck hat direkten Einfluß sowohl auf die Luftkräfte, als auch auf den Schub luftatmender Triebwerke. Auch wichtige Beschränkungen hängen direkt vom Staudruck ab, so dass die Optimierung zusätzlich vereinfacht wird. Spezielle Regler werden vorgestellt, um ein Staudruckprofil, das durch Optimierung gewonnen wurde, wieder in die traditionellen Steuerungen (wie z. B. Lastfaktoren) umzusetzen.

Zur Erzeugung einer Startschätzung kann die Horizontalsteuerung für Aufstiegsfahrzeuge durch Vorgabe einer Azimut-Drehrate erfolgen. Zur Optimierung sollte allerdings auf eine variable Steuerung umgeschaltet werden.

Für Wiedereintrittsfahrzeugen ist meist der Anstellwinkel als Funktion der Mach-Zahl aus thermischen Gründen vorgegeben. Diese Definition kann auch bei der Optimierung zur Bestimmung der zweiten Lagesteuerung beibehalten werden.

Ergebnisse

Die vorgestellten Lenkgesetze wurden in umfangreichen Testrechnungen geprüft. Für Raketenträger ergibt sich bei Verwendung der Lenkgesetze während der Optimierung ein erheblicher Zeitgewinn (mit einem Faktor zwischen zwei und vier). Allerdings ist die erzielte Nutzlast um bis zu 10% niedriger als bei Optimierung mit freien Steuerungen.

Verwendet man allerdings das Bi-Lineare-Tangens Gesetz zusammen mit einer optimalen Unterstufensteuerung, sind die Ergebnisse praktisch identisch zu den optimalen Flugbahnen. Hieraus kann man schließen, dass die Verluste bereits durch die Lenkung in den ersten Bahnteilen auftreten. Weitere Forschungsarbeit sollte sich somit vor allem mit der Lenkung in den atmosphärischen Bahnteilen befassen.

Wenn man die Bi-Lineare-Tangens Lenkung mit dem Required-Velocity Konzept vergleicht, so fällt auf, dass letztere nur als reiner Startwertschätzer tauglich ist. Aber selbst bei dieser Anwendung erzeugt das Bi-Lineare-Tangens Lenkgesetz einen glatteren Verlauf des Nickwinkels und führt zu Flugbahnen, die die energetischen Endbedingungen besser erfüllen.

Dies lässt sich auf die Tatsache zurückführen, dass es auf Optimalitätskriterien beruht, während das Lenkgesetz von Battin eher eine ingenieursmässige Abschätzung darstellt.

Bei den luftgestützen Fahrzeugen führt die Anwendung der reduzierten Bewegungsgleichungen zu erheblich kürzeren Rechenzeiten. Die Genauigkeit der erzielten Lösungen im Vergleich zum Optimum ist sehr hoch. Als zusätzlicher Vorteil werden Oszillationen unterdrückt, die sonst oft auftreten und die durch Zusatzterme unterdrückt werden müssen. Durch Verwendung des Staudruck lassen sich die Pfadbeschränkungen als Funktion einer Steuerung ausdrücken. Hierdurch wird die Optimierung weiter vereinfacht.

Auch für luftatmende Träger erwies sich das Staudruckprofile in Zusammenhang mit den reduzierten Differentialgleichungen als adäquate Steuerung. Die Optimierungszeit kann wesentlich verkürzt werden. Nicht nur der Zustandsvektor kann verkürzt werden, auch die Anzahl der Stützstellen kann reduziert werden. Somit ist die Anzahl der Parameter, die zur Diskretisierung der Flugbahn benötigt werden viel kleiner.

Als weitere Vorteil kann der Staudruck nun durch Beschränkung der Optimierungsparameter eingehalten werden und muss nicht mehr als nichtlineare Beschränkung formuliert werden. Bei dem vorgestellten Beispiel kann so auf die meisten Auswertungen der Pfadbeschränkungen verzichtet werden, was eine fühlbare Zeitersparnis bringt.

Allerdings muss man beachten, dass mit dem Lenkgesetz oft nicht die gleiche Optimierungsgenauigkeit erzielt werden kann. Da die Steuerungen nur mit wenigen Parameter beschrieben werden, ist es für den Optimierer schwieriger, alle Zwischen- und Endbedingungen einzuhalten. Ein scheinbares Paradox tritt auf, wenn die Flugbahn mit einem Kollokationsverfahren diskretisiert wird. Obwohl nur eine schlechte Kollokationsgenauigkeit erzielt wird, kann das Ergebnis in einer abschließenden Simulation erstaunlich genau sein. Da die schnellen Zustandsvariablen eliminiert sind, genügt anscheinend eine geringere Genauigkeit der Lösung.

Resümee

Die präsentierten Ergebnisse zeigen, dass die vorgestellten Lenkgesetze für alle drei Arten von Fahrzeugen zuverlässig Startschätzungen liefern, die im Konvergenzbereich der Optimierungssoftware liegen. Sie können für eine große Anzahl verschiedener Konfigurationen und Missionen verwendet wer-

den. Durch die Einbettung in eine vorhanden Benutzerumgebung ist komfortables Arbeiten möglich.

Die Lenkgesetze sind durch eine kleine Anzahl von Parametern charakterisiert, die durch Optimierung an die jeweilige Mission angepasst werden können. Das Ergebnis ist zwar meist etwas weniger genau, kann aber in wesentlich kürzerer Zeit berechnet werden. Dies kann gut für Systemstudien verwendet werden, bei denen sehr viele Bahnen für verschiedene Konfigurationen berechnet werden. Hierbei kommt es mehr auf die relative Leistung an und weniger auf das absolut beste Ergebnis.

Vom wissenschaftlichen Standpunkt ist die Kombination von singulärem Störungsansatz mit Parameteroptimierung interessant. Schnelle Zustände werden als kontinuierliche, glatte Steuerungen modelliert. Dadurch kann der größte Nachteil der singulären Störungen vermieden werden, die Notwendigkeit zu Grenzschichtbetrachtungen an Stellen, an denen die schnelle Zustände springen oder an denen Randbedingungen nicht erfüllen.

Abstract

In aerospace engineering achieving the best possible performance is a must. Due to the extremely high energy needed, the technical task of placing a satellite in outer space is daunting. The payload's percentage of the launch mass is often almost negligible. Even a minor deterioration of the performance can endanger the success of a mission. For this reason, programs are commonly used to optimize the trajectories of aerospace vehicles.

Developed by the IFR, ASTOS® is a software packet that simplifies the task of trajectory optimization considerably. However, ASTOS, like most optimization programs, needs a kind of starting solution, an initial guess. One way to describe an initial guess is by specifying the control values for every point of the trajectory. It is often much more simple to define a guidance law: an algorithm which computes the value of a control depending on the state vector.

This thesis presents guidance laws for three different kinds of aerospace vehicles: rocket launchers, air-breathing launchers and reentry vehicles. These guidance laws are characterized by a small number of free parameters, which are directly related to the trajectory problem. Therefore they can be easily estimated by the user. Moreover, the guidance laws are constructed in a way that makes them suitable for optimization. The small number of parameters and the robust performance expedite the optimization process considerably.

Description of Supported Vehicle Types

ASTOS is designed to handle different kinds of aerospace vehicles. Since some of these vehicles pose very specific problems for the optimization, a classification of the main categories is needed. This thesis concentrates on three different types of aerospace vehicles: conventional and advanced launcher, as well as reentry vehicles with moderate to high lift capability.

The archetypical *conventional launcher* is the classic rocket, launched vertically from a fixed site. However in the last decade several concepts have evolved that change this notion. For instance, the Pegasus vehicle is carried by an aircraft to a high altitude and then released. It pulls up from horizontally flight, supported by its wing. The concept of Sea-Launch Ltd. is similar in that the launch site can be chosen accordingly to the mission's needs. The rocket is launched vertically from a swimming platform.

The feature all conventional launchers have in common is the use of rocket motors. This type of engine is fed with fuel and an oxidizer that the vehicle carries along. It does not need any ambient air for propulsion.

Except for a few cases where lift is actively used, the atmosphere is just a cause for negative effects. Therefore rocket vehicles usually get out of the dense atmosphere soon after launch. However, when the ascent is too steep, energy is spent to lift the fuel to high altitudes: this is called gravity loss. Therefore rocket trajectories tend to have almost horizontal acceleration segments after leaving the atmosphere. Some even show a dip before an upper stage is ignited.

As these examples show, the greatest problem for modelling and optimization of conventional launchers is posed by the great variety of staging concepts and mission profiles. Therefore a guidance law must be especially versatile.

The main characteristic of an *advanced launcher* is that, during part of the trajectory, the engines are using ambient oxygen for combustion. This can be a huge saving, since for normal rockets the oxidizer accounts for a large percentage of the total fuel weight.

In order to use air breathing engines for an extended period of time, the trajectories of advanced launchers are almost horizontal in parts. Since the velocity is typically far from the velocity of a circular orbit, some aerodynamic lift capacity is useful (although not strictly required by our definition of an advanced launcher). In some projects, the extended acceleration and

climb phase is used to obtain a favorable starting place for the upper stage. This can be achieved by a cruise phase or by an unsteady pseudo-cruise.

ASTOS currently treats *reentry vehicles* with medium or high lift to drag ratio in the range of 0.5 to 2.0. Such a spacecraft will typically have some sort of wings or other devices to generate lift. Rocket parts (like a reusable lower stage) could be treated similarly, while capsules with very low lift capability may lack sufficient control authority for proper guidance.

All reentry vehicles have one thing in common – their relatively high specific energy must be dissipated by using aerodynamic drag. Specific constraints and cost functionals ensue. The reentry corridor is very narrow – sometimes almost non-existent. In addition, European projects demanded a high cross range – which is difficult to achieve, given the limited lift capability of the proposed vehicles.

The Role of an Initial Guess Generator

Besides specifying a model and a phase sequence, a user has to supply an initial estimate of the optimal controls. A good initial guess will simplify the solution process – in some cases it is even impossible to achieve a solution without it. In the presence of several local minima, the initial guess can also influence the outcome of the solution. For these reasons it is worthwhile to develop an initial guess which is as close to the solution as possible.

ASTOS includes a wide range of modelling options, which allow the modelling of a large variety of aerospace vehicles. Because of this flexibility, and also because of the multitude of possible missions which can be optimized, a large number of control options is available, which can be used to specify an initial guess.

Since ASTOS uses optimization techniques which need a discretization of the control history and of the state history, the most straight forward way to specify an initial guess is by giving starting values for the states and tables for the control history. These tables could be obtained by using the optimal solution of a similar problem, by using external tools for trajectory computation or by a trial and error procedure.

For obvious reasons, none of these approaches is satisfactory. Therefore the possibility of specifying feedback control laws is introduced. This allows to specify controls not only depending on time, but also on the current state.

Objective of Advanced Guidance Laws

There is little literature on guidance laws specifically designed for an initial guess generator. Therefore, guidance laws that are used for the real time guidance of aerospace vehicles are examined. The purpose of these guidance laws is to control a vehicle in real time in a way as to guaranty the achievement of certain target conditions – without necessarily satisfying any intermediate constraints.

A conventional control law is often designed to handle just a single mission, f.i. it may rely on a pre-computed trajectory. An IGG control law, however, should handle a wide range of initial and final conditions, as well as different kinds of models and different phase structures.

Furthermore, since the control discretization used for optimization is often quite coarse, the controls used for the initial guess should be smooth and without high frequency content. If in addition an initial guess is close to the optimal solution and satisfies most of the path constraints, it will lead to fast optimizations.

The initial guesses obtained with previously implemented guidance laws proved to be sufficiently close to the optimal solution. However, it is recognized that improved control laws could make it easier and faster to obtain an optimal solution. In addition, it was observed that especially advanced launcher and reentry missions require a very long optimization time. This is partly due to the different time scales involved and to the large number of parameters for the control approximation.

For these reasons, an initial guess generator using a novel set of guidance laws is implemented. Some of the guidance laws allow to describe a control history which is very close to the optimum with a small number of parameters. Therefore these guidance laws can be used for optimization in their own right. The resulting savings of a huge number of control discretization parameters shortens the time needed for optimization considerably.

Guidance Laws for Conventional Launchers

For conventional launchers, the guidance laws are implemented as controls of the Euler angles yaw and pitch. The roll angle is of little importance for the aerodynamic models used.

The yaw angle is used for the horizontal guidance. Two simple guidance laws are available: one is to set the yaw angle equal to the heading angle, keeping the projection of the rocket tangentially to its ground track. The second option uses the inclination of a target orbit and sets the yaw to the heading of this orbit, calculated for the current declination. The inclination used for steering is optimizable and may deviate from the inclination of the actual target orbit.

For the vertical guidance, a sequence of guidance strategies is provided. Until the rocket clears the launch pad, the pitch is set to the same value as the flight-path angle. Then a push-over maneuver is initiated: the pitch angle is deviated from the flight-path angle with a constant rate and then slowly driven back. While the timing is constant (with user definable time constants), the pitch over rate is optimizable. The temporary deviation is used to set a defined flight-path angle at the entry of the gravity turn maneuver.

Once the rocket gets out of the dense atmosphere, the upper stage guidance is applied. Two options are available: the required velocity concept by Battin and a bi-linear tangent law.

The latter is based optimal control theory, applied to the motion of a point mass in the vertical plane. It states that the tangens of the pitch angle should always be of the same value as the quotient of two linear functions of the time. The free parameters of this functions are optimizable.

Guidance Laws for Advanced Launchers and Reentry Vehicles

For air breathing launcher a guidance concept is presented that is based on the dynamic pressure as a pseudo-control. Since the dynamic pressure by definition harbors the air density (which depends primarily on the altitude), this control can be used to replace the variables of the vertical motion, altitude and flight-path angle. These variables are considered “fast” as compared to the variables of the horizontal motion and therefore removing them not only reduces the size of the state vector, but also reduces the number of integration steps needed.

This quantity influences the aerodynamical forces and the thrust directly, as well as some important path constraints. These facts are further accelerating the optimization.

The horizontal control can be specifying a constant turn rate as a first estimate. Also for reentry vehicle a dynamic pressure control and the described state vector reduction are proposed. Since for reentry vehicles the angle of attack as a function of the Mach number is often given by aero-thermal considerations, this is used as the second attitude control.

Results

Using the guidance law which describes the control time history with a small number of parameters can speed up the optimization time for conventional launcher missions considerably (by a factor between two and four). However, there is a penalty in the form of a smaller payload (on the average by 10% less).

The bi-linear tangent law in conjunction with an optimal lower stage guidance consistently shows an almost identical performance to an optimized control. It can be concluded that this guidance law is appropriate for the upper stage, however, that the gravity turn and the yaw guidance options are often sub-optimal. More research should be devoted to find better control laws for the atmospheric phases of the trajectory.

Using the bi-linear tangent law as a pure (non-optimizing) initial guess generator, when compared to the required velocity guidance, has the advantage of giving a smooth control time history and also a better performance. This can be attributed to the fact that the bi-linear law is based on an optimum criterion, whereas the required velocity guidance is rather an engineering “rule of thumb” approach.

The reduced equations of motion for optimization of reentry trajectories do often result in tremendously reduced optimization times. Part of this is due to the fact that the optimizer Tropic can be used, since the frequency content of the solution is reduced.

The accuracy of the solution obtained is very high, when compared to the optimal trajectory. As an additional benefit, control oscillations, which otherwise must be smoothed by using a penalty term, can hardly occur.

Using the dynamic pressure as control simplifies the relation of the most important path constraints. The constraints formulae do contain the pseudo-control directly, a fact which further simplifies the optimization process.

The dynamic pressure profile in conjunction with the reduced order differential equations proved to be effective also for advanced launchers. The optimization time is considerably less than the time needed for optimization with conventional controls. The size of the parameter vector is reduced, partly because of the smaller state vector, but also because of a smaller number of collocation points needed.

It should be noted, however, that the guidance law does not achieve the same accuracy during optimization. Since the optimal controls are described by very few parameters only, it is more difficult to satisfy all path and boundary constraints. Still, when using collocation, the reduced order solution is often as precise in the final simulation than the full order one. This is due to the fact, that the fast part of the state vector is not present and therefore larger intervals for the collocation are admissible.

As an additional benefit, the guidance law allows to model the dynamic pressure constraints as box constraints on the parameters which are treated much more efficiently by the optimizer. For the example given, most path constraint evaluation points can be therefore eliminated. This reduction in evaluations speeds up optimization additionally.

Conclusion

The results presented for three types of vehicles show that the new guidance laws are reliably supplying an initial guess. The proposed control options can be adapted for a wide range of missions and allow to model attitude controls close to the optimal ones. The implementation of the guidance laws within the ASTOS environment makes the usage very simply.

In addition, the control laws are described by a small number of parameters, which can be adapted during an optimization. The result is less accurate than a full scale optimization, but it is obtained considerably faster. This property can be used in system studies, where a large number of trajectories must be computed and computation time is more important than total accuracy.

From a scientific point of view, this thesis treats the adaptation of the theory of singular perturbations to parameter optimization. It is shown, that this combination offers distinct advantages when compared to the traditional approach of using indirect optimization. When the fast members of the state vector as pseudo-controls are modelled as continuos functions, which are dif-

ferentiable to the required degree, the separate treatment of boundary layers can be avoided. Since the user can control the frequency content of the solution by selecting the discretization of the pseudo-control, a solution can be achieved, which is flyable by the vehicle – and not just of theoretical interest.

1 Introduction

ASTOS® is an optimization tool for aerospace vehicles. The acronym stands for aerospace trajectory optimization software. Formerly known as Altos, it has been developed for eight years by the IFR.

The optimum is – according to Webster's Ninth Collegiate Dictionary – the "greatest degree attained or attainable under implied or specified conditions". So optimization is a method to minimize or maximize a performance criterion in the presence of constraints.

Obtaining the best performance is especially important for aerospace vehicles since these vehicles are almost always operated at the very edge of technology. Even a slight deterioration from the nominal performance can make a planned mission impossible.

The payload of a launcher f.i. is usually only a few per cent of the take-off mass: a small improvement has a big pay-off. Even when a mission is already well-defined, saving some fuel during launch, which can later be used for maintaining the position, may prolong the useful life of the satellite considerably. In other cases optimization may improve the security margin and minimize the risk for crew and ground personal.

1.1 The Role of an Initial Guess Generator (IGG)

The above mentioned missions as well as many others can be optimized with ASTOS. However, besides specifying a model and a phase sequence, a user

has to supply an initial estimate of the optimal controls as well as of the trajectory. That is, ASTOS, as almost all kinds of optimization programs, requires the user to specify a guess of the solution when starting. For programs which do not strictly require an initial guess, supplying a good guess often will help speed up the optimization process. In the presence of several local minima, the initial guess can also influence the outcome of the solution. For these reasons it is worthwhile to develop an initial guess which is as close to the solution as possible.

ASTOS includes a wide range of options, which allow the modelling of practically all kinds of aerospace vehicles. Because of this flexibility, and also because of the multitude of possible missions which can be optimized, a large number of control options is available, which can be used to specify an initial guess.

Since ASTOS uses optimization techniques which need a discretization of the control history and of the state history, the most straight forward way to specify an initial guess is by giving starting values for the states and tables for the control history. These tables could be obtained by using the optimal solution of a similar problem, by using external tools for trajectory computation or by a trial and error procedure, which often involves guessing a short starting trajectory and extending it piece by piece.

For obvious reasons, none of these solutions is satisfactory. Therefore the possibility of specifying feedback control laws is introduced. This allows to specify controls not only depending on time, but also on the current state (see [2],[3],[4]).

1.2 Objective of Advanced Guidance Laws

Several guidance laws for typical missions were previously implemented. Notably these include the required velocity concept of Battin (see [9]) for rockets, the Shuttle Guidance for high-lift reentry vehicles (see [30]) and a guidance for air breathing launchers based on the energy method dating back to Kaiser (see [42]).

The initial guesses obtained proved to be sufficiently close to the optimal solution. However, it is recognized that improved control laws could make it easier and faster to obtain an optimal solution.

In addition, it was observed that especially advanced launcher and reentry missions require a very long optimization time. This is partly due to the different time scales involved and to the large number of parameters for the control approximation. The time scale problem also prohibits in some cases the use of the optimization code Tropic, which uses collocation instead of numerical integration.

For these reasons, an initial guess generator using a set of guidance laws is implemented. Some of the guidance laws allow to describe a control history which is very close to the optimum with a small number of parameters. Therefore these guidance laws can be used for optimization in their own right. The resulting savings of a huge number of control discretization parameters shortens the time needed for optimization considerably.

Another guidance law involving the dynamic pressure as control is devised for aerospace planes with a prolonged trajectory in the atmosphere. Together with a reduced set of differential equations, this allows for a time separation of the horizontal and the vertical motion. Neglecting the fast time scale during optimization results in much reduced integration times and also allows the application of a collocation scheme for discretization.

In contrast to the traditional energy state approximations (see e.g. [23]) the continuity and the smoothness of the altitude is preserved. Therefore the trajectories can be easily followed by simple controllers.

1.3 Structure of the Thesis

In the next chapter the basic types of vehicles treated by the initial guess generator are defined. Characteristics of the vehicles are introduced, as well as an outline for a typical mission. In addition, the specific problems an initial guess must treat for all three classes are discussed.

Chapter 3 states the formulation of the optimization problem. Two sets of differential equations of motion are presented. Together with the control options treated subsequently these form the dynamic system. Several path constraints which have an influence on the construction of the initial guess generator are discussed, as well as some of the major cost functions implemented in ASTOS.

Next, traditional guidance laws are discussed, as well as their suitability for an advanced initial guess generator. Novel guidance laws are pre-

sented and their advantages are shown, as compared to the previous solutions.

Optimization results for all vehicle types prove the benefits of the advanced guidance laws. Finally a conclusion sums up the important points.

2 Classification of Vehicles

ASTOS is designed to handle different kinds of aerospace vehicles. Since some of these vehicles pose very specific problems for the optimization, a classification of the main categories is needed. This thesis concentrates on three different types of aerospace vehicles: conventional and advanced launcher, as well as reentry vehicles with moderate or high lift capability.

2.1 Conventional Launcher

The archetypical conventional launcher is the classic rocket, launched vertically from a fixed site. However in the last decade several concepts have evolved that change this notion.

For instance, the Pegasus vehicle by Orbital Science Corp. is carried by an aircraft to an altitude of about 11.9 km and then released (see Fig. 2.1). It pulls up from horizontally flight, supported by its wing (see [34], [54]). This procedure gives the rocket an initial velocity and allows it to stay out of the densest part of the atmosphere. The aircraft can also be used to shuttle the assembled vehicle to a convenient launch site.

The concept of Sea-Launch Ltd. (see [88]) is similar in that the launch site can be chosen according to the customer's needs. The rocket is launched vertically from a swimming platform (see Fig. 2.2). A command vessel is used for assembly of the vehicle and for launch control operations.

Fig. 2.1: Launch of a Pegasus vehicle carried by a L-1011 airplane
Photography by courtesy of Orbital Science Corp. [87]

Fig. 2.2: Launch platform and command vessel.
Photography by courtesy of Sea Launch Ltd. [88]

The feature these vehicles have in common is the use of rocket motors. This type of engine is fed – besides fuel – with an oxidizer that the vehicle carries along. It does not need any ambient air for propulsion.

Except for a few cases where lift is actively used, the atmosphere is just a cause for negative effects. Therefore rocket vehicles usually get out of the dense atmosphere soon after launch. However, when the ascent is too steep, energy is spent to lift the fuel to high altitudes: this is called gravity loss. Therefore rocket trajectories tend to have almost horizontal acceleration segments after leaving the atmosphere. Some even show a dip before an upper stage is ignited.

A typical mission for a conventional rocket launcher begins with a vertical launch. After clearing the launch pad, the vehicle is tilted slightly, in order to achieve curved trajectory. When a suitable state is reached, the vehicle enters a gravity turn maneuver, in which the launcher axis is aligned with the velocity vector. In this way the losses due to atmospheric drag are minimized. Once out of the dense atmosphere, an upper stage guidance assures that the vehicle reaches the target orbit. For some missions it is preferable to enter a coast arc before the final ignition of the upper stage.

Currently most rocket launchers are expandable, that means along the trajectory rocket stages are jettisoned as their tanks are emptied. However, there are several projects for wholly or partially reusable launchers, e.g. the Kistler K-1 vehicle (see [86]). After separation, the first stage will enact a retro burn and return to the launch site. The upper stage will stay in orbit for about 24 hours to deliver the payload and then re-enter the atmosphere for a soft landing (see Fig. 2.3). Missions of this complexity require a new way of modelling, including optimization of a branched trajectory.

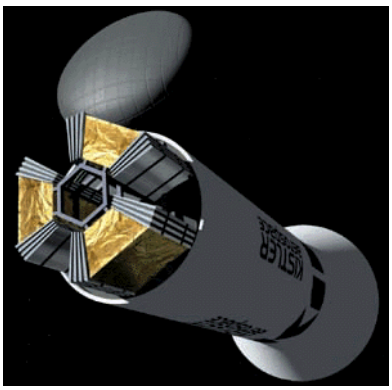

Fig. 2.3: Kistler K-1 upper stage releasing the payload
The payload door will serve as a heat shield during reentry
Picture by courtesy of Kistler Aerospace Corp. ([86]).

Rocket propulsion can also be used for landing: without atmosphere, like a lunar lander, or with aerodynamic help for deceleration, like the proposed DC-X vehicle, the Delta Clipper.

As these examples show, the greatest problem for modelling and optimization of conventional launchers is posed by the large variety of staging concepts and mission profiles.

2.2 Advanced Launcher

The main characteristic of an advanced launcher is that, during a part of the trajectory, the engines are using ambient oxygen for combustion. Since for conventional rockets the oxidizer accounts for a large percentage of the total fuel weight, this can be a huge saving. For instance, for the combination of liquid hydrogen and liquid oxygen at stochiometric combustion, this is almost 90%. However, currently at least the upper stage must be propelled by a conventional rocket engine since the problems of combustion at extremely high speeds are not yet solved.

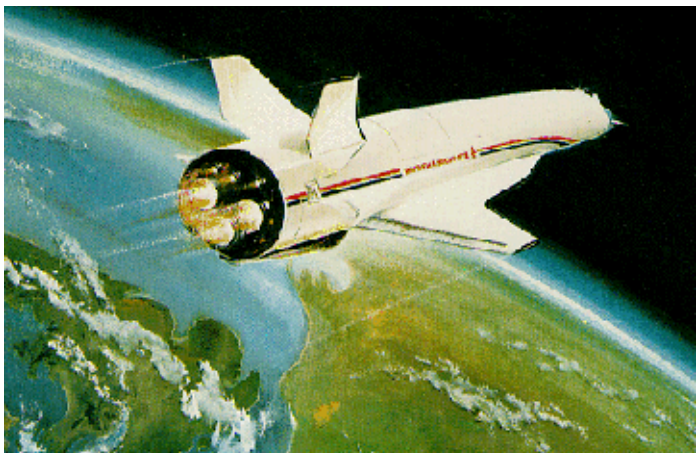

Fig. 2.4: Artist's view of the British Hotol vehicle
Picture by courtesy of British Aerospace Corp. ([89])

In order to use air breathing engines for an extended period of time, the trajectories of advanced launchers are almost horizontal in parts. Since the velocity is typically far from the velocity of a circular orbit, some aerodynamic lift capacity is useful – although not strictly required by the definition of an advanced launcher.

In some projects, the extended acceleration and climb phase is used to obtain a favorable starting place for the upper stage. This can be achieved by a cruise phase or by an unsteady pseudo-cruise.

Currently there are two major ideas for advanced launching vehicles. For a "single stage to orbit" vehicle (SSTO) all propulsion systems are mounted on the same vehicle which will achieve orbital velocity. There is no

jettisoning of stages. After fulfilling its mission, the orbiter returns back to earth. An example is the British Hotol project, which is discontinued (see Fig. 2.4).

The concurrent “two stages to orbit” projects (TSTO) consist of an atmospheric vehicle with advanced propulsion and a smaller upper stage with rocket propulsion. The upper stage, which is released at sub-orbital speed, reaches the orbit with rocket power, while the lower stage – in most concepts – returns to base. The cancelled Sänger II project may serve as an example (see Fig. 2.5). Pegasus will also fit in the scheme of an advanced launcher, if the carrier aircraft is taken into account.

Fig. 2.5: Sänger II vehicle (Artist’s view)
Picture by courtesy of Mrs. Karen Buchholz.

Several problems are encountered during optimization of advanced launcher trajectories. No advanced launchers exist yet, therefore the experimental data is quite limited. Models are calculated by costly computer simulations. Often there are only a few data points available, located on a narrow band around a nominal trajectory. An optimization must be restricted to trajectories which stay within this narrow corridor.

At the high speeds involved, the phugoid motion covers a considerable altitude difference. This alters the characteristic of this motion, since the density cannot be considered constant (see [29]). As Bayer and Sachs pointed out ([11]), there is the possibility of saving a small amount of fuel by using

the phugoid motion. Since the effect is only a fraction of a percent of the total fuel, and since this flight path would be rather difficult for a guidance scheme to follow, this mode should be suppressed by optimization.

From the numerical point of view, long trajectories like the ones proposed for advanced launchers, pose the problem of differing time scales. The fastest motion of the set of differential equations has a time constant which is much smaller than the time constant of the slowest motion – or than the total flight time. Therefore the solution of the optimal control problem must go into great details. This requires a large number of parameters for the control discretization, causing the optimization time to increase significantly.

2.3 Reentry Vehicles

A very different type of vehicle is used for reentry calculations. Lift and drag are produced to achieve aerodynamic control. There is normally no propulsion. However, in a few studies, some propulsion is used to control the final touchdown.

Fig. 2.6: Artist's view of X-38 reentering the atmosphere
Picture by courtesy of NASA ([90], ref. ED97-43903-1)

ASTOS currently treats reentry vehicles with medium or high lift to drag ratio in the range of 0.5 to 2. Such a spacecraft will typically have some sort of wings or other devices to generate lift, like the X-38 (see Fig. 2.6). Rocket parts like a re-usable lower stage could be treated similarly, while

capsules with very low lift capability may lack sufficient control authority for proper guidance.

All these vehicles have one thing in common – their relatively high specific energy must be dissipated by using aerodynamic drag. Specific constraints and cost functionals ensue. Especially European projects demanded a high cross range – which is difficult to achieve, given the limited lift capability of the proposed vehicle.

As a special feature, also the optimization of six degrees of freedom models (6 DOF) is possible in ASTOS. An internal controller is used to translate the commanded attitude angles into a momentum applied around the major axis.

In a typical reentry mission, the vehicle is in a low earth orbit. At a certain point, the vehicle is decelerated by a de-orbit impulse of its rocket motor. The new orbit is designed to enter the atmosphere, which is used for further deceleration. Lift capability of the spacecraft is used to approach the landing site and to achieve favorable conditions for landing.

Some special problems are encountered during reentry optimizations. Since the specific energy, which must be dissipated, is very high, some stringent constraints must be heeded. The reentry corridor is very narrow – sometimes almost non-existent.

Again, a phugoid motion due to density differences can ensue. Special constraints are introduced to avoid problems of controllability. An equilibrium glide condition, corresponding to the loft ceiling of a conventional airplane, is often used to suppress this motion. For the optimization, again, the large difference in time scales poses a problem, especially when optimizing with a six degrees of freedom model.

3 Formulation of the Optimization Problem

In [1] the standard formulation of the "multi-phase optimal control problem (MPOCP)" of a dynamic system is specified:

"Given *m* phases with possibly optimizable phase separation times

$$t^j \in \{t^0 < t^1 < t^2 ... < t^m\}, t^m = t^f \tag{3.1}$$

let the state vectors $x^j \in R^{n^j}$, $j \in \{1, ...,m\}$ be governed by the ordinary differential equations

$$\dot{x}^j = f^j(x^j, u^j, p^j, t), t \in \{t^{j-1}, t^j\}, j \in \{1, ...,m\} \tag{3.2}$$

where $p^j \in R^{n_p^j}$ is a vector of model parameters and $u^j(t) \in R^{n_u^j}$ are control functions. Then the optimization problem consists of finding optimal control functions, model parameters and phase separation times to minimize a scalar cost functional. Minimize

$$I = \phi^0(x^1(t^0), u^0(t^0), p^1, t^0) + \sum_{j=1}^{m} \phi^j(x^j(t^j), u^j(t^j), p^j, t^j) + \sum_{j=1}^{m} \int_{t^{j-1}}^{t^j} L(x^j(t), u^j(t), p^j, t)dt \tag{3.3}$$

with respect to $u^j(t), p^j, t^0, t^j, j \in \{1, ...,m\}$.

This cost functional is a combination of Mayer and Lagrange terms. In addition to the Eq. (3.2) the solution is required to satisfy separable multipoint boundary conditions

$$\psi^0(t^0, x^1(t^0), u^1(t^0), p^1) \geq 0 \tag{3.4}$$

at the initial time,

$$\psi^j(t^j, x^j(t^j), u^j(t^j), p^j) \geq 0, j \in \{1,...,m\} \tag{3.5}$$

at the phase time-points t^j, pure parameter constraints

$$w^j(p^j) \geq 0, j \in \{1, ...,m\}, \tag{3.6}$$

path constraints

$$g^j(t, x^j(t), u^j(t), p^j) \geq 0, t \in [t^{j-1}, t^j], j \in \{1, ...,m\}, \tag{3.7}$$

and phase transition conditions

$$\begin{bmatrix} x^{j+1}(t^j) \\ u^{j+1}(t^j) \\ p^{j+1} \end{bmatrix} = h^j(t^j, x^j(t^j), u^j(t^j), p^j), j \in \{1, ...,m-1\}.” \tag{3.8}$$

Some of the equations (3.1) to (3.8), which are of particular interest for the discussion of the initial guess generator, are explained in more detail below. Note, that the presence of the control u in the boundary conditions ψ is only sensible for direct optimization procedures.

3.1 Differential Equations of Motion

Several sets of equations of motion are implemented in ASTOS. Besides a set based on orbital elements and equations for the rotational dynamics, there are two sets of equations dealing with the motion of a mass point of a spherical, rotating planet: one is a system based on inertial velocity components, the second is the flight-path velocity system.

These well known equations are only quoted for convenience. A detailed description of the terms involved can be found in [5].

It should be noted that using ASTOS, the differential equations can be switched at each phase boundary. The phase connect conditions Eq. (3.8) will be adjusted accordingly.

3.1.1 Inertial Velocity System

This system is described in [14]. The radius vector is given in spherical, planet relative coordinates (see Fig. A.1). Its derivative with respect to time is

$$\frac{d}{dt}\begin{bmatrix} R \\ \lambda \\ \delta \end{bmatrix} = \frac{1}{r}\begin{bmatrix} V_R \\ \dfrac{V_\lambda}{R\cos\delta} - \omega_E \\ \dfrac{V_\delta}{R} \end{bmatrix}, \tag{3.9}$$

where R, λ, δ are the radius, the longitude and the declination, respectively, V_R, V_λ, V_δ are the velocity components in the corresponding directions, and ω_E is the angular velocity of the rotation of the planet.

The derivative of the velocity vector is given by

$$\frac{d}{dt}\begin{bmatrix} V_R \\ V_\lambda \\ V_\delta \end{bmatrix}_L = \frac{1}{R}\begin{bmatrix} V_\lambda^2 + V_\delta^2 \\ V_\lambda(V_\delta\tan\delta - V_R) \\ -V_\lambda^2\tan\delta - V_R V_\delta \end{bmatrix}_L + \frac{\vec{F}}{m}, \tag{3.10}$$

where $\vec{F}$ is the sum of all forces acting on the vehicle, like gravity, aerodynamic forces and thrust. The index L denotes the local horizontal coordinate system.

These differential equations are especially useful for rocket launchers, when a vertical flight is part of the trajectory since the differential equations of motion accommodate vertical flight. Note that the differential equations show a discontinuity for flight over the poles ($\delta = \pm\pi/2$).

3.1.2 Flight-Path System

While the definition of the radius vector is the same, the differential equation is expressed in the terms of the flight-path velocity vector (see Fig. A.2):

$$\frac{dR}{dt} = V\sin\gamma, \tag{3.11}$$

$$\frac{d\lambda}{dt} = \frac{V\cos\gamma\sin\chi}{R\cos\delta}, \tag{3.12}$$

$$\frac{d\delta}{dt} = \frac{V\cos\gamma\cos\chi}{R} \tag{3.13}$$

with the planet-relative velocity V, the flight-path angle γ, and the azimuth χ. The equations of motion are, for the velocity:

$$\begin{aligned}\frac{dV}{dt} = & -g\sin\gamma + g_\delta\cos\chi\cos\gamma + \\ & + \frac{T\cos\varepsilon\cos\nu - D}{m} + \\ & + \omega_E^2 R\cos\delta(\cos\delta\sin\gamma - \sin\delta\cos\gamma\cos\chi)\end{aligned}, \tag{3.14}$$

for the heading angle:

$$\begin{aligned}\frac{d\chi}{dt} = & -\frac{g_\delta\sin\chi}{V\cos\gamma} + \frac{V\cos\gamma}{R\cos\delta}\sin\chi\sin\delta + \\ & + \frac{(L + T\sin\varepsilon)\sin\mu_a + (T\cos\varepsilon\sin\nu - Y_a)\cos\mu_a}{mV\cos\gamma} + \\ & + 2\omega_E(\sin\delta - \cos\chi\cos\delta\tan\gamma) + \frac{\omega_E^2 R\cos\delta}{V\cos\gamma}\sin\chi\sin\delta\end{aligned}, \tag{3.15}$$

and for the flight-path angle:

$$\frac{d\gamma}{dt} = -\frac{g}{V}\cos\gamma - \frac{g_\delta}{V}\cos\chi\sin\gamma + \frac{V}{R}\cos\gamma + \\ + \frac{(Y_a - T\cos\varepsilon\sin\nu)\sin\mu_a + (L + T\sin\varepsilon)\cos\mu_a}{mV} + \\ + 2\omega_E\sin\chi\cos\delta + \frac{\omega_E^2 R\cos\delta}{V}(\sin\delta\sin\gamma\cos\chi + \cos\delta\cos\gamma) \quad . \quad (3.16)$$

The component of the gravity in meridional direction g_δ is often neglected, the component in longitudinal direction is zero for simple planet models.

Note that for the dynamic equations the first lines denote the influence of the external forces and the centrifugal forces due to the vehicle's motion, while the last line contains the Coriolis acceleration (terms including $2\omega_E$) and the centrifugal acceleration due to the rotation of the earth (denoted by $r\omega_E^2$). The equations for movement over a non-rotating planet can be obtained by setting ω_E to zero.

The thrust incidence angles ε and ν are taken in the air-path system. For a rocket with the thrust aligned with the body x axis, ν will be equal to the side slip angle and ε equal to the angle of attack. For a definition of ε and ν please refer to Fig. A.5.

3.2 Attitude Controls

The attitude controls describe the orientation of the vehicle with respect to an axis system. The orientation influences the size and direction of the aerodynamic force and of the thrust force.

There are three major possibilities to specify attitude controls in ASTOS: aerodynamic angles, Euler angles and load factors. Two of these methods offer the option of specifying a full set of three attitude angles or a reduced set of controls of two angles only. In the latter case, the side slip angle is set to zero.

3.2.1 Transformations

In order to define the attitude control angles, it is necessary to describe the axis systems used and the coordinate rotations needed to transform a vector

from one to another. For a detailed description of the different axis systems mentioned in Table 3.1 please refer to Appendix A.

Table 3.1: Axis systems

Index	Axis System
V	local vertical system
AV	air-path vertical system
T	trajectory system
A	air-path system
B	body-fixed system

Each transformation is described by a transformation matrix $T_i(\delta)$, which denotes a rotation around the axis *i* by the angle δ. Transformations are given in the form:

$$\mathbf{T}_{AV}^{A} = \mathbf{T}_1(\mu_a), \tag{3.17}$$

which means: to transform a vector from the AV system to the A system, a rotation around the first axis by the angle μ_a is necessary. Three basic matrices are used, one for each the three rotations around an axes:

$$\mathbf{T}_1(\Phi) = \begin{bmatrix} 1 & 0 & 0 \\ 0 & \cos\Phi & \sin\Phi \\ 0 & -\sin\Phi & \cos\Phi \end{bmatrix}, \tag{3.18}$$

$$\mathbf{T}_2(\Theta) = \begin{bmatrix} \cos\Theta & 0 & -\sin\Theta \\ 0 & 1 & 0 \\ \sin\Theta & 0 & \cos\Theta \end{bmatrix}, \tag{3.19}$$

$$\mathbf{T}_3(\Psi) = \begin{bmatrix} \cos\Psi & \sin\Psi & 0 \\ -\sin\Psi & \cos\Psi & 0 \\ 0 & 0 & 1 \end{bmatrix}. \tag{3.20}$$

When several rotations are needed, they are done from the right to the left:

$$\mathbf{T}_A^B = \mathbf{T}_2(\alpha)\mathbf{T}_3(-\beta)\,. \tag{3.21}$$

First the rotation around the third axis and then the rotation around the second axis is effected. A summary of the different transformation sequences is given in Fig. 3.1.

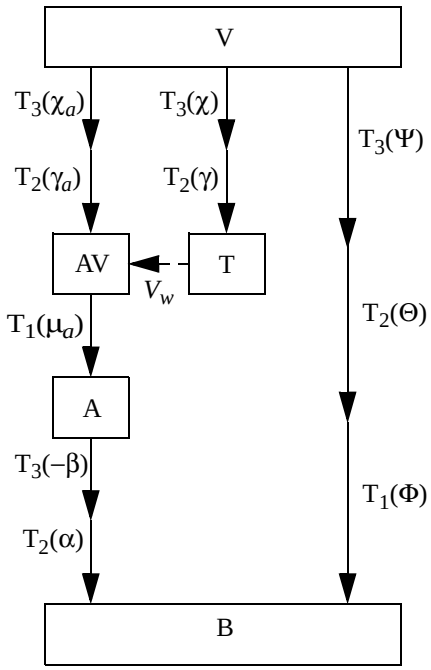

Fig. 3.1: Angular transformations from local vertical system to body system.

3.2.2 Aerodynamic Angles

The most common way to describe the control of aircraft like vehicles are the aerodynamic angles: air-path velocity bank angle μ_a, side slip angle β and angle of attack α (see Figs. A.4 and A.5). The reference frame is the vertical air-path axis system AV, which is identical to the trajectory axis system when no wind is present (V_W=0).

For vehicles with a distinct plane of symmetry, the aerodynamic angles have the advantage of relating the body axis directly to the air-path velocity. The aerodynamic models are also given as functions of the angle of attack

This reduces the amount of transformations needed, especially when the flight-path equations of motion are used.

As output functions, the Euler angles Ψ, Θ, and Φ are computed from the identity of both ways of doing the transformations $\mathbf{T}_V^B$:

$$\mathbf{T}_1(\Phi)\mathbf{T}_2(\Theta)\mathbf{T}_3(\Psi) = \mathbf{T}_2(\alpha)\mathbf{T}_3(-\beta)\mathbf{T}_1(\mu_a)\mathbf{T}_2(\gamma_a)\mathbf{T}_3(\chi_a)\,. \qquad (3.22)$$

In order to simplify the computation of the yaw and the pitch angle, the x axis of the body-fixed system is transformed into the vertical axis system:

$$\begin{bmatrix} c_x \\ c_y \\ c_z \end{bmatrix}_V = \mathbf{T}_A^V \; \mathbf{T}_B^A \begin{bmatrix} 1 \\ 0 \\ 0 \end{bmatrix}_B \qquad (3.23)$$

and

$$\begin{bmatrix} c_x \\ c_y \\ c_z \end{bmatrix}_V = \mathbf{T}_3(-\Psi)\mathbf{T}_2(-\Theta)\mathbf{T}_1(-\Phi) \begin{bmatrix} 1 \\ 0 \\ 0 \end{bmatrix}_B . \qquad (3.24)$$

Note that the transformation of (3.23) is computed numerically and that the roll angle rotation is invariant on the x axis. When the matrices and the vector (3.24) are multiplied:

$$\begin{bmatrix} c_x \\ c_y \\ c_z \end{bmatrix}_V = \begin{bmatrix} \cos\Psi & -\sin\Psi & 0 \\ \sin\Psi & \cos\Psi & 0 \\ 0 & 0 & 1 \end{bmatrix} \begin{bmatrix} \cos\Theta & 0 & \sin\Theta \\ 0 & 1 & 0 \\ -\sin\Theta & 0 & \cos\Theta \end{bmatrix} \begin{bmatrix} 1 & 0 & 0 \\ 0 & \cos\Phi & -\sin\Phi \\ 0 & \sin\Phi & \cos\Phi \end{bmatrix} \begin{bmatrix} 1 \\ 0 \\ 0 \end{bmatrix} , \qquad (3.25)$$

a simple vector equation results:

$$\begin{bmatrix} c_x \\ c_y \\ c_z \end{bmatrix}_V = \begin{bmatrix} \cos\Theta\cos\Psi \\ \cos\Theta\sin\Psi \\ -\sin\Theta \end{bmatrix}. \tag{3.26}$$

Taking the into account the signs of c_x and c_y, the attitude angles can be computed easily using (3.23) and (3.26). For the roll angle, the z axis of the vertical system is used for similar computations:

$$\mathbf{T}_A^B \; \mathbf{T}_V^A \begin{bmatrix} 0 \\ 0 \\ 1 \end{bmatrix}_V = \begin{bmatrix} c_x \\ c_y \\ c_z \end{bmatrix}_B = \mathbf{T}_1(\Phi)\mathbf{T}_2(\Theta)\mathbf{T}_3(\Psi) \begin{bmatrix} 0 \\ 0 \\ 1 \end{bmatrix}_V \tag{3.27}$$

or

$$\begin{bmatrix} c_x \\ c_y \\ c_z \end{bmatrix}_B = \begin{bmatrix} -\sin\Theta \\ \sin\Phi\cos\Theta \\ \cos\Phi\cos\Theta \end{bmatrix}. \tag{3.28}$$

The roll angle can be computed using the c_y and c_z components of the transformed vector.

3.2.3 Reduced Aerodynamic Angles

When no data is available relating the aerodynamic coefficients to the side slip angle – and when no wind is present – this member of the attitude control vector can be set to zero. This will result in a vanishing side force.

In this model the angle of attack can be positive or negative, since there is no ambiguity due to the missing definition of an attitude angle, unlike the reduced Euler angles described below.

3.2.4 Euler Angles

When the orientation of the vehicle is given in reference to the local vertical axis system V (see Fig. 3.1), the Euler angles yaw Ψ, pitch Θ, and roll Φ are used (see also Fig. A.6).

This control system is especially useful for parts of the trajectory during which the aerodynamic angles are not well defined, f.i. during the vertical launch of a rocket. Some launcher guidance schemes are also easier expressed in Euler angles.

As additional output variables, the aerodynamic angles are computed. By observing that

$$\mathbf{T}_A^B \; \mathbf{T}_{AV}^A \begin{bmatrix} 1 \\ 0 \\ 0 \end{bmatrix}_{AV} = \begin{bmatrix} c_x \\ c_y \\ c_z \end{bmatrix}_B = \mathbf{T}_L^B \; \mathbf{T}_{AV}^L \begin{bmatrix} 1 \\ 0 \\ 0 \end{bmatrix}_{AV}, \tag{3.29}$$

the angle of attack and the side slip angle can be obtained from:

$$\begin{bmatrix} \cos\beta\cos\alpha \\ \sin\beta \\ \cos\beta\sin\alpha \end{bmatrix} = \begin{bmatrix} c_x \\ c_y \\ c_z \end{bmatrix}_B . \tag{3.30}$$

The air-path bank angle is computed similarly from:

$$\mathbf{T}_A^{AV} \begin{bmatrix} 0 \\ y \\ 0 \end{bmatrix}_A = \begin{bmatrix} c_x \\ c_y \\ c_z \end{bmatrix}_{AV} = \mathbf{T}_L^{AV} \mathbf{T}_B^L \; \mathbf{T}_A^B \begin{bmatrix} 0 \\ y \\ 0 \end{bmatrix}_A \tag{3.31}$$

or

$$\begin{bmatrix} c_x \\ c_y \\ c_z \end{bmatrix}_{AV} = y \begin{bmatrix} 0 \\ \cos\mu_a \\ \sin\mu_a \end{bmatrix} . \tag{3.32}$$

3.2.5 Reduced Euler Angles

This kind of controls is meant for vehicles which show a rotational symmetry around the x axis of the body system and for which specifying a roll angle control would not make sense. However, in order to comply with other con-

Table 3.2: Axis systems for axisymmetric bodies

Index	Axis System
TF	total force system
TA	total angle of attack system

trol models, notably the reduced aerodynamic angles, an artificial roll angle is computed. It does not correspond to any characteristics of the vehicle, but rather to the direction of the resulting aerodynamic force. In this way it is possible to set the side slip angle to zero, which allows a smooth transition to and from the reduced aerodynamic angles (see Fig. 3.2 and Table 3.2).

The total angle of attack α_t, the bank angle of the total force system μ_t and the corresponding roll angle Φ' are computed as additional output functions (see Fig. A.7).

The total angle of attack is the angle between the air-path velocity $\vec{v}_a$ and the body x axis (denoted by $\vec{x}_b$):

$$\cos\alpha_t = \frac{\vec{v}_a \bullet \vec{x}_b}{|\vec{v}_a| \cdot |\vec{x}_b|}. \tag{3.33}$$

Since the vector

$$\vec{y} = \vec{v}_a \times \vec{x}_b \tag{3.34}$$

is perpendicular to both $\vec{v}_a$ and $\vec{x}_b$, it is along the y axis of the total force system TF. Therefore it can be used directly as test vector in formula (3.31). The aeroballistic roll angle Φ' can be computed analogous to (3.27) and (3.28). If the air-path velocity and the body x axis are parallel, the total angle of attack is zero and the bank angle is undefined.

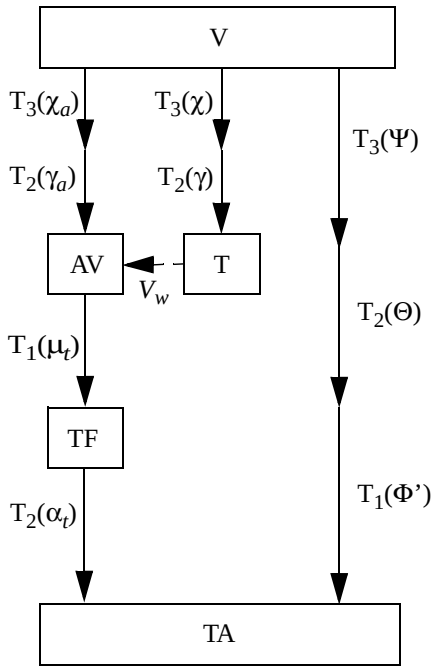

Fig. 3.2: Angular transformations for reduced attitude controls

Please note that this way of computation is tailored to vehicles that show a symmetric lift characteristic, i.e. the magnitude of lift is the same for positive and negative angle of attack. Especially the lift must be zero for a vanishing angle of attack.

3.2.6 Load Factor Controls

With this option, the control variables are the horizontal and the vertical load factor. There is no third component, since the side slip angle is set to zero. This implies that the side force is vanishing, too.

A load factor is defined as the ratio of the applicable aerodynamic force component and the vehicle's weight. In accordance with [7], the norm of the local gravity vector is used. In high speed flight, when the centrifugal and Coriolis accelerations cannot be neglected, a vertical load factor balancing the gravity will be slightly less than one, however.

The total angle of attack and the flight-path bank angle are computed, conserving the sign of the bank angle. Therefore the discussion of

Section 3.2.2 and Section 3.2.3 applies. The tangent of the bank angle defined by ratio of the load factors, observing the correct sign:

$$\mu_t = \operatorname{atan}(n_h, n_v) \; . \tag{3.35}$$

The aerodynamic model must provide a method to calculate the angle of attack that corresponds – for the current Mach number – to a given lift coefficient:

$$c_L(\alpha_t, M) = \frac{qS}{mg}\sqrt{n_h^2 + n_v^2} \, . \tag{3.36}$$

The side slip angle β is always zero. Therefore the total angle of attack system is used (see Section A.3.2 on page 162). Note that a negative vertical load factor will result in a positive total angle of attack and a vehicle orientation that will point the top part of the aircraft towards the planet.

3.3 Path Constraints

A path constraint $g^j \geq 0$ (see Eq. (3.7)) is enforced during the whole phase j. It is called “active” when it has an influence on the optimal trajectory. For an active path constraint, the trajectory can pass along the constraint for part or for all of the phase or there can be just a finite set of touch points in a phase. Path constraints are always of the inequality type (an equality constraint could be eliminated by reducing the state and control vectors).

The most important path constraints are discussed subsequently. These are the dynamic pressure, the heat load, the normal load and the loft ceiling. Note that in all these constraints the dynamic pressure plays a prominent role. This fact will be used later for derivation of atmospheric guidance laws.

The axial acceleration, a path constraint which depends on the atmosphere only to a very limited extend, is especially important for rocket launchers.

3.3.1 Dynamic Pressure

The dynamic pressure is one of the most important quantities in flight mechanics. All aerodynamic forces and moments are proportional to it. Also

the actuator forces for the aerodynamic control surfaces depend on the dynamic pressure. It is a function of the air density and of the air speed:

$$q = \frac{1}{2}\rho V^2 \leq q_{max}. \tag{3.37}$$

The unit is that of a pressure, force per area: $[q] = N/m^2$.

3.3.2 Heat Rate

The stagnation point heat rate is a measure for the amount of energy that the ambient medium will dissipate to the vehicle per unit of time. A heuristic formula is given by [24] and by [61] as

$$\dot{Q} = C\rho^n V^m \leq \dot{Q}_{max}. \tag{3.38}$$

In the case of free stream enthalpy, the parameters are C=1/2, n=1, and m=3, or:

$$\dot{Q} = \frac{1}{2}\rho V^3 = qV \leq \dot{Q}_{max}. \tag{3.39}$$

For hypersonic heating, when only a small fraction of the available heat is conducted to the vehicle, the literature suggests n=1/2, and m=3.0 or m=3.15:

$$\dot{Q} = 2^n C q^n V^{m-2n}. \tag{3.40}$$

The constant C must be chosen according to the effective stagnation point radius. Note that the unit of C must be consistent with the other parameters.

The unit of the heat load is thermal power dissipation per area: $[\dot{Q}] = W/m^2$.

3.3.3 Normal Load Factor

The normal load relates the acceleration due to aerodynamic forces to the local acceleration due to gravity by

$$n = \frac{\left|(-D, Y_a, -L)^T\right|}{m\left|\vec{g}(\vec{r})\right|} \leq n_{max}. \tag{3.41}$$

It is the acceleration that a passenger would feel in the absence of a thrust force. Note, that the choice of a local $\grave{g}(\grave{r})$ is mandated by [7].

When the lateral force Y_a is neglected (and with the short hand g for gravity), the normal load is

$$n = q\sqrt{c_D^2 + c_L^2}\ \frac{S}{mg} \le n_{max}. \tag{3.42}$$

Normal load is dimensionless: $[n] = 1$.

3.3.4 Loft Ceiling

This constraint is dictated by controllability considerations, rather than being a strict limit. It states that the vertical lift component must be large enough to balance all other accelerations in Eq. (3.16):

$$\frac{L_{max}}{m} + \left(\frac{V^2}{R} - g\right)\cos\gamma + a_{\omega_E} \ge 0, \tag{3.43}$$

where a_{ω_E} stands for the Coriolis and the centrifugal acceleration due to the planet's rotation. This equation can be rewritten as

$$a_{Lmax} = \frac{S}{m} q c_{Lmax} \ge \left(g - \frac{V^2}{R}\right)\cos\gamma - a_{\omega_E}, \tag{3.44}$$

where c_{Lmax} is the maximum achievable lift factor and usually depends only on the Mach number.

The unit of the lift acceleration is: $[a_{Lmax}] = m/s^2$.

A similar limit exists for vehicles entering at hyperbolic speed. The "no-skip" condition ensures that the vehicle will not leave the atmosphere anymore (called "over-shoot" or "skip-out"):

$$\frac{L_{max}\cos|\mu|_m}{m} \le \left(g - \frac{V^2}{R}\right)\cos\gamma - a_{\omega_E}. \tag{3.45}$$

Note, that the centrifugal acceleration can be larger than the gravity acceleration. The maximum bank angle modulus $|\mu|_m$ is given by flight control con-

siderations. When it is larger than $\pi/2$, the lift is oriented downwards. Otherwise the L_{max} should be replaced by the minimum possible lift.

3.3.5 Axial Acceleration

The fuel of a rocket launcher is typically a large percentage of the total mass at launch time. When the fuel of a stage is depleted while the thrust is kept constant, the acceleration of the vehicle is steadily increasing. At some point the thrust must be reduced, in order not to destroy the launcher or the payload:

$$a_T = \frac{T(t) - D}{m(t)} \leq a_{Tmax}. \tag{3.46}$$

Since the thrust is mostly aligned with the major axis of the vehicle, the acceleration is called “axial”. Usually the drag can be neglected for rockets.

The unit is $[a_{Tmax}] = m/s^2$.

3.4 Cost Functions

While it is often a difficult task just to satisfy all constraints, there are still open parameters which can be chosen to the cost function. While in the general formulation, a cost functional can have an integral part called Lagrange term (see Eq. (3.3)), in ASTOS this is only used for control smoothing:

$$I = \phi^0(x^1(t^0), u^0(t^0), p^1, t^0) + \sum_{j=1}^{m} \phi^j(x^j(t^j), u^j(t^j), p^j, t^j) \quad . \tag{3.47}$$

Cost functions involving the ratio of launch mass to final mass are of particular interest for launch vehicles, while for reentry vehicles a typical task is to reduce the heat load on the vehicle, or – during planning of the mission – it is important to optimize the maneuverability, represented by the achievable cross range.

3.4.1 Maximum Payload

This cost function is the sum of the masses of all payloads:

$$I = -\sum m_{PL,\,i}\,. \tag{3.48}$$

This can be used to size a satellite during the design phase, or to assess how much fuel a satellite can use for station keeping.

For this criterion, the mass of at least one payload is variable. In the case of several payloads, usually the scaling parameters of all but the one to be sized are set to be constant.

Note that the cost function is conveniently calculated at t_0, since the mass of the payloads is constant during the flight.

3.4.2 Maximum Final Mass

In this case, the total mass at the final time t_f or at the time when the last payload is jettisoned is used as cost function:

$$I = -\sum m_i\Big|_{t_f}\,. \tag{3.49}$$

The mass of the payloads is held constant. It is assumed that savings in upper stage propellant during ascent can be used as additional propellant in the payload – for station keeping, f. i.

3.4.3 Minimum Fuel

While holding the payload masses constant, the sum of the fuel of all tanks at launch time is minimized:

$$I = \sum m_F\Big|_{t_0}\,. \tag{3.50}$$

This assumes that at least one of the tanks has a variable filling capability.

3.4.4 Minimal Heat Load

Widely used for reentry vehicles, the accumulated stagnation point heat load is a measure for the thickness (and weight) of the thermal insulation needed.

The heat load is the integral of the stagnation point heat rate (see Eq. (3.38)):

$$I = \int_{t_0}^{t_f} \dot{Q} dt . \tag{3.51}$$

Most of this energy will be radiated into the ambient, only a small fraction is actually conducted through the insulation.

3.4.5 Cross Range

When evaluating the capabilities of a reentry vehicle, the achievable cross range is important, f.i. to assess how many landing sites must be planned for emergency returns.

The cross range is defined as the distance of the landing site from the initial orbital plane (see Fig. 3.3). Note that this involves parameters both from t_0 and t_f (denoted by the indices 0 and *f*):

$$\sin\delta_C = \left(\frac{\vec{R}_0 \times \vec{V}_0}{|\vec{R}_0 \times \vec{V}_0|} \right) \cdot \frac{\vec{R}_f}{|\vec{R}_f|} = \vec{i}_0 \cdot \frac{\vec{R}_f}{|\vec{R}_f|}, \tag{3.52}$$

where $\vec{i}_0$ is the unit vector in the direction of the angular momentum of the initial orbit. All vectors are expressed in the inertial frame.

In order to maximize the (positive) cross range when turning to the right

$$I = -\delta_C \tag{3.53}$$

or to minimize the (negative) cross range when turning to the left

$$I = \delta_C \tag{3.54}$$

the sign of the cost function must be chosen accordingly.

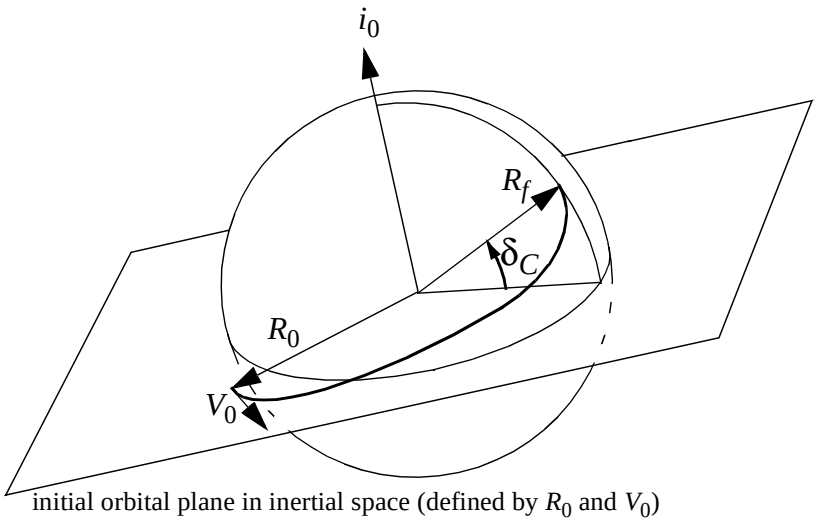

Fig. 3.3: Definition of cross range for reentry

3.4.6 Trajectory Smoothing

For trajectory smoothing an additional term can be used together with any of the other cost functions. An additional member of the state vector is defined, whose differential equation is the square of the derivative of the flight-path angle:

$$x_S = c \cdot \int_{t^0}^{t^f} \dot{\gamma}^2 \; dt\,. \tag{3.55}$$

If the constant c is not set otherwise by the user, its value is zero.

4 Guidance Laws

There is little literature on guidance laws specifically designed for an initial guess generator. Therefore, guidance laws that are used for the real time guidance of aerospace vehicles are examined: conventional launchers (see [9], [31], [59], [60], [70]), advanced launchers (see [14], [21], [46], [47], [55], [56], [58]) and reentry vehicles (see [13], [17], [19], [23], [25], [26], [30], [36], [41], [48], [49], [73], [84]). The purpose of these guidance laws is to control a vehicle in real time in a way as to guaranty the achievement of certain target conditions – without necessarily satisfying any intermediate constraints.

While a conventional control law is often designed to handle just a single mission, an IGG control law for the ASTOS software should handle a wide range of initial and final conditions, as well as different kinds of models and different phase structures.

Since the control discretization used for optimization is often quite coarse, the controls used for the initial guess should be smooth and without high frequency content. A small number of abrupt changes can be modelled, when these changes happen at well-defined times.

If in addition an initial guess is close to the optimal solution and satisfies all or at least some of the path constraints, it will lead to fast optimizations.

If a controller is used within an IGG, it faces some severe restrictions. There cannot be any integral stage, since this would extend the state vector.

Also a differential block is not feasible, since the integrator of the IGG is allowed to select evaluation times at random order. No information obtained in a previous step can be used, so also output filtering techniques must be avoided. However, the whole state vector can be considered exactly known and no measurement noise must be taken into account. In addition, an IGG control law should generate the state history with minimal computation effort.

4.1 Conventional Launcher

An overview is given for some typical guidance schemes. The three guidance schemes used in ASTOS will be discussed in greater detail in the subsequent sections. A guidance scheme for a vertically launched rocket involves typically four sections. In an initial phase the vehicle accelerates vertically until the launch pad is cleared. Then some maneuver is made to achieve a well defined interface to the subsequent gravity turn. Finally a guidance is executed in order to reach the target orbit conditions.

4.1.1 Previous Work

Skalecki and Martin ([69]) propose guidance by parameter optimization. The optimizer is only used to satisfy all constraints, so this is actually a targeting scheme, rather than optimization.

Similarly, the optimization described by Gath ([27]) can be used for the parts of the trajectory outside of the atmosphere. The optimization with an indirect method is reported to be very robust, and no initial guess is needed. Due to the use of a primer vector, the result is a three dimensional guidance scheme.

In [55], an altitude profile is used for guidance. It is specified as a cubic spline with two sectors. The coefficients are optimized to achieve the proper target orbit. The guidance of the Pegasus vehicle uses a pre-computed pitch profile for the lower stage guidance (see [54]).

However these guidance schemes either need some pre-computations or involve a specific kind of optimization on their own. Therefore they do not qualify for the initial guess generator.

4.1.2 Pitch Push-Over

A gravity turn normally cannot be flown from the start of the launcher. There must be some push-over maneuver to get the trajectory out of the vertical and to establish a well defined flight-path angle. The pitch program is according to:

$$\begin{aligned}
\Theta &= \gamma && \text{for} \quad t_i \le t \le t_{acc}, \\
\Theta &= \gamma - \frac{t - t_{acc}}{t_{po} - t_{acc}}\,\Delta\Theta && \text{for} \quad t_{acc} \le t \le t_{po}, \\
\Theta &= \gamma - \Delta\Theta e^{-(t - t_{po})/t_c} && \text{for} \quad t_{po} \le t \le t_{i+1}, \\
&\text{or} \\
\Theta &= \gamma - \frac{t_{i+1} - t}{t_{i+1} - t_{po}}\Delta\Theta && \text{for} \quad t_{po} \le t \le t_{i+1},
\end{aligned} \tag{4.1}$$

where $t_i \le t_{acc} < t_{po} < t_{i+1}$ are the initial time of the phase, the end of an acceleration time, the end of the pitch-over rotation, and the phase final time, respectively. When the time constant t_c is not specified, the last formula is used for reducing the difference between pitch and flight-path angle.

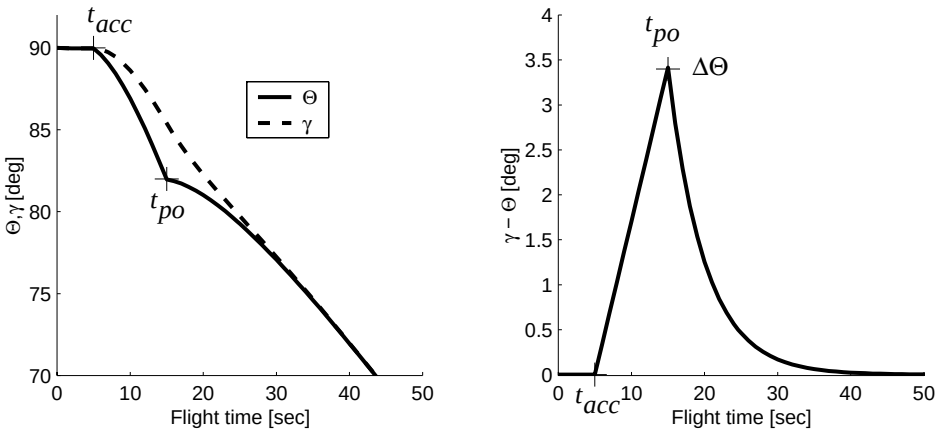

Fig. 4.1: Pitch over maneuver and comparison to flight-path angle

The pitch difference $\Delta\Theta$ characterizes the amount of pitch over. It is the only optimizable parameter.

4.1.3 Gravity Turn

The gravity turn is the most elementary – and the most widely used – control law for the first stages of rocket launchers. In the vertical plane the trajectory is governed only by the gravitational acceleration. Thrust serves just for acceleration along the current velocity vector.

In ASTOS there are two slightly different ways to specify a gravity turn ([37]). When using aerodynamic angles as control option, the angle of attack can be fixed to zero. Note that the bank angle becomes undefined and that there is no controllability in the horizontal direction.

When using Euler angles controls, the gravity turn option sets the pitch equal to the flight-path angle. The yaw angle can be used to steer in the horizontal plane. Like this, the angle of attack can deviate from zero.

Since the gravity turn does not have any control parameters on its own, the trajectory is extremely sensitive with respect to the state vector at the beginning of the maneuver.

4.1.4 Required Velocity Concept

This guidance concept was introduced by Battin (see [9]). It is often called Q-Guidance. Several research papers at the IFR have shown the merits of the concept (see f.i. [59], [60], [70]).

The base of the guidance is the observation, that, for a given radius that a velocity vector can be computed, that a vehicle on a given elliptic orbit should have (the result is definite, except for the sign of the radial component). This velocity is called the “required velocity” (V_{req}).

The task of the guidance law is to reduce the difference between the required velocity and the current velocity to zero (see Fig. 4.2):

$$\vec{V}_d = \vec{V}_{req} - \vec{V}_{curr}\,. \tag{4.2}$$

In the most basic form, the net acceleration (thrust acceleration minus net gravity) is applied in the direction of the velocity difference:

$$\frac{\vec{T}}{m} - \vec{g}_n \parallel \vec{V}_d\,. \tag{4.3}$$

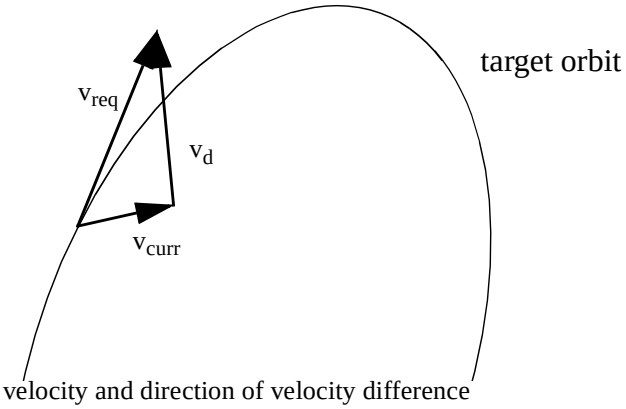

Fig. 4.2: Required velocity and direction of velocity difference

In a simple geometric procedure, a circle with a radius equal to the thrust acceleration is drawn around the tip of the gravity acceleration. The point where this circle intersects the direction of the velocity difference gives the direction of the thrust. This procedure is shown graphically in Fig. 4.3.

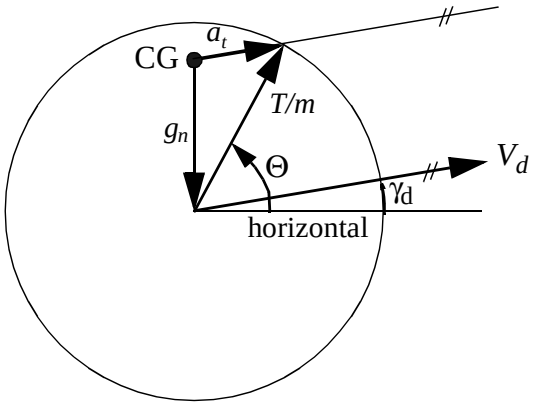

Fig. 4.3: Applying thrust to reduce the velocity difference
Note that the total acceleration a_t is parallel to V_d.

In the triangle formed by g_n, the thrust acceleration T/m and the total acceleration a_t, the following formulas hold:

$$\frac{\sin(90^0 - \Theta)}{a_t} = \frac{\sin(90^0 + \gamma_d)}{T/m} \tag{4.4}$$

and

$$a_t^2 = \left(\frac{T}{m}\right)^2 + g_n^2 - \frac{T}{m} g_n \cos(90^0 - \Theta). \tag{4.5}$$

Note that the angle Θ and the length of a_t are unknowns. The latter is easily eliminated to obtain:

$$\frac{1 - \sin^2\Theta}{\cos^2\gamma_d} = 1 + \left(\frac{mg_n}{T}\right)^2 - \frac{mg_n}{T}\sin\Theta. \tag{4.6}$$

With the abbreviations

$$p = -\frac{mg_n}{T}\cos^2\gamma_d,$$

$$q = \cos^2\gamma_d - 1 + \left(\frac{mg_n}{T}\right)^2 \cos^2\gamma_d, \tag{4.7}$$

the pitch Θ can be computed from the solution of a quadratic equation:

$$\sin\Theta_{1,2} = -\frac{p}{2} \pm \sqrt{\left(\frac{p}{2}\right)^2 - q}. \tag{4.8}$$

The sign of the square root is chosen according to the radial component of V_d. Note that the effective gravity g_n is the local gravity minus the centrifugal acceleration.

By setting the pitch angle in this way, the velocity difference is steadily reduced. Once the difference is sufficiently small, the engine is shut off. It must be observed that part of the thrust is used to balance the gravitational acceleration. Therefore this guidance can only be used when the thrust force is larger than the effective gravitational force. For many rockets this is not the case at the beginning of the upper stage burn, when the tank is still full and the horizontal velocity is too small to balance the gravity. Also this concept can only be used when the altitude of the launcher is in between apogee and perigee altitude of the target orbit.

In ASTOS, if any of these conditions is not true, simply a default pitch is foreseen, which can be specified by the user. However, at the moment, when the Q-guidance can be used, a large jump in the pitch control occurs.

This guidance scheme does not have any optimizable parameters, it is too rigid for optimization.

4.1.5 Bi-Linear Tangent Law

The bi-linear tangent law is the solution of a very simple control problem, the "maximum velocity transfer to a rectilinear path" (see [12]):

> "Consider a particle of mass *m*, acted upon by a force of magnitude *ma*. We assume planar motion and use an inertial coordinate system *x, y* to locate the particle; the velocity components of the particle are *u, v.* The thrust-direction angle $\beta(t)$ is the control variable of the system.
> ...
> We wish to transfer the particle to a path parallel to the *x*-axis, a distance *h* away, in a given time *T* with the maximum value of *u(t)*."

As shown in [12], pp. 59 and pp. 82, and in Appendix B.1, the optimal control law for this problem is:

$$\tan\beta = \frac{c_2 t + c_4}{c_1 t + c_3}. \tag{4.9}$$

This is called "bi-linear tangent law", since the tangent of the control angle is the ratio of two linear functions. The coefficients must be chosen in order to satisfy the end conditions. With the assumptions of constant thrust acceleration, this can be done analytically.

In the special case when no end condition depends on the coordinate *x*, the coefficient c_1 is zero and the guidance law becomes

$$\tan\beta = \frac{c_2}{c_3} t + \frac{c_4}{c_3}, \tag{4.10}$$

which is the "linear tangent law". In this form, the guidance law is proposed for the upper stage of the Kistler K-1 vehicle ([31]).

Application to the Guidance of Rockets

Although this bi-linear tangent law is valid only for a flat planet and a constant gravitational acceleration, it can be used with good results also for the guidance of rockets (see [60]). The control angle β is replaced by the pitch angle Θ, and the distance h by the perigee altitude of the target orbit. Maximizing the horizontal velocity is then equivalent to maximizing the apogee of the orbit.

The application is limited to trajectory parts where the above assumptions are approximately true and where the atmospheric drag can be neglected.

For optimization, the formulation of in Eq. (4.9) poses some difficulties. Although there are four constants, one is redundant and could be replaced by one – provided it is not equal to zero! Since this is not known a priori, one cannot simply divide by one of the constants.

In addition, during iterations the denominator may vanish. This would introduce a jump in the control angle, which may trip the numerical integration algorithm. Finally, it is difficult to estimate good upper and lower bounds for the coefficients.

To avoid these problems, the guidance law is rewritten. Since the pitch angle is known to be within the interval of $-\pi/2$ to $+\pi/2$ (a value outside this range would reduce the horizontal velocity component instead of increasing it), using the initial and the final pitch angle offers a convenient way to specify two of the necessary constants. As a third parameter, a measure of the curvature was chosen.

$$\tan\theta = \frac{c\tan\theta_0 + (\tan\theta_f - c\tan\theta_0)\hat{t}}{c + (1-c)\hat{t}} \text{ with } \hat{t} = \frac{(t-t_0)}{(t_f-t_0)}. \tag{4.11}$$

It can easily be seen, that a given c has the opposite curvature effect than the reciprocal value $1/c$. In order to make the relationship symmetric, an exponent was introduced:

$$\tan\theta = \frac{a^{\xi}\tan\theta_0 + (\tan\theta_f - a^{\xi}\tan\theta_0)\hat{t}}{a^{\xi} + (1-a^{\xi})\hat{t}} \tag{4.12}$$

with an arbitrary constant $a > 1$.

A value of a=100 allows a ξ in the interval of [-1, +1] to cover a wide range of curvatures (see Fig. 4.4). For ξ=0, the linear tangent law will result.

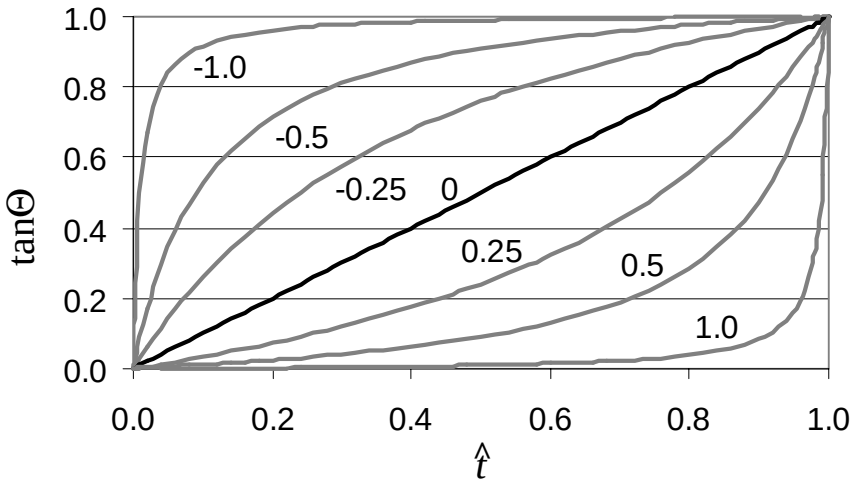

Fig. 4.4: Effect of the curvature parameter ξ for a base of a=100
The end values are $\tan\Theta_0$=0, and $\tan\Theta_f$=1, respectively. For other values, the graph is stretched accordingly

4.1.6 Horizontal Guidance

While some rockets are restricted to a constant yaw during the powered flight, most can have a steering, which greatly improves the versatility. In ASTOS two methods for guessing the yaw angle are implemented.

The first corresponds to the gravity turn. The yaw is simply set to the current heading angle:

$$\Psi = \chi . \tag{4.13}$$

The trajectory depends largely on the starting value, which should be specified by the user according to the mission. The heading angle can be chosen in the earth-relative frame for the atmospheric part of the trajectory or in the inertial frame for the upper stage.

The second method is called “target inclination”. The yaw is set to the value that corresponds to an orbit with the given inclination, at the current latitude:

$$\begin{aligned} \Psi &= \Psi_0 \quad \text{for northward flight} \\ \Psi &= \pi - \Psi_0 \quad \text{for southward flight} \end{aligned} \tag{4.14}$$

with Ψ_0 given by

$$\sin\Psi_0 = \cos i_t \cos\delta . \tag{4.15}$$

The target inclination i_t can be optimized. It will be close, but not necessarily identical to the inclination i required by the end conditions. The direction of Ψ – either northward or southward flight – can either be chosen by the user or obtained from the current velocity vector.

Note that the only rocket guidance law implemented for aerodynamic angles, the gravity turn, does not require any additional horizontal guidance.

4.2 Advanced Launcher

While the vertical motion of advanced launchers has been treated extensively in the literature (see [14], [46], [47], [55], [56], [58]), there are only very few solutions for the horizontal guidance (e.g. [21]).

Since advanced launchers are in many respects similar to high-performance aircraft, some literature concerning fighter aircraft maneuvers is considered ([16], [21], [28], [67], [68]).

4.2.1 Vertical Guidance

4.2.1.1 Theory of Singular Perturbations

Many publications deal with the ascent guidance of advanced vehicles using the method of singular perturbations (e.g. [21], [47]). This method is based on the observation that in many systems of differential equations it is possible to identify a “fast” and a “slow” subset of the state vector. Some variables can reach a given final state very fast, while others are changing on a much slower time scale:

$$\hat{\dot{x}} = \begin{pmatrix} \hat{\dot{x}}_F \\ \hat{\dot{x}}_S \end{pmatrix}. \tag{4.16}$$

In more formal terms, the left hand side of the “fast” equations is multiplied by a small constant ε. (see e.g. [16] for further discussion of the procedure). Sometimes it is possible to identify a system parameter that can serve as the ε, otherwise it must be introduced arbitrarily (this is called “forced singular perturbation”):

$$\begin{aligned} \dot{x_S} &= f_S(t, (x_S, x_F)^T, u), \\ \varepsilon\dot{x_F} &= f_F(t, (x_S, x_F)^T, u). \end{aligned} \tag{4.17}$$

To solve the optimization problem of the slow manifold, the constant ε is set to zero, resulting in additional algebraic conditions, which can be used to eliminate some of the original controls:

$$\begin{aligned} \dot{x_S} &= f_S(t, (x_S, x_F)^T, u), \\ 0 &= f_F(t, (x_S, x_F)^T, u) \ . \end{aligned} \tag{4.18}$$

After the trajectory of the slow variables is solved, all differential equations are divided by the constant ε. The limit $\varepsilon \to 0$ results in

$$\begin{aligned} 0 &= f_S(t, (x_S, x_F)^T, u), \\ \dot{x_F} &= f_F(t, (x_S, x_F)^T, u). \end{aligned} \tag{4.19}$$

On the fast time scale the slow variables can be considered constant. The fast variables are used to satisfy the remaining boundary constraints. Since this results in short transients at the beginning and at the end of the trajectory, the regions are called “boundary layers”.

Problems

In general the method of singular perturbations is used in conjunction with indirect optimization techniques. Then the reduction of the size of the state vector is especially advantageous.

However, in the presence of active path constraints, in which not all of the neglected states show up, a jump in the pseudo-control may occur. Since a state – even a fast one – cannot change in an instant, such a solution is not physically sensible. These points should be subject to another boundary layer investigation.

The assumption that the fast variables reach an equilibrium so quickly that for most of the trajectory they can be considered constant (second part of Eq. (4.18)) is a contradiction to the use of the fast variables as pseudo-controls. However, in most papers, the equation is not used any further.

4.2.1.2 Energy State Approximation

For solving the ascent of advanced launchers with the singular perturbation method, very often the “Energy State Approximation” (or ESA for short) is used. The variables of the vertical motion, altitude h (or equivalently, the radius R) and flight-path angle γ, are identified as the fast variables. The slow state members are the mass and the specific energy e, which replaces velocity (hence the name of the approximation).

The velocity V is expressed in terms of e and h:

$$V = \sqrt{2(e - gh)} \tag{4.20}$$

when a constant gravitational acceleration g is assumed, or in terms of the radius R for a spherical gravitational field:

$$V = \sqrt{2\left(e + \frac{\mu_E}{R}\right)}. \tag{4.21}$$

Most papers neglect the horizontal dynamics (position and heading). Then the differential equations are (see e.g. [22]):

$$\begin{aligned}
\dot{e} &= V\frac{(T\cos\varepsilon - D)}{m} \\
\dot{m} &= -f(R, e, \phi, \alpha) \\
\varepsilon\dot{\gamma} &= \frac{(T\sin\varepsilon + L)\cos\mu_a}{mV} + \frac{V\cos\gamma}{R} - \frac{\mu_E\cos\gamma}{VR^2} \\
\varepsilon\dot{R} &= V\sin\gamma
\end{aligned} \quad , \tag{4.22}$$

where $T\cos\varepsilon$ is the thrust component in flight-path velocity direction, and $T\sin\varepsilon$ is the component perpendicular to it (ν is considered to be equal to zero).

Corban, Calise and Flandro ([22]) solve sub-problems by making further simplifications, like setting the flight-path angle to zero and assuming that the thrust is always aligned with the velocity. As a minor result, it is shown that the throttle setting will be of a bang-bang type (only zero or one), when both thrust and fuel rate are a linear function of the throttle.

In [47], Lovell and Schmidt use the ESA for the fast evaluation of neighboring vehicle design. Schultz et al. ([66]) also use the ESA, and propose it for reentry as well.

Kremer and Mease ([44]) treat the control problem for boundary layers, observing several kinds of constraints.

Hermann and Schmidt [33] examine the conditions for the time scale separation in detail. Points along the trajectory are reported, where potential energy is traded for kinetic energy instantaneously.

A few papers also deal with the horizontal guidance problem when using the ESA for fighter aircraft.

Cliff and Well used forced singular perturbation in three time scales ([21]): fast variables (γ,h), and slow (position x, y, and fuel weight W_f). Energy and heading χ are considered of intermediate speed. The model was based on a flat earth, but included correction terms for the centrifugal acceleration. In the solution intermediate transients both for the energy and for the heading angle were observed, independent of each other.

In [68], Shinar, Well, and Järmark compare two concepts for high performance aircraft: one based on the energy state approximation and one based on indirect optimization with a simplified model. Both results are compared to off-line optimization. Due to the setting (a steadily moving target airplane), there is a change of χ only in the initial boundary. Further on, all motion takes place in a vertical plane.

In a paper about the range optimization of a fighter aircraft ([67]), Seywald et al. show that a great number of different switching structures are possible when a bound on the normal load factor is present.

4.2.1.3 Energy Method

One of the earliest references to optimization in aerospace technology is the energy climb investigated by Kaiser ([42]), a geometric procedure to minimize the time to climb for an aircraft by selecting, for each velocity, the altitude where the specific excess power is the highest.

When the energy is monotonously increasing, the state variables can be derived with respect to energy instead of time. With

$$m' = \frac{dm}{de} = \frac{dm}{dt}\,\frac{dt}{de} = \frac{\dot{m}}{\dot{e}}, \tag{4.23}$$

the second equation of Eq. (4.22) becomes:

$$m' = -\frac{f(R, e, \phi, \alpha)m}{V[T_C(R, e, \phi, \alpha) - D(R, e, \alpha)]}\ . \tag{4.24}$$

Note that since the derivative of the specific energy with respect to itself is always unity, this is the only differential equation left of the slow manifold. The reciprocal formula

$$\frac{de}{dm} = \frac{1}{m'} = -\frac{V[T_C(R, e, \phi, \alpha) - D(R, e, \alpha)]}{f(R, e, \phi, \alpha)m} \tag{4.25}$$

describes the amount of energy gained for each small amount of fuel spent. Since there is only one state left – the mass – and due to the assumption, that the energy is monotonously, the Bellman principle can be applied. The most fuel efficient trajectory is achieved, when at every point along the trajectory, the energy gained for every bit of fuel spent is maximized.

Of the variables involved on the right hand side (R, e, ϕ, and α), energy replaces the time as the independent variable. The angle of attack α is given by the vertical balance of forces – at least as a zeroth order approximation. This leaves the throttle factor ϕ and the radius R to be chosen.

Therefore, for every energy level, an optimal altitude and an optimal throttle factor can be computed. Since these depend only on the atmosphere, the engine and the aerodynamic model, the computations can be done offline, before launch. Schnepper shows in [64] that in general the best perfor-

mance is achieved at a bound of the permissible flight region, e.g. at the maximum dynamic pressure bound.

It must be kept in mind, however, that this method completely ignores the horizontal dynamics and therefore cannot satisfy any positional boundary constraints. In his thesis ([10]), Baunach compared the energy-method very favorably with result obtained by optimizing a full model. For a long part of the trajectory, the vehicle did fly along the dynamic pressure boundary, as predicted, but there were also cruise-like parts of the trajectory, which cannot be treated adequately.

4.2.1.4 Other Vertical Guidance Concepts

A problem for optimization of advanced launchers is the hypersonic phugoid oscillation. While it was pointed out, that this can be used to save a very small amount of fuel, as compared to a conventional trajectory ([11]), it poses a major problem for a guidance logic.

In their paper Landiech, Aumasson, and Droz [46] use the flight-path angle γ as a control, in order to avoid oscillations. This can be regarded as singular perturbation, too. However the authors use a controller to obtain the angle of attack and introduce a fast time scale again into the integration.

Schnepper ([64]) achieves suppression of the phugoid by using a penalty term on $\dot{\gamma}$. The solution presented flies along the upper dynamic pressure bound during most of ascent, and at the lower bound during descent.

As a model reduction, Paus ([56]) uses the flight-path angle and the heading angle as “virtual” controls. A controller using feedback linearization computes the real controls α and μ_a. The reference flight-path angle is split into two parts: one (called pre-control γ_p) is the angle needed to follow the dynamic pressure boundary, while only γ_c, the second part, is optimized. As an initial guess γ_c is set to zero.

4.2.2 Horizontal Guidance

Both Paus ([56]) and Baunach ([10]) use a linear function as an estimate for the optimal azimuth. This is reported to be within the convergence region of the optimizer.

In [14], Buhl, Ebert, and Wolf give a heuristic for the return of a lower stage in a two stage to orbit configuration (TSTO). After the release of the

upper stage, the lower stage vehicle flies a circle until the heading is toward the landing site. Altitude and velocity are kept constant, the thrust of the ram-jet engines compensates the drag. The angle of attack is selected to achieve the best lift to drag ratio. Once the heading is aligned to the landing site, the circle is finished. Again the altitude and velocity are kept constant. Finally, when the runway can be reached by a glide, the engines are shut off. The angle of attack is again set for best glide (minimal L/D).

Again, for fighter aircraft, some other guidance laws are given, but for situations much different from an advanced launcher ascent ([28], [68]).

A common guidance law is proportional navigation (see e.g. [77]). A pursuer aircraft has to turn into a collision course with a target aircraft, which flies at constant speed (and direction). The turn command is proportional to the current change rate of the line of sight. Once this change rate is zero, the collision course is reached and there is no control activity anymore. This is similar to the result of [68], which describes a singular perturbation for the heading angle and gives a guidance law for the initial boundary layer.

Grimm and Hans [28] describe the optimal turn to a given heading in minimal time, when no load factor constraint is active.

The aircraft solutions tend to have a short phase of heading change and then a longer phase with constant heading. However several publications describe the supersonic ascent as a long, unsteady curve ([39], [63], [64]). Therefore the base assumptions (like "χ is a fast variable") do not hold and these schemes cannot be applied.

A simple guidance law is implemented. It consists of computing the horizontal load factor corresponding to a constant heading turn rate, derived from eqn. (3.15):

$$n_h g = \dot{\chi} v \cos\gamma + g_\delta \sin\chi - \frac{(V\cos\gamma)^2}{R} \sin\chi \tan\delta - \\ - 2\omega_E V \cos\gamma (\sin\delta - \cos\chi \cos\delta \tan\gamma) - \omega_E^2 R \cos\delta \sin\chi \sin\delta . \quad (4.26)$$

For simplicity, the thrust incidence angles ν and ε are set to zero. Otherwise, the bank angle cannot be easily eliminated. Note that no side force exists for load factor controls, anyway.

4.3 Reentry Vehicles

Several guidance schemes have been proposed for reentry. The most successful – and the most elaborate – is the Shuttle guidance, which is described in section 4.3.1. Some other guidance laws and their (lack of) suitability for an initial guess generator are discussed in this section.

Closed Form Predictions

The earliest attempts to solve the reentry problem were made using closed form predictions: Wingrove ([82]), Tannas ([73]), and Hankey ([29]) give some formulas which are valid under specific assumptions. While Tannas states that the cross range in general cannot be predicted, Causey and Sohoni ([17]) give downrange and cross range estimates by assuming a constant bank angle. They also achieve targeting in both dimensions by linearizing the ranges over μ_a and α.

Usually the assumptions are very stringent and do not allow trajectory planning for a complex set of constraints. Most of the formulas also predict just one variable and are not suited for two dimensional targeting.

Reference Trajectory Guidance

Many papers have been published, describing reentry guidance with precomputed trajectory profiles. Some examples:

Buhl et al. ([13], [14]) report a technique for energy management using a reference profile.

Marcus and Kriegsman define a density vs. speed profile ([49]) to obtain a range estimation. The lift is maximized. In a second mode, a reference table $h(V)$ is used.

In [58], Pignie, Delpy, and Carmona are tracking a reference profile with a PI controller for the angle of attack.

Pesch ([57]) and Kugelmann ([45]) use the solution of a two point boundary value problem as a reference trajectory. The latter paper shows how the linearization of the necessary conditions for optimality can be used as a sensitivity matrix for the controls. For the guidance, only a matrix-vector multiplication is used for every step.

Jouhaud's guidance scheme involves the solution of an optimal control problem, linearized around a reference trajectory, by using the maximum principle ([41]). The optimal control will bring the vehicle to the final conditions. The resulting three dimensional acceleration vector is mapped to the two controls α and μ_a and, at low velocity, to the speed brakes.

All these guidance schemes are not suitable for an IGG, since a reference trajectory must be computed a priori.

Targeting with few Parameters

In order to reduce the computational load on board of the vehicle, several guidance schemes which are specified by a very small number of parameters (down to two), have been proposed.

Burkhardt, Schöttle, and Zimmermann show in several publications ([15], [65], [84]) guidance laws for capsules. Targeting is achieved by adapting two parameters, the ranges are computed by numerical integration. The concept of "minimal control effort" is introduced, which reduces the amount of energy needed.

Fuhry designs a guidance with just two free parameters for the Kistler K-1 vehicle ([26]): the magnitude of the bank angle $|\mu_a|$ and the timing of a single bank reversal. The prediction is done by numerical integration, the targeting by linearization. All path constraints must be satisfied by choosing appropriate initial conditions, therefore the margin for velocity and flight-path angle at the entry interface are extremely small.

A similar concept is presented by Ishijima and Matsumoto ([35]), however several bank reversals are foreseen, initiated by a conventional dead band switch.

These guidance laws offer a fast computation and targeting, but due to the small number of parameters not all constraints, which make up the small entry corridor for high lift vehicles, can be fulfilled – even when optimizing the free parameters.

ESA and Reduced Order Systems

The energy state approximation (see Section 4.2.1.2) has also been used to solve the reentry problem. E.g. Schultz et al. ([66]) apply it and solve the reduced problem by using the maximum principle.

For mission design studies, Ardema, Bowles, Chou, and Windhorst, ([20], [81]) employ the energy-state approximation, reducing the system to the integration of a single variable: energy (see also 4.2.1.3). Several different cost criteria are investigated. Due to the reduction of the state vector, no targeting is possible.

A different approach is used by Mease, Teufel, et al. ([51], [75]). By using energy as the independent variable, replacing the radius with a reference radius and setting $\cos\gamma=1$, a reduced order system is found. The drag D and the ratio of the vertical part of the lift and the drag ($L\cos\mu_a/D$) are used as controls.

Chern, Yang, Vinh, and Hanson ([18], [76]) use a normalized set of differential equations with the Chapman variables

$$Z = \frac{\rho S c_L^*}{2m}\sqrt{Rh_S}\,,\ \nu = \frac{V^2}{gR}\,. \tag{4.27}$$

A quadratic polar is assumed, with c_L^* the lift coefficient for the best lift to drag ratio. By setting $\gamma \approx 0$ (equilibrium glide condition) and also $\dot{\gamma} \approx 0$, the altitude variable Z is eliminated. It is shown, that for maximizing cross range the optimal bank angle is given by:

$$\tan\mu = \frac{1-\nu}{\nu}\frac{\cos\delta\sin(\lambda_f-\lambda)}{\cos(\lambda_f-\lambda)\sin\chi - \cos\chi\sin\delta\sin(\lambda_f-\lambda)}\,. \tag{4.28}$$

for a given final longitude λ_f. The solution does not take path constraints into account (as do Chern, Yang, and Sheen in [19]). In addition, it shows large oscillations, which are in contradiction to the original assumption of equilibrium glide.

In order to protect the upper surface from excessive heat load current vehicles fly in the post stall region for a large part of the trajectory. Therefore the lift coefficient for best glide slope, c_L^*, cannot be used for theses trajectories.

4.3.1 Shuttle Guidance Law

Probably the guidance law most referred to is the Shuttle reentry guidance. Since its inception in the early seventies, numerous papers have been published, analyzing this guidance scheme or modifying it for special purposes.

An excellent description of the guidance logic is given by Harpold and Graves in [30]. Additional information can be found at Arrington and Jones ([8]), as well as at Joosten ([40]).

4.3.1.1 Angle of Attack Profile

During a long part of the reentry, the Space Shuttle encounters very high thermal loads. Since only the lower surface of the orbiter is designed to withstand the heat, the upper part of the shuttle is kept sheltered on the lee side by flying at a high angle of attack. This is a post stall condition, with the drag almost as large as the lift. Only at a much lower speed the nose is taken down, changing over to a normal flight regime.

The higher the initial angle of attack, the lower will be the total heat load. However a high angle of attack does limit the cross range capability (note that the necessary down range can be achieved by proper timing of the deorbit impulse). Therefore the maximum angle of attack that satisfies the cross range requirements is flown in the high speed regime.

Before every Shuttle mission, the angle of attack profile (f.i. as a function of the Mach number or of the velocity) is specified. During flight, there are only small deviations from the prescribed profile for modulating the drag during bank reversals.

4.3.1.2 Side Slip Angle

Due to thermal considerations the side slip angle should be zero, and the side force can be neglected for the design of the guidance. Therefore the attitude controls correspond to the case described in Section 3.2.3.

4.3.1.3 Velocity Bank Angle

During the initial phase of the reentry the orbiter flies normally at wings-level attitude ($\mu_a=0^o$). During a steep entry, all the available lift is needed for a pull-up maneuver. When the entry is more shallow (f.i. due to a small deorbit impulse), the excessive lift is dumped by turning the orbiter sideways ($\mu_a=\pm 90^o$).

When the aerodynamic forces reach a suitable level, the drag controller mode is initiated and used to compute the bank angle.

4.3.1.4 Drag Profile

It has been shown that the major path constraints for reentry can be expressed as functions of the dynamic pressure and the velocity (see section “Path Constraints” on page 65). Therefore the flight corridor could be specified in a diagram of q vs. V. However, the dynamic pressure cannot be directly measured in hypersonic flight.

Since the angle of attack profile is prescribed for every shuttle flight, the drag acceleration (which is easier to estimate) can be used instead of q:

$$d(V) = \frac{D}{m} = c_D(\alpha(M), M)\frac{qS}{m} = c_D(V)\frac{qS}{m} \tag{4.29}$$

for a sufficiently well know aerodynamic model. This also allows a convenient estimate of the range that still can be flown by analytical formulas.

During the shuttle entry, the drag profile is specified by a series of simple functions of the velocity or, for the last part of the trajectory, of the specific energy. This sequence consists of:

Temperature Control

The drag is a quadratic fit to the heat rate constraint:

$$d(V) = c_1 + c_2 V + c_3 V^2 . \tag{4.30}$$

For increased flexibility, two such segments with different coefficients are used.

Equilibrium Glide

Equilibrium glide is defined as $\dot{\gamma} = 0$. When neglecting the Earth’s rotation (by setting ω_E=0), setting cosγ=1, and applying all lift vertically (cosμ=1), equation (3.16) becomes:

$$d(V) = \frac{g}{c_L / c_D}\left(1 - \frac{V^2}{gR}\right). \tag{4.31}$$

Finally gr is replaced by a constant V_S^2, which is varied for ranging:

$$d(V) = \frac{g}{c_L / c_D}\left(1 - \frac{V^2}{V_S^2}\right). \tag{4.32}$$

Constant Drag Acceleration

This phase can be used to control the normal load, since – for constant lift to drag ratio – a constant drag corresponds to constant normal load:

$$d(V) = c_4. \tag{4.33}$$

Transition Phase

In the final part of the supersonic reentry, when the flight-path becomes steeper and the change in potential energy cannot be neglected anymore, the specific drag is modulated as a linear function of the specific energy:

$$d(e) = d_f + c_5(e - e_f). \tag{4.34}$$

In this way, when approaching the final energy e_f, a drag deceleration d_f compatible with the final approach is reached.

4.3.1.5 Range Control

The distance covered during reentry is:

$$\dot{s} = V\cos\gamma. \tag{4.35}$$

When neglecting the rotation of the Earth as well as the lateral gravity component g_δ, and for small flight-path angles (when $\sin\gamma \approx 0$), Eq. (3.14) becomes:

$$\dot{V} = -d. \tag{4.36}$$

These two equations can be combined to compute the distance travelled for a velocity range, given a drag profile as a function of the velocity:

$$s = -\int \frac{V}{d(V)} dV. \tag{4.37}$$

At lower speed, when the flight-path angle cannot be neglected anymore, the range is integrated over the specific energy. Observing that $e = V^2/2 + gh$, the derivative of the energy with respect to time is

$$\dot{e} = V\dot{V} + g\dot{h} = -Vd \tag{4.38}$$

and the integration of the distance covered for an energy range is given by:

$$s = -\int \frac{1}{d(e)} de. \tag{4.39}$$

These integrals are easily solved for the drag profiles given by eqns. (4.30), (4.32), (4.33), and (4.34).

During the flight the resulting distance that can be still covered with the nominal drag profile is compared to the actual distance to the target site. When there is a difference, the profile is adjusted.

By changing just a single parameter of the current segment (either the level of the drag or the final velocity of a segment), sufficient reserves are kept for adjustments necessary during later parts of the flight. This is important, since during the communication black out at hypersonic speed, navigational errors accumulate and must be corrected when the radio link is reestablished.

4.3.1.6 Drag Controller

Since the drag acceleration cannot be steered directly, a controller is used to achieve the commanded profile. While the angle of attack is used for short period drag control (f.i. during a bank reversal), the magnitude of the bank angle is the main control.

The vertical part of the lift $L\cos\mu_a$ is the control input in the differential equation of the flight-path angle (see Eq. (3.16), with some simplifications):

$$\dot{\gamma} = \left(\frac{V}{R} - \frac{g}{V}\right)\cos\gamma + \frac{L\cos\mu_a}{mV}. \tag{4.40}$$

The flight-path angle and the velocity make up the differential equation of the altitude (Eq. (3.11)), which is the major influence for the air density. Therefore the drag can be controlled by the bank angle via two integrations.

The bank angle controller compares the commanded drag d_0 and the actual drag. In order to improve the response to drag errors, also the difference between the actual altitude rate $\dot{h}$ and an estimated rate $\dot{h}_0$ computed from the drag profile is taken into account:

$$\cos\mu_C = \cos\mu_0 + \frac{c_D}{c_L}[f_1(d - d_0) + f_2(\dot{h} - \dot{h}_0) + f_4\int(d - d_0)dt] . \quad (4.41)$$

The term $\cos\mu_0$ is derived from the equilibrium glide condition $\dot{\gamma} = 0$ and from the curvature of the drag profile. The integral term is used to offset measurement errors in the altitude rate and can be neglected for a numerical simulation, in which the state is know exactly.

The two remaining gains are determined by pole placement and analytical computation of the gain scheduling.

4.3.1.7 Lateral Steering

Since the guidance logic does not supply an estimate for the cross range capability, the targeting scheme is rather simple.

Whenever the azimuth to the target becomes larger than a predefined azimuth error, a bank reversal is initiated, i.e. the sign of the bank angle is reversed. The dead band is around 12^o for high and 18^o for intermediate velocities. Below 1.4 km/s, the band is narrower again, to ensure guidance accuracy.

During bank reversals, the vertical part of the lift is larger than required by the drag controller. To avoid large deviation from the drag profile, the angle of attack is temporarily reduced, reducing the drag.

Note that in order to ensure lateral control authority, several bank reversals must be planned along the trajectory. The angle of attack profile is designed for the total cross range needed, which includes reserves for the cross range lost due to changing the direction of the turn.

4.3.1.8 Literature on the Shuttle Guidance

Since the inception of the guidance scheme, a large body of literature was published, analyzing and enhancing it.

Hechler [32] adapted the guidance to the needs of Hermes, the proposed European shuttle. The bank angle – the controller output – shows large

peaks, whenever a new segment of the profile is reached or when the profile is updated for ranging.

In [72], Strohmaier, et al. compare the trajectories obtained by a Shuttle guidance to an optimized one. Due to variations of the angle of attack, a lower heat load and higher cross range is achieved. The cross range requirements of a landing in Europe do not allow bank reversals.

Mease and Kremer analyze the controller part of the Shuttle guidance and propose modifications to extend the domain of applicability ([50]). Down and cross range, however, are not considered.

Ishizuka, Shimura, and Ishimoto describe a Shuttle guidance with “free form” subarcs instead of closed functions ([36]). Each subarc is defined by a few parameters. Range is estimated by numerical integration.

Lu et al. ([48]) define the drag profile by a piece wise linear function. The integrals for both cost function and range are solved analytically. The profile is computed a priori to achieve the necessary range at the lowest accumulated heat load. When deviations occur during the flight, the whole profile is scaled to reach the target.

The application of the Shuttle law on the reentry of a low lift capsule was investigated by Metzler in [53]. Also Frank ([25]) applies the guidance law to capsules, but he uses the derivative of the distance that can be covered, which is proportional the reciprocal value of the drag acceleration:

$$\frac{ds}{de} = s' = \frac{\cos\gamma}{d(e)} \approx \frac{1}{d}. \tag{4.42}$$

This simplifies the analytical integration considerably. One of the free conditions of the spline is used to achieve the appropriate ranging.

4.3.1.9 Conclusions

The Shuttle Guidance Law has proven its robustness and its precision in 100 controlled landings up to now. It is designed for on-line control of a real aircraft. The design principles involve robustness, simple measurement and little computational requirements on board.

While robustness is an issue, the other considerations are of less importance for an initial guess generator. Since all quantities are known without

uncertainties, also one that would be difficult to measure can be used as reference profile.

The biggest disadvantage of the shuttle guidance is its inability to estimate the cross range. Also the down range can only be estimated, with the assumption that the flight-path will not deviate too much from the original orbital plane. Matching the different segments for ranging purposes involves complicated – and error prone – formulas.

The lateral ranging is done by a dead band switch initiating bank reversals. This technique needs a large cross range reserve. For missions that require a high cross range capability, this scheme cannot be used. From the point of view of an initial guess generator, fast changes in the controls are also not desirable.

By its definition the drag profile is continuos, but it has sharp bends at the junctions of the different segments. Since the estimate of the altitude rate corresponds to the derivative of the commanded drag, this leads to sharp peaks in the control output.

4.3.2 Adaptation of the Shuttle Guidance for the IGG

4.3.2.1 Cross and Down Range Prediction

The shuttle guidance uses a fast analytical prediction for ground range. However this only works well for trajectories that stay close to the original orbital plane, since only the curved path is predicted and not the actual down range. For trajectories generating a significant cross range from the orbital plane, the prediction will be too far off the linear down range.

In addition, there is no way to predict and correct the cross range. For a trajectory like the one originally proposed for Hermes, generating sufficient cross range to reach Istres in the South of France form an orbit of an inclination of 28.5^{o} is a major task. There is not enough cross range reserve for guidance by multiple bank reversals.

Therefore, for the guidance a scheme is developed that uses a numerical integration, which is much slower, but can exactly predict cross and down range at the same time.

The shuttle achieves its ranging capability by selecting a single parameter of the drag profile at a time and linearizing the predicted range for this

parameter. Due to the numerical integration of the new guidance this is more difficult, but an optimizer can be used to achieve the required cross and down range, while satisfying the path constraint and minimizing a cost function at the same time!

4.3.2.2 Dynamic Pressure Control

The shuttle guidance uses drag deceleration as pseudo-control for the reasons explained above. But in the IGG, using drag poses some problems.

For the estimate of the bank angle the second derivative of the drag deceleration is needed. This involves the second derivative of the drag coefficient c_D. But since the drag coefficient depends on the angle of attack, which can be an optimizable control, no information is known about the first derivative of the coefficient, let alone the second.

Therefore instead of drag deceleration dynamic pressure is chosen. This eliminates the problem of the drag coefficient and makes many expressions simpler. All important path constraints can be expressed as easy in terms of dynamic pressure as in terms of drag deceleration, or even easier.

Since the range prediction is done by numerical integration, it is not hindered by this choice, either.

4.3.2.3 Cubic Spline

The shuttle uses a profile which is defined in segments. At the junction points the profile is continuous, but it may show discontinuous slopes.

Therefore, since the estimate of the altitude rate depends directly on the derivative of the dynamic pressure, a change in the slope of the profile will introduce a jump in the altitude rate. The altitude rate being part of the controller equation, it will also create a discontinuity in the bank angle. Since it is very desirable for an initial guess generator to produce smooth controls, these jumps should be avoided.

In addition, if at the beginning of a phase the commanded dynamic pressure and/or altitude rate differ from the starting conditions, the controller can show undesirable behavior, like overshooting and several oscillations of the bank angle. Therefore the profile should be continuous and – at least – once differentiable, even across the segment boundaries.

The different functions used for the shuttle drag profile all can be written as polynomials of velocity of degree two or less. However, when enforcing the continuity as defined above, a piece wise profile defined by quadratic polynomials is generally very oscillatory. Given a series of points and a starting slope, the equations defining the coefficients are already used up. There is no degree of freedom left to smooth the curvature.

Cubic splines however are known to minimize the bending energy of the curve. This type of spline is continuously differentiable twice. When comparing the number of parameters and the number of conditions, it is seen that there are two degrees of freedom left, for which arbitrary conditions can be imposed. A common set of conditions describes the “natural spline”: the curvature at both ends of the spline to set to zero.

Formulas exist for prescribing the slopes at both sides. Fortunately this possibilities can be mixed: the slope on one side is prescribed and the remaining degree of freedom is used, arbitrarily, to set the curvature at the other side to zero (for details see appendix B.2).

4.4 Reduced Order Equations

While the Shuttle Guidance type of initial guess generator produces accurate results that are within the convergence region of the optimal solution, it is not very well suited for an optimization itself. The presence of the controller inside the simulation introduces a fast time scale, which makes integration very time consuming. Therefore a modified approach is considered.

It has been observed, that the time scale of some subsets of the state vector are separated (see also Section 4.2.1.1). For numerical integration, treating only the slower subset will save a large part of the computation time.

The vertical dynamic (altitude and flight-path angle) can be considered faster than the horizontal motion (velocity, azimuth, longitude and latitude). Although the accelerating forces are of the same magnitude in horizontal and vertical direction, the distances covered are different by orders of magnitude: the altitude is constricted to be between 0 and 120 km, but the downrange is about 10,000 km. While the flight-path angle is in the range of a few degrees, the azimuth can cover a quarter of the circle easily.

The time separation can be achieved by neglecting the fast dynamics or by regarding it as a pseudo-control. For the method of singular perturbations,

usually both is done. While the flight-path angle as the fastest state is completely removed, the altitude becomes a control.

Singular perturbations are normally used in conjunction with indirect optimization methods. This results in controls, that can have a discontinuity at the time points when a path constraints becomes active, that does not directly depend on controls (the constraint is of an order higher than zero). However, using a state element as pseudo control, a discontinuity is not physically feasible: states don't jump.

By using parameter optimization, this problem can be avoided. The discretization of the control can be chosen to be continuous and even differentiable. As discussed, the dynamic pressure is well suited as a control, since it contains the vertical motion and since the major path constraints can be expressed in terms of velocity and dynamic pressure. Then the flight-path equations of motion (eqns. (3.11) – (3.16)) become:

$$\frac{d\lambda}{dt} = \frac{V\cos\gamma\sin\chi}{R\cos\delta}, \tag{4.43}$$

$$\frac{d\delta}{dt} = \frac{V\cos\gamma\cos\chi}{R}, \tag{4.44}$$

$$\begin{aligned}\frac{dV}{dt} = & -g\sin\gamma + g_\delta\cos\chi\cos\gamma + \\ & + \frac{T\cos\varepsilon\cos\nu - c_D Sq}{m} + \\ & + \omega_E^2 R\cos\delta(\cos\delta\sin\gamma - \sin\delta\cos\gamma\cos\chi)\end{aligned}, \tag{4.45}$$

$$\begin{aligned}\frac{d\chi}{dt} = & -\frac{g_\delta\sin\chi}{V\cos\gamma} + \frac{V\cos\gamma}{R\cos\delta}\sin\chi\sin\delta + \\ & + \frac{(c_L Sq + T\sin\varepsilon)\sin\mu_a + (T\cos\varepsilon\cos\nu - c_Y Sq)\cos\mu_a}{mV\cos\gamma} + \\ & + 2\omega_E(\sin\delta - \cos\chi\cos\delta\tan\gamma) + \frac{\omega_E^2 R\cos\delta}{V\cos\gamma}\sin\chi\sin\delta\end{aligned}, \tag{4.46}$$

Note that the radius and the flight-path angle are algebraic variables and are not governed by differential equations. While in ASTOS the radius is computed by inverting the atmospheric density model, it could be replaced by a constant value with only a small loss of accuracy. The flight-path angle can be estimated by (see Section B.3 on page 172):

$$\sin\gamma = \frac{h_S}{V^2 + 2gh_S}\left(2\frac{T - c_D Sq}{m} - \frac{\dot{q}V}{q}\right), \tag{4.47}$$

or, when the dynamic pressure is given as a function of the velocity:

$$\sin\gamma = \frac{h_S(2 - Vq'/q)}{V^2 + gh_S(2 - Vq'/q)}\frac{T - c_D Sq}{m}. \tag{4.48}$$

The air-path bank angle can be estimated as (see Section B.4 on page 174):

$$\begin{aligned}\frac{c_L Sq\cos\mu}{m} = {} & \left(g - \frac{V^2}{R}\right)\cos\gamma + \frac{h_S}{V^2\cos\gamma}\left[2\ddot{V} - 4\frac{\dot{V}^2}{V} - \frac{\ddot{q}V}{q} + \frac{V\dot{q}^2}{q^2} + \frac{\dot{q}\dot{V}}{q}\right] - \\ & -2\omega_E V\sin\chi\cos\delta - R\omega_E^2\cos\delta(\sin\delta\sin\gamma\cos\chi + \cos\delta\cos\gamma)\end{aligned}, \tag{4.49}$$

or, when the dynamic pressure is given as a function of the velocity:

$$\begin{aligned}\frac{c_L Sq\cos\mu}{m} = {} & \left(g - \frac{V^2}{R}\right)\cos\gamma + \frac{\dot{V}^2 h_S}{\cos\gamma}\left[-\frac{4}{V^2} - \frac{q''}{q} + \frac{Vq'^2 + q'q}{q^2V}\right] - \\ & -2\omega_E V\sin\chi\cos\delta - R\omega_E^2\cos\delta(\sin\delta\sin\gamma\cos\chi + \cos\delta\cos\gamma)\end{aligned}. \tag{4.50}$$

Note that for the reentry vehicles the thrust is zero. For air breathing launchers it is expected that the thrust varies with the dynamic pressure.

4.5 Dynamic Pressure Controller

In order to convert a dynamic pressure profile back to traditional controls the estimates of (B.34) and (B.39) are not sufficiently exact. Using this estimates, the vertical motion is unstable. Therefore a controller is needed to stabilize the trajectory integration.

Due to the limitations a controller inside an initial guess generator faces, a rather simple design must be used. Just like the shuttle guidance, a design with an auxiliary feedback of the altitude rate (for which a commanded rate can be easily computed) is chosen. Pole placement is used to compute the free parameters of the controller as function of the current state using gain scheduling.

The vertical lift acceleration can be split into two parts:

$$l_V = \frac{L}{m}\cos\mu = l_{V0} + l_{VC}. \tag{4.51}$$

The first is needed to offset the external forces and can be computed from Eq. (3.16) by setting $\dot{\gamma}$ to zero, assuming that the side force, the thrust and the meridional component of the gravity are negligible:

$$\begin{aligned} l_{V0} = &\left(g - \frac{V^2}{R}\right)\cos\gamma - \\ &- 2\omega_E V \sin\chi\cos\delta - R\omega_E^2\cos\delta(\sin\delta\sin\gamma\cos\chi + \cos\delta\cos\gamma), \end{aligned} \tag{4.52}$$

while the second part is supplied by the controller:

$$l_{VC} = K_q(q_0 - q) + K_{\dot{h}}(\dot{h}_0 - \dot{h}). \tag{4.53}$$

With this, the differential equation for the flight-path angle becomes:

$$\dot{\gamma} = \frac{l_{VC}}{V}. \tag{4.54}$$

For simplicity, a term for the curvature of the dynamic pressure profile (like in Eq. (B.34) or Eq. (B.39)) is neglected.

Fig. 4.5 shows the structure of the controller. For the time scale of the controller the commands and the velocity can be considered constant. For small flight-path angles, sinγ is replaced by γ. The right most block contains the linearization of the atmosphere and the conversion from density to dynamic pressure.

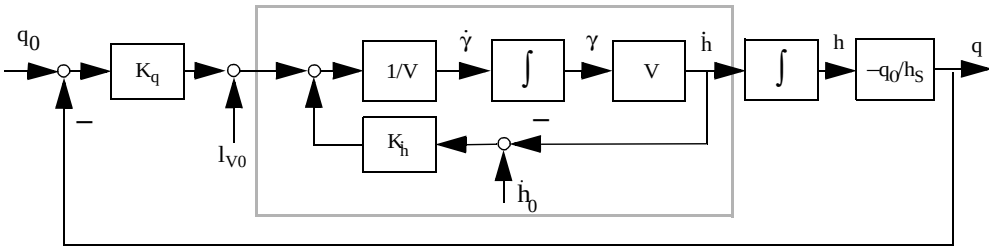

Fig. 4.5: Structure of the controller

The inner loop in Fig. 4.5 (surrounded by the grey box) can be replaced by its closed loop transfer function (see Fig. 4.6):

$$F_1 = \frac{1/s}{1 + K_{\dot{h}}/s} = \frac{1}{s + K_{\dot{h}}}. \tag{4.55}$$

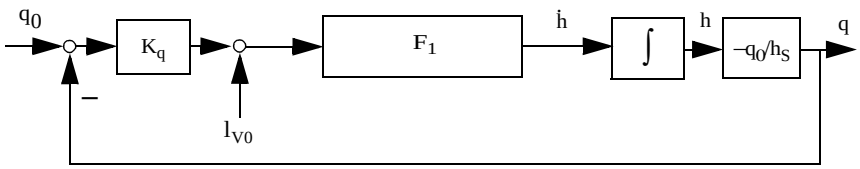

Fig. 4.6: Controller without inner loop

The transfer function of the forward part can be replaced by

$$F_2 = K_q F_1 \frac{1}{s}\left(-\frac{q_0}{h_S}\right) = -\frac{q_0 K_q}{h_S} \frac{1}{s^2 + K_{\dot{h}} s}. \tag{4.56}$$

With this the transfer function of the complete controller can be written as:

$$F = \frac{F_2}{1 + F_2} = \frac{-q_0 K_q / h_S}{s^2 + K_{\dot{h}} s - q_0 K_q / h_S}. \tag{4.57}$$

Comparing the coefficients with the standard form of a second order transfer function

$$F = \frac{K\omega_0{}^2}{s^2 + 2\zeta\omega_0 s + \omega_0^2} \tag{4.58}$$

yields the gains:

$$K_{\dot{h}} = \frac{1}{2\zeta\omega_0}, \; K_q = -\frac{\omega_0^2 h_S}{q_0}, \; K = 1. \tag{4.59}$$

The frequency ω_0 and the damping ζ can be chosen by the user, the gains $K_{\dot{h}}$ and K_q will be computed accordingly.

4.6 Dynamic Pressure Controller Based on Load Factor Controls

This controller is an alternate formulation to the one described in the previous section. It consists of two cascaded loops (see Fig. 4.7). In the outer loop, the current dynamic pressure q is compared to the commanded one, q_0. The difference is transformed into a required altitude rate using a user supplied time constant. In the inner loop, this altitude rate, and a component which depends on the slope of the dynamic pressure profile, is divided by a second time constant, in order to obtain the required vertical acceleration, which is then converted into the vertical lift.

In the following a locally exponential atmosphere is assumed:

$$\rho \approx \rho_0 e^{-h/h_S}. \tag{4.60}$$

A part of the required altitude rate can be attributed to the change in dynamic pressure:

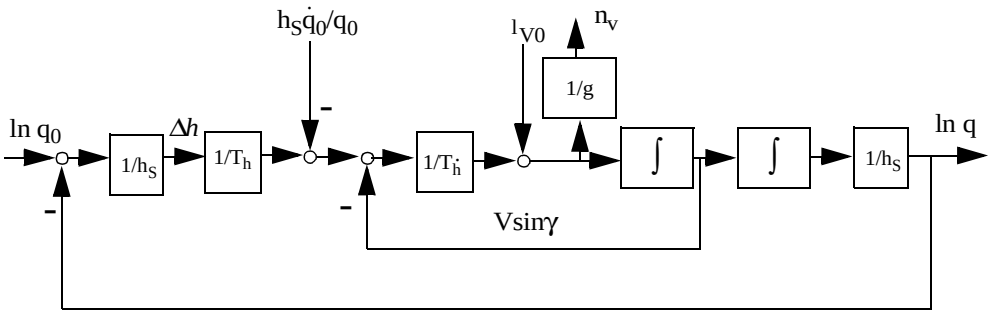

Fig. 4.7: Dynamic pressure controller based on load factors

$$\dot{q_0} = \frac{1}{2}V^2\dot{\rho} + \rho V\dot{V} = q_0\left(\frac{\dot{\rho}}{\rho} + 2\frac{\dot{V}}{V}\right) = q_0\left(2\frac{\dot{V}}{V} - \frac{\dot{h}}{h_S}\right), \tag{4.61}$$

or, since the velocity change is usually very small compared to the (supersonic) velocity:

$$\dot{h_{\dot{q}}} = -h_S\ \frac{\dot{q_0}}{q_0}. \tag{4.62}$$

Since for a given velocity, the dynamic pressure is proportional to the density, the difference of the current altitude h and h_0, the one corresponding to the commanded dynamic pressure is:

$$\Delta h = h_S\left(\ln\frac{\rho_0}{2q/V^2} - \ln\frac{\rho_0}{2q_0/V^2}\right) = h_S \ln\frac{q_0}{q}. \tag{4.63}$$

By choosing a suitable time constant T_h for the altitude, we can get a commanded altitude rate:

$$\dot{h_C} = \frac{\Delta h}{T_h} - h_S\ \frac{\dot{q_0}}{q_0}. \tag{4.64}$$

This value can be compared with the current altitude rate $V\sin\gamma$ and divided by a time constant to get the altitude acceleration needed:

$$\ddot{h}_C = \frac{\dot{h}_C - V\sin\gamma}{T_{\dot{h}}}. \tag{4.65}$$

When inserting this term into the differential equation of the flight-path angle (Eq. (3.16)), with the approximation

$$\ddot{h}_C = \dot{V}\sin\gamma + V\dot{\gamma}\cos\gamma \approx V\dot{\gamma} \tag{4.66}$$

one can determine the vertical load factor:

$$n_V g = \ddot{h}_C + \left(g - \frac{V^2}{R}\right)\cos\gamma - \\ -2\omega_E V\sin\chi\cos\delta - R\omega_E^2\cos\delta(\sin\delta\sin\gamma\cos\chi + \cos\delta\cos\gamma). \tag{4.67}$$

The time constants of the two loops are user definable and should differ by a factor of five, at least, in order to satisfy the time separation condition. An additional term for the curvature of the dynamic pressure profile can be added, but normally this is not necessary (see Section B.4 on page 174).

4.7 Summary of Guidance Laws

4.7.1 Conventional Launcher

A summary of the guidance laws available for conventional launchers is given in Table 4.1. Note that the required velocity concept is missing, since it cannot be used during optimizations. The values for the constant or the linear laws can be supplied by the user, otherwise they are taken from the attitude controls of the previous phase.

Table 4.1: Guidance laws for conventional launchers

Control Law	Parameter	Source	Optimizable	Attitude Control
Target orbit	i_t	user supplied	yes	Ψ
Tangential	–	–	–	
Constant yaw	Ψ_c	user / comp.	yes	
Linear yaw	Ψ_0 Ψ_f	user / comp. user / comp.	yes yes	
Optimal yaw	$\Psi(t)$	user supplied	yes	
Push over	t_{acc} t_{po} $\Delta\Theta$ t_c	user supplied user supplied user supplied user supplied	no no yes no	Θ
Gravity turn	–	–	–	
Bi-linear tangent law	Θ_0 ξ Θ_f	computed computed computed	yes yes yes	
Constant pitch	Θ_c	user / comp.	yes	
Linear pitch	Θ_0 Θ_f	user / comp. user / comp.	yes yes	
Optimal yaw	$\Theta(t)$	user supplied	yes	

4.7.2 Advanced Launcher

Specific control options for advanced launchers are supplied by the load factor attitude controls. The dynamic pressure profile can be specified either as a function of time or as a function of flight-path velocity (see Table 4.2).

Table 4.2: Guidance laws for advanced launchers

Control Law	**Parameter**	**Source**	**Optimizable**	**Attitude Control**
Constant turn rate	$\dot{\chi}$	user supplied	yes	n_h
Optimal horizontal load factor	$n_h(t)$	user supplied	yes	
Dynamic pressure velocity profile	V_0 $q(V_0)$ $q'(V_0)$ V_i $q_i(v_i)$	computed computed computed user supplied computed	yes yes yes no yes	n_v
Dynamic pressure time profile	t_0 $q(t_0)$ $q'(t_0)$ t_i $q_i(t_i)$	computed computed computed user supplied computed	yes yes yes no yes	
Optimal vertical load factor	$n_v(t)$	user supplied	yes	

4.7.3 Reentry Vehicles

Reentry vehicles are typically controlled by using the aerodynamic angle control options. Very often the angle of attack is not optimizable since it is given by aero-thermodynamic considerations. Therefore the options of specifying the angle of attack either as a function of the time or as a function of the Mach number exist (see Table 4.3). The dynamic pressure profile is only available as a function of the velocity.

Table 4.3: Guidance laws for reentry vehicles

Control Law	**Parameter**	**Source**	**Optimizable**	**Attitude Control**
angle of attack profile	t_i $\alpha_i(t_i)$	user supplied user supplied	no no	α
	t_i $\alpha_i(t_i)$	user supplied user supplied	no no	
Constant angle of attack	α_c	user / comp.	yes	
Linear angle of attack	α_0 α_f	user / comp. user / comp.	yes yes	
optimal angle of attack	$\alpha(M)$ or $\alpha(t)$	user supplied	yes	
Dynamic pressure profile	V_0 $q(V_0)$ $q'(V_0)$ V_i $q_i(v_i)$	computed computed computed user supplied computed	yes yes yes no yes	μ_a
Constant bank angle	μ_c	user / comp.	yes	
Linear bank angle	μ_0 μ_f	user / comp. user / comp.	yes yes	
optimal bank angle	$\mu_a(t)$	user supplied	yes	

5 Comparison of Optimal and Guidance Law Solutions

The guidance laws described in the previous chapter are tested with the initial guess generator. For all three types of vehicles a typical mission is discussed in detail, comparing the result obtained with the guidance laws to the optimal solution. For several other missions only a summary of the numerical results is given.

5.1 Conventional Launcher

5.1.1 Escape Mission

The mission is to deliver a payload into an escape orbit given by the declination of the asymptote and the excess speed (i.e. the speed the craft would have at “infinite” distance from the central body). This kind of orbit can be used f.i. for interplanetary missions. The aim of the optimization is to maximize the payload mass delivered.

Phase Structure

The start is affected with both the first stage main engine H150 and both solid propellant boosters P230 of the Ariane V launch vehicle thrusting. The boosters are jettisoned when empty. The phase structure is described in Table 5.1.

Table 5.1: Phase Structure of escape mission

	Duration (seconds)	**Active Propulsion**	**Aerodynamic**	**Boundary Constraints**	**Path Constraints**	**Remarks**
1	0 - 123	H150 + 2 P230	Ariane 5		$-10.5° \le \chi \le 91.5°$	P230s are jettisoned at end
2	123 - $t_{f,2}$	H150	Ariane 5	$\dot{Q} \le 1135$ W/m^2		fairing jettisoned at end
3	$t_{f,2}$ - 580.509	H150	Ariane 5		$\dot{Q} \le 1135$ W/m^2	H150 jettisoned at end
4	580.509 - 1370.117	L7	Ariane 5	$V_\infty =$ 2.5 km/s $\delta_{asymptote} = -12°$	$\dot{Q} \le 1135$ W/m^2	

During the second and the third phase only the first stage main engine is burning. The separation is marked by jettisoning of the payload fairing. This time is optimizable and depends on the heat flux condition. After the third phase, the first stage is separated. During the final phase the upper stage engine L7 is used.

Constraints

For range safety reasons an azimuth constraint is demanded for the first phase. However since the azimuth for vertical take-off is undefined it cannot be imposed for the first few seconds of flight time. Therefore it can only be imposed for the second phase. In this particular phase, however, the constraint is inactive anyway.

After the jettisoning of the payload fairing, the heat flux may not raise above a certain limit. Therefore the time when this limit is reached marks the end of the second phase.

It should be noted that due to a dip into the denser atmosphere the heat flux constraint will again be active in the last phase. Therefore the constraint must be activated and checked in both phases.

The parameters of the escape orbit supply the final boundary constraints for the last phase. The excess velocity describes the kinetic energy the craft would have at a very large distance to the earth and the declination of the asymptote the elevation angle above the equator at this point. Both must be understood as limits with the flight time approaching infinity.

5.1.1.1 Reference Solution

The optimal solution is computed using the optimization routine Tropic. The controls pitch and yaw are optimizable in all phases. The result is the best obtainable, as can be seen in Table 5.2.

Table 5.2: Comparison of execution times and results of escape mission

	nominal	**optimal**	**guidance law**	**bi-linear law, lower stage optimization**
Iteration		91	17	271
Execution time		201 s	54 s	320 s
Payload	6159 kg	6346 kg	5799 kg	6341 kg
Declination of asymptote	-12^o	-12.004^o	-12.09^o	-12.004^o
Escape velocity	2.5 km/s	2.499 km/s	2.42 km/s	2.499 km/s

5.1.1.2 Guidance Law

Guidance laws, as described in Section 4.1, are used to reduce the number of parameters to define the attitude controls. The parameters and their respective values are summed up in Table 5.3.

In the first phase a pitch-over maneuver of optimizable magnitude defines the state in which the vehicle enters the gravity turn, which is flown for the next two phases. In the final phase, the bi-linear tangent law is used.

Since for the escape orbit setting the inclination in the higher phases does not make sense, only in the first phase the target inclination option is

used for the yaw angle. This defines the plane in which the remainder of the trajectory is flown, setting the yaw tangential to the trajectory. In this way, the yaw history is described by a single optimizable parameter. The guidance laws are described in detail in Section 4.1 on page 74.

Table 5.3: Horizontal and vertical guidance laws and parameters of escape mission

Control Law	**Phase**	**Para-meter**	**Esti-mate**	**Lower Bound**	**Upper Bound**	**Opt. Value**
Target orbit	1	i_t	20^o	-180^o	180^o	22.854^o
Tangential	2,3,4	–				
Pitch push over	1	t_{acc}	5 s	–	–	–
		t_{po}	10 s	–	–	–
		$\Delta\Theta$	3.4^o	-18^o	18^o	3.4197^o
		t_c	5 s	–	–	–
Gravity turn	2,3	–				
Bi-linear tangent	4	Θ_0	2.028^{o*}	-90^o	90^o	-4.6222^o
		ξ	0^*	-1	1	0.2107
		Θ_f	-9.396^{o*}	-90^o	90^o	19.066^o

* computed

Comparing the trajectory to the optimal one reveals remarkable differences (see Figs. 5.1 and 5.2). The limitations of the attitude controls do greatly influence all state histories. The altitude rate is effected by the rigid gravity turn and therefore is much higher during the first part of the trajectory, and the dip into the denser atmosphere is later than for the optimal solution.

During rocket ascent, not all of the available thrust can be used for velocity increment. Therefore several formulas for estimates of the incurred losses due to external forces are given in literature. The losses are computed in the form of a velocity decrement. The drag loss is the integral of the drag force (which is by definition opposed to the flight-path velocity vector):

$$\Delta v_D = \int_{t_0}^{t_f} \frac{D}{m}\, dt, \tag{5.1}$$

while the gravity loss occurs when the velocity vector is not perpendicular to the gravity vector (note, that for negative flight-path angle there is a gain):

$$\Delta v_g = \int_{t_0}^{t_f} g \sin\gamma \; dt . \tag{5.2}$$

Another source of losses is due to misalignment of the thrust and the velocity vector during maneuvers. The following formula assumes that the thrust is aligned with the vehicle x-axis:

$$\Delta v_T = \int_{t_0}^{t_f} \frac{T}{m}(1 - \cos\alpha_t) \; dt . \tag{5.3}$$

When comparing these kinds of losses it can be seen that the guidance law solution incurs less drag than the optimal solution. Also the losses due to misalignment of the thrust vector are very small, since most of the trajectory is flown in the gravity turn mode (see Table 5.4).

Table 5.4: Sources of losses of escape mission

	optimal	**guidance law**	**bi-linear law, lower stage optimization**
Drag loss	157 m/s	102 m/s	158 m/s
Gravity loss	2251 m/s	2464 m/s	2245 m/s
Alignment loss	126 m/s	4 m/s	131 m/s
Total losses	2534 m/s	2570 m/s	2534 m/s

However, since the trajectory is much steeper in the beginning, higher gravity losses occur. Most of the fuel is burned at higher altitudes, this accounts for the reduction of 10% of the payload.

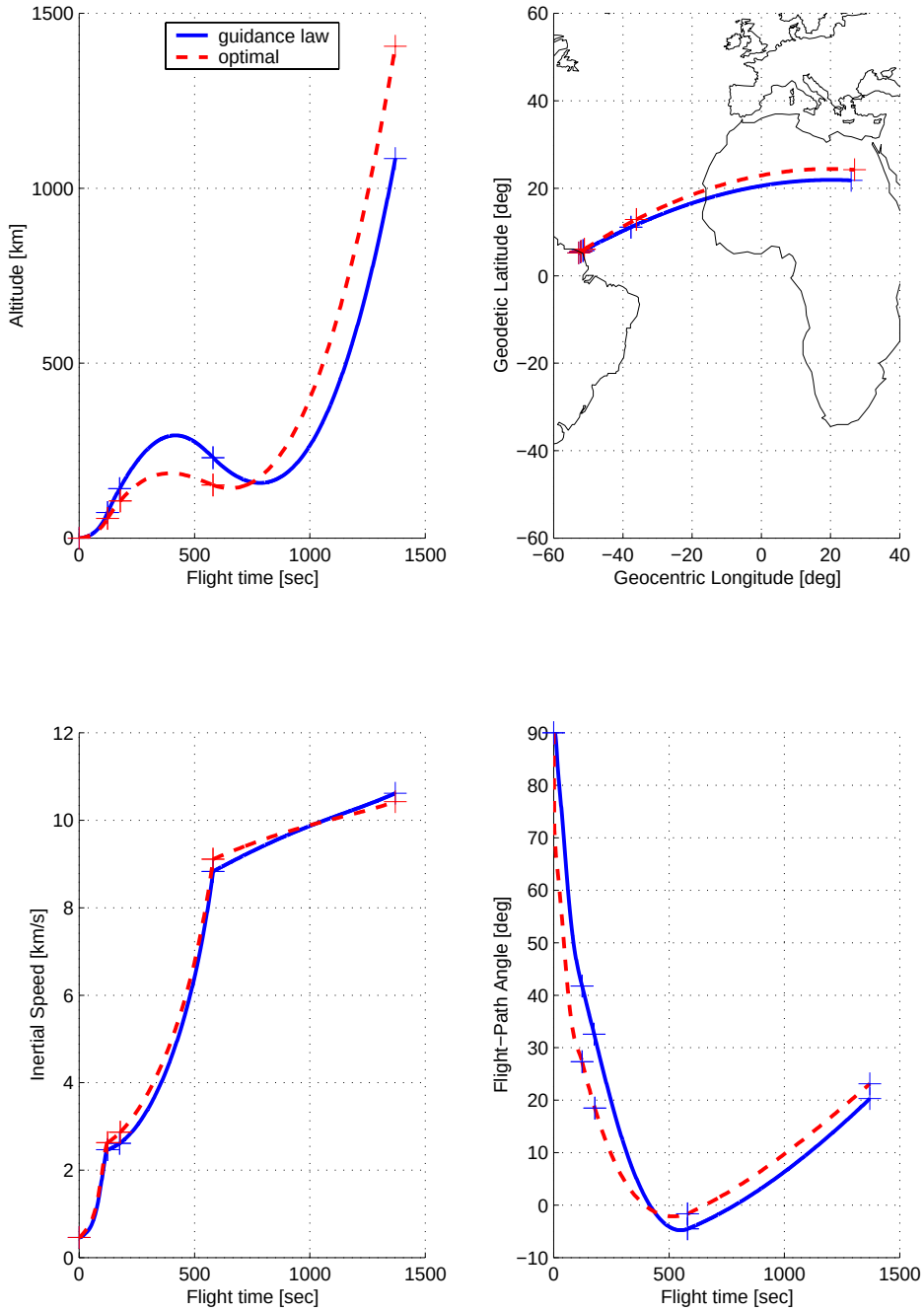

Fig. 5.1: Comparison of states for escape mission
The markers show the phase boundaries.

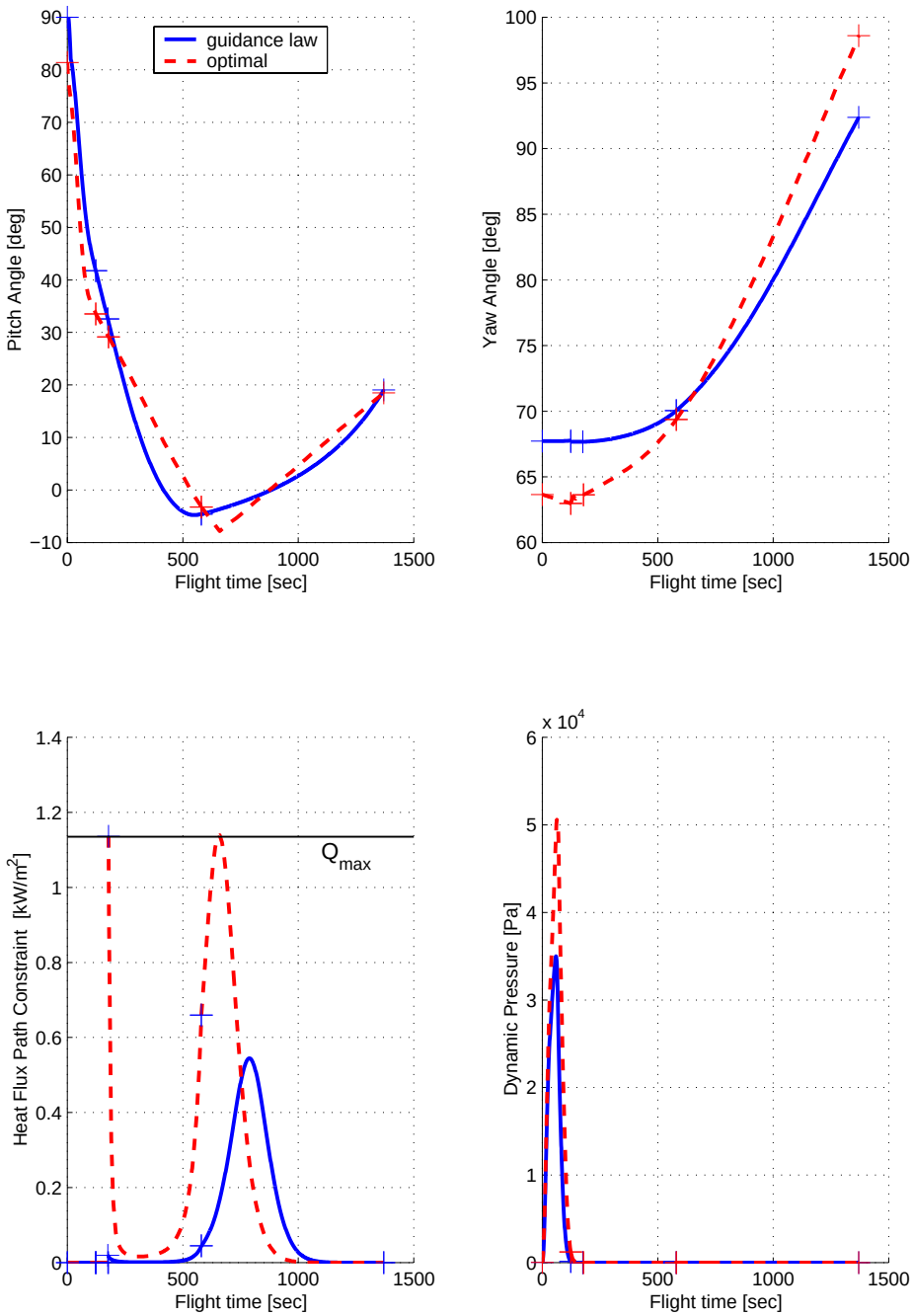

Fig. 5.2: Comparison of controls and constraints for escape mission

5.1.1.3 Optimal Lower Stage Control

In order to identify the reason for the loss in payload, an optimization with a mixed guidance scheme was performed. The phase sequence is described in Table 5.1. While the yaw was optimizable in all phases, the pitch was optimizable only in the lower stages, the upper stage being guided by the bi-linear tangent law (see Table 5.5).

Table 5.5: Guidance laws and parameters for partially optimal control

Control Law	**Phase**	**Parameter**	**Estimate**	**Lower Bound**	**Upper Bound**	**Opt. Value**
Optimal yaw	1,2,3,4	–		-180^o	180^o	
Optimal pitch	1,2,3	–		-90^o	90^o	
Bi-linear tangent	4	Θ_0	2.051^{o*}	-90^o	90^o	-8.111^o
		ξ	0^*	-1	1	0.0738
		Θ_f	-9.437^{o*}	-90^o	90^o	19.338^o

* computed

All variables of the resulting trajectory are practically identical to the optimum. In addition, the payload is almost the same, and the end conditions are satisfied to the same degree as for the optimal solution. Therefore it can be assumed that the bi-linear tangent law is very close to the optimal solution.

The lower stage guidance however is not very well modelled. This is also visible in the first graph of Fig. 5.2: in the first phase the optimal pitch is well below the guidance law solution. The pitch history of the optimization with upper stage guidance, however, is indistinguishable from the optimum (see Fig. 5.3). The losses of this solution are practically similar to the losses of the optimal solution (see Table 5.4).

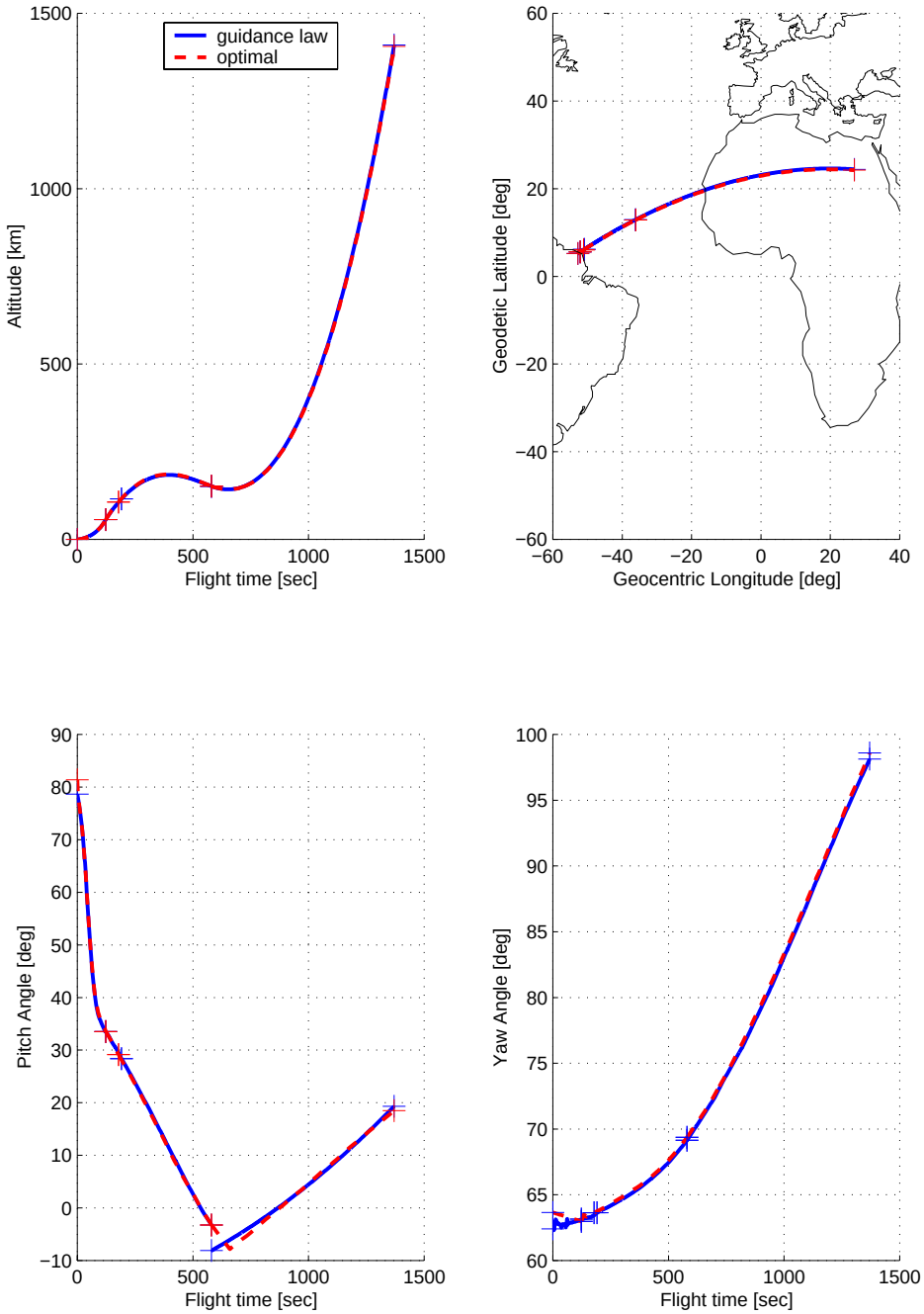

Fig. 5.3: Optimal solution vs. solution with upper stage guidance

5.1.2 Molnija Orbit

The mission is to deliver a payload with maximal mass into a Molnija orbit. This is a highly elliptic twelve hour orbit with an inclination that allows to cover the ground between the arctic circles. The perigee is chosen to be the southernmost point of the orbit. The phase structure is described in Table 5.6.

Table 5.6: Phase Structure of Molnija orbit mission

	Duration (seconds)	**Active Propulsion**	**Aerodynamic**	**Boundary Constraints**	**Path Constraints**	**Remarks**
1	0 – 123	H150 + 2 P230	Ariane 5		$-10.5° \le \chi \le 91.5°$	P230s are jettisoned at end
2	$123 - t_{f,2}$	H150	Ariane 5	$\dot{Q} \le 1135$ W/m^2		payload fairing jettisoned at end
3	$t_{f,2}$ – 580.509	H150	Ariane 5	$h_p \le$ 50 km, $\delta_{ip} \le 50^o$	$\dot{Q} \le 1135$ W/m^2	H150 jettisoned at end
4	580.509 – $t_{f,4}$	-	Ariane 5			coast arc
5	$t_{f,4} - t_{f,5}$; Δt_{fix} = 789.609	L7	Ariane 5	h_a = 40067 km, h_p = 300 km, i = 63.4°, ω = 270°		

By virtue of the special inclination, the argument of the perigee will not drift due to the oblateness of the earth. Therefore this orbit is well suited for communication satellites in the northern part of Europe, Asia and America.

In addition to the conditions of the ASTOS test case 2, a splash down constraint was introduced, preventing the H150 stage from falling on inhabited areas in Australia.

The results of different optimizations are shown in Table 5.7. The relatively large deviation of apogee and perigee altitude can be attributed to the special kind of trajectory. After a long coast arc, the launcher descends towards perigee altitude. Since a deviation of a few kilometers in altitude does have a sizable impact on the air density, even an extremely small error at the beginning of the coast arc can result in a large deviation of the final part of the trajectory.

Table 5.7: Comparison of execution times and results of Molnija orbit mission

	nominal	**optimal**	**guidance law**	**bi-linear law, lower stage optimization**
Iteration		80	42	50
Execution time		140 s	56 s	62 s
Payload	6315kg	6908 kg	5999 kg	6558 kg
Perigee altitude	300 km	298 km	193 km	299.8 km
Apogee altitude	40067 km	40073 km	41960 km	40045 km
Perigee argument	-90^o	-89.9^o	-89.2^o	-89.99^o
Inclination	63.4^o	63.4^o	63.6^o	63.4^o

The sequence of control laws for the “guidance law” case and the corresponding parameters are shown in Table 5.8. A comparison of the different kinds of losses incurred is given in Table 5.9. It can be seen, that the guidance law solution has much higher losses than the others. Therefore the payload is lower.

Table 5.8: Guidance laws and parameters of Molnija orbit mission

Control Law	Phase	Parameter	Estimate	Lower Bound	Upper Bound	Opt. Value
Target orbit	1	i_t	63.4^o	-180^o	180^o	76.667^o
Target orbit	2	i_t	63.4^o	-180^o	180^o	66.861^o
Target orbit	3	i_t	63.4^o	-180^o	180^o	65.448^o
Linear	4	Ψ_0 Ψ_f	27.909^{o*} 27.909^{o*}	-180^o -180^o	180^o 180^o	25.787^o 27.906^o
Target orbit	5	i_t	63.4^o	-180^o	180^o	60.799^o
Push over	1	t_{acc} t_{po} $\Delta\Theta$ t_c	5 s 10 s 2.6^o 3.5 s	– – -18^o –	– – 18^o –	– – 2.403^o –
Gravity turn	2,3	–				
Linear	4	Θ_0 Θ_f	3.415^{o*} 3.415^{o*}	-90^o -90^o	90^o 90^o	4.832^o 4.391^o
Bi-linear tangent	5	Θ_0 ζ Θ_f	0^{o*} 0^* 0^{o*}	-90^o -1 -90^o	90^o 1 90^o	9.782^o -0.0818 -8.766^o

* computed

Table 5.9: Sources of losses of Molnija mission

	optimal	guidance law	bi-linear law, lower stage optimization
Drag loss	103 m/s	94 m/s	109 m/s
Gravity loss	2158 m/s	2720 m/s	2402 m/s
Alignment loss	126 m/s	52 m/s	89 m/s
Total losses	2387 m/s	2866 m/s	2600 m/s

5.1.3 GTO

The mission is to deliver the payload to a transfer orbit with an apogee suitable for insertion into a geostationary orbit. The aim of the optimization is to maximize the payload mass delivered into the transfer orbit. Since the

Table 5.10: Phase Structure of GTO mission

	Duration (seconds)	**Active Propulsion**	**Aerodynamic**	**Boundary Constraints**	**Path Constraints**	**Remarks**
1*	0 – 11.6	L220 + 2 PAP + 2 PAL	Ariane 44LP		$\chi \leq 91.5°$	
2	11.6 – 44.959 (0–44.959)	L220 + 2 PAP + 2 PAL	Ariane 44LP		$\chi \leq 91.5°$	PAPs jettisoned at end
3	44.959 – 143.658	L220 + 2 PAL	Ariane 42L		$\chi \leq 91.5°$	PALs jettisoned at end
4	143.658 – 211.355	L220	Ariane 40		$q\alpha \leq$ 5.9°kPa †, $q \leq$ 1.88 kPa †	L220 jettisoned at end
5	211.355 – 299.925	L33	Ariane 40	$\dot{Q} \leq 1135$ W/m^2		fairing jettisoned at end
6	299.925 – 342.19	L33	Ariane 40		$\dot{Q} = 1135$ W/m^2	L33 jettisoned at end
7	342.19 – 1068.371	H10	Ariane 40	$h_a =$ 35786 km, $h_p =$ 185 km, $i = 7°$, $\omega = 180°$		

* only when optimizing with a control law; else the next phase starts at t=0

† final six seconds of the phase only

impulse for the final circularization is fixed and can be computed analytically using the assumptions of Hohmann, it is not considered part of the optimization problem. The phase structure is shown in Table 5.10 and the results in Table 5.11. Note that the solution with yaw guidance does not satisfy the inclination and the perigee argument constraints. Therefore it has a better payload than the solution with optimized yaw, using a guidance law for the pitch only.

Table 5.11: Comparison of execution times and results for GTO mission

	nominal	**optimal**	**guidance law**	**guidance law, yaw optimized**
Iteration		116	42	79
Execution time		196 s	61	145 s
Payload	5785 kg	5899 kg	5549 kg	5486 kg
Perigee altitude	185 km	187 km	185 km	168 km
Apogee altitude	35786 km	35914 km	35784 km	36739 km
Perigee argument	180^o	171^o	136^{o*}	180.3^o
Inclination	7^o	6.99^o	5.2^{o*}	6.99^o

* constraints not enforced

The control law sequence for the case with optimizable yaw and the corresponding parameters are shown in Table 5.12. Again, the guidance law solution shows the largest total loss, while the losses for the mixed solution are similar to the losses of the optimal solution.

Table 5.13: Sources of losses of GTO mission

	optimal	**guidance law**	**guidance law, yaw optimized**
Drag loss	144 m/s	78 m/s	140 m/s
Gravity loss	1453 m/s	1824 m/s	1472 m/s
Alignment loss	140 m/s	46 m/s	156 m/s
Total losses	1737 m/s	1948 m/s	1768 m/s

Table 5.12: Guidance laws for the GTO mission case with optimized yaw

Control Law	Phase	Para-meter	Esti-mate	Lower Bound	Upper Bound	Opt. Value
Optimal yaw	1 – 7	–		-180^o	180^o	
Vertical pitch	1	–				
Push over	2	t_{acc} t_{po} $\Delta\Theta$ t_c	0 s 19.2s 0.6^o 2.5 s	– – -18^o –	– – 18^o –	– – 0.5498^o –
Gravity turn	3,4,5,6	–				
Bi-linear tangent	7	Θ_0 ζ Θ_f	45.06^{o*} 0^* -29.25^{o*}	-90^o -1 -90^o	90^o 1 90^o	21.60^o -0.267 -7.592^o

* computed

5.1.4 Sun-Synchronous Orbit

The mission is to deliver a payload to a sun-synchronous circular orbit. For a certain range of orbit radii, the orbit can be inclined such that the drift of the ascending node due to the oblateness of the Earth is the same as the angular velocity of the Earth around the sun (see boundary constraints in Table 5.14). Like this, the orientation of the orbit towards the sun remains the same. This can be used f.i. for Earth observation satellites which can always view a part of the Earth under the same light conditions, e.g. at dawn and dusk.

The objective is to maximize the final mass, which includes the payload and the remaining fuel, which can be used to deliver a second payload or for house keeping operations.The guidance laws and parameters used can be seen in Table 5.15.

The optimization using guidance laws for all stages takes about one third of the normal optimization time, while delivering almost the same payload. Using the bi-linear tangent law in the upper stage only is even slightly faster, while offering the same performance as a full optimization (see Table 5.16). An estimate of the losses is given in Table 5.17.

Table 5.14: Phase Structure of the SSO mission

	Duration (seconds)	**Active Propul-sion**	**Aerody-namic**	**Boundary Con-straints**	**Path Con-straints**	**Remarks**
1	0 - 129.1	H155 + 2 P230	Ariane 5		$\chi \leq 91.5°$	P230s jettisoned at end
2	129.1 - $t_{f,2}$	H155	Ariane 5	$\dot{Q} \leq 1135$ W/m^2		fairing jettisoned at end
3	$t_{f,2}$ - 567.764	H155	Ariane 5		$\dot{Q} \leq 1135$ W/m^2	H155 jettisoned at end
4	567.764 - $t_{f,4}$	L9	Ariane 5	$h_a = h_p =$ 800 km i = 98.6°		

Table 5.15: Horizontal and vertical guidance laws and parameters of SSO mission

Control Law	**Phase**	**Para-meter**	**Esti-mate**	**Lower Bound**	**Upper Bound**	**Opt. Value**
Optimal yaw	1 – 4	–		-180^o	180^o	
Push over	1	t_{acc} t_{po} $\Delta\Theta$ t_c	6 s 10 s 1.3^o 2.5 s	– – -18^o –	– – 18^o –	– – 2.425^o –
Gravity turn	2	–				
Bi-linear tangent	3	Θ_0 ζ Θ_f	21.3^{o*} 0^* 21.3^{o*}	-90^o -1 -90^o	90^o 1 90^o	43.96^o -0.0642 21.34^o
Bi-linear tangent	4	Θ_0 ζ Θ_f	35.7^{o*} 0^* 35.7^{o*}	-90^o -1 -90^o	90^o 1 90^o	23.23^o -0.0688 -24.67^o

* computed

Table 5.16: Comparison of execution times and results for the SSO mission

	nominal	**optimal (Promis)**	**optimal (Tropic)**	**guidance law***	**bi-linear law, lower stage optimization**
Iteration		32	163	67	62
Execution time		379	249 s	87 s	79 s
Final mass	13800 kg	14013 kg	13930kg	13817 kg	13967 kg
Perigee altitude	800 km	799.99 km	799.98 km	799.85 km	799.98 km
Apogee altitude	800 km	800.00 km	800.6 km	800.1 km	800.5 km
Inclination	98.6^o	98.5999^o	98.5998^o	98.5999^o	98.5999^o

* see Table 5.15

Table 5.17: Sources of losses of SSO mission

	optimal (Tropic)	**guidance law**	**bi-linear law, lower stage optimization**
Drag loss	123 m/s	82 m/s	115 m/s
Gravity loss	2488 m/s	2636 m/s	2508 m/s
Alignment loss	393 m/s	434 m/s	373 m/s
Total losses	3004 m/s	3152 m/s	2996 m/s

5.2 Reentry Vehicle

5.2.1 X-38 Return to Captieux

The X-38 is an experimental hypersonic reentry vehicle currently in planning stage. It may evolve into a crew rescue vehicle (CRV) for the international space station. Just like the space shuttle, the X-38 will enter the atmosphere at very high speed. During the flight towards the landing site, several severe conditions exist that would easily destroy the vehicle, if not properly controlled (see Table 5.18, and also Section 3.3).

Table 5.18: Constraints of the X-38 return to Captieux

Initial Boundary Constraints	**Path Constraints**	**Final Boundary Constraints**
initial orbit: $i = 51.6^{o}$ $r = 6838$ km entry altitude: $h = 121.9$ km	$\dot{Q} \le 1175\text{kW/m}^2$ $n_{max} \le 2$ $q \le 14364\text{Pa}$ $\gamma \le 0$ $\alpha_{min}(M) \le \alpha \le \alpha_{max}(M)$	$24.1\text{km} \le h \le 25.1\text{km}$ $645\text{m/s} \le v \le 845\text{m/s}$ Landing site: $\delta_T = 44.4^{o}$ $\lambda_T = 0.4^{o}$

The phase structure is presented in Table 5.19. For this case, the angle of attack was optimizable in a corridor of $\pm 5^{\circ}$ around the nominal profile. With a fixed α profile, no convergence could be achieved. The results of all optimizations is shown in Table 5.20.

Table 5.19: Phase structure of optimal solution

Phase	**Duration (seconds)**	**Differential Equations**	**Control Laws**
1	0 – 1221	flight-path equations	AoA: optimal bank angle: optimal

The optimal solution obtained with Promis shows very rough control histories. Therefore a smoothing term which penalizes variations of the atti-

tude controls was introduced. This did reduce the optimization time considerably for this test case (however, this cannot be generalized). The slight improvement of the cost function and the slightly shorter flight time of 1187 seconds can be attributed to the fact that the “rough” solution is not converged to the same accuracy.

Table 5.20: Comparison of execution times and results for X38 mission to Captieux

	nominal	**optimal***	**optimal, smoothed**	**reduced ode**
Iteration		93	35	96
Execution time		28650 s	5003 s	1075 s
Optimizer		Promis SNOPT		Tropic
Integ. heatload		958 MJ/m^2	951 MJ/m^2	942 MJ/m^2
Final velocity	645–845 m/s	845 m/s	845 m/s	832 m/s
Final altitude	24.1–25.1 km	25.1 km	24.2 km	26.0 km
Target distance	< 30 km	30 km	14.9 km	48 km

* reduced optimization accuracy

5.2.1.1 Reduced Order Solution

Although the solution with reduced differential equations is not perfectly converged (the convergence criteria are missed by a small margin), it does compare very well to the optimal solution, see Figs. 5.4 to 5.6. After an initial pull-up maneuver, the trajectory follows two path constraints: first the heat flux constraint, than the normal load constraint. This is the expected behavior for a minimum heat load reentry, since by maximizing the drag, the flight time is minimized, and this lowers the heat flux integral.

While the optimal solution consists of a single phase only, for the reduced solution two phases are needed (see Table 5.21). During the first phase the bank angle is fixed at 0^o, in order to obtain the highest possible lift in the vertical direction for a pull-up maneuver. When almost level flight is achieved, the dynamic pressure control mode is initiated for phase two. The phase timing is optimizable. The guidance law is described in detail in Section 4.3 on page 89.

The dynamic pressure profile is defined by a cubic spline. The slope of the spline at the beginning of the phase is the same as the one at the end of the first phase in order to avoid a jump in the required altitude rate. The first point of the spline is therefore given in terms of initial flight-path velocity, dynamic pressure and its derivative with respect to the velocity. Since these three parameters must be adapted to the situation at the end of the first phase, all three are optimizable.

Table 5.21: Horizontal and vertical guidance laws of reduced order solution

Phase	**Duration (seconds)**	**Differential Equations**	**Control Laws**
1	0 – 322	flight-path equations	AoA: optimal bank angle: vertical
2	322 – 1187	reduced flight-path equations	AoA: optimal dynamic pressure

Table 5.22: Specification of dynamic pressure profile

Parameter	**at Velocity**	**Estimate***	**Lower Bound***	**Upper Bound***	**Optimal Value**
V_0	–	7503 m/s	3751 m/s	11254 m/s	7507 m/s
q	V_0	1529 Pa	0 Pa	4587 Pa	1719 Pa
dq/dV	V_0	-2.78 sPa/m	-8.93 sPa/m	8.93 sPa/m	-2.44 sPa/m
q_1	500 m/s	14364 Pa	7182 Pa	15800 Pa	9862 Pa
q_2	1000 m/s	14364 Pa	7182 Pa	15800 Pa	12929 Pa
q_3	2000 m/s	14364 Pa	7182 Pa	15800 Pa	13538 Pa
q_4	3000 m/s	14364 Pa	7182 Pa	15800 Pa	11696 Pa
q_5	4000 m/s	14364 Pa	7182 Pa	15800 Pa	11728 Pa
q_6	4500 m/s	14364 Pa	7182 Pa	15800 Pa	11660 Pa
q_7	4750 m/s	12303 Pa	6152 Pa	13534 Pa	11902 Pa
q_8	5000 m/s	9868 Pa	4934 Pa	10855 Pa	10001 Pa
q_9	5500 m/s	6550 Pa	3275 Pa	7205 Pa	6539 Pa
q_{10}	6000 m/s	4505 Pa	2253 Pa	4956 Pa	4506 Pa
q_{11}	7000 m/s	2322 Pa	1161 Pa	2554 Pa	2322 Pa
q_{12}	7200 m/s	2057 Pa	1029 Pa	2263 Pa	2055 Pa
q_{13}	7400 m/s	1828 Pa	914 Pa	2011 Pa	1849 Pa

* computed

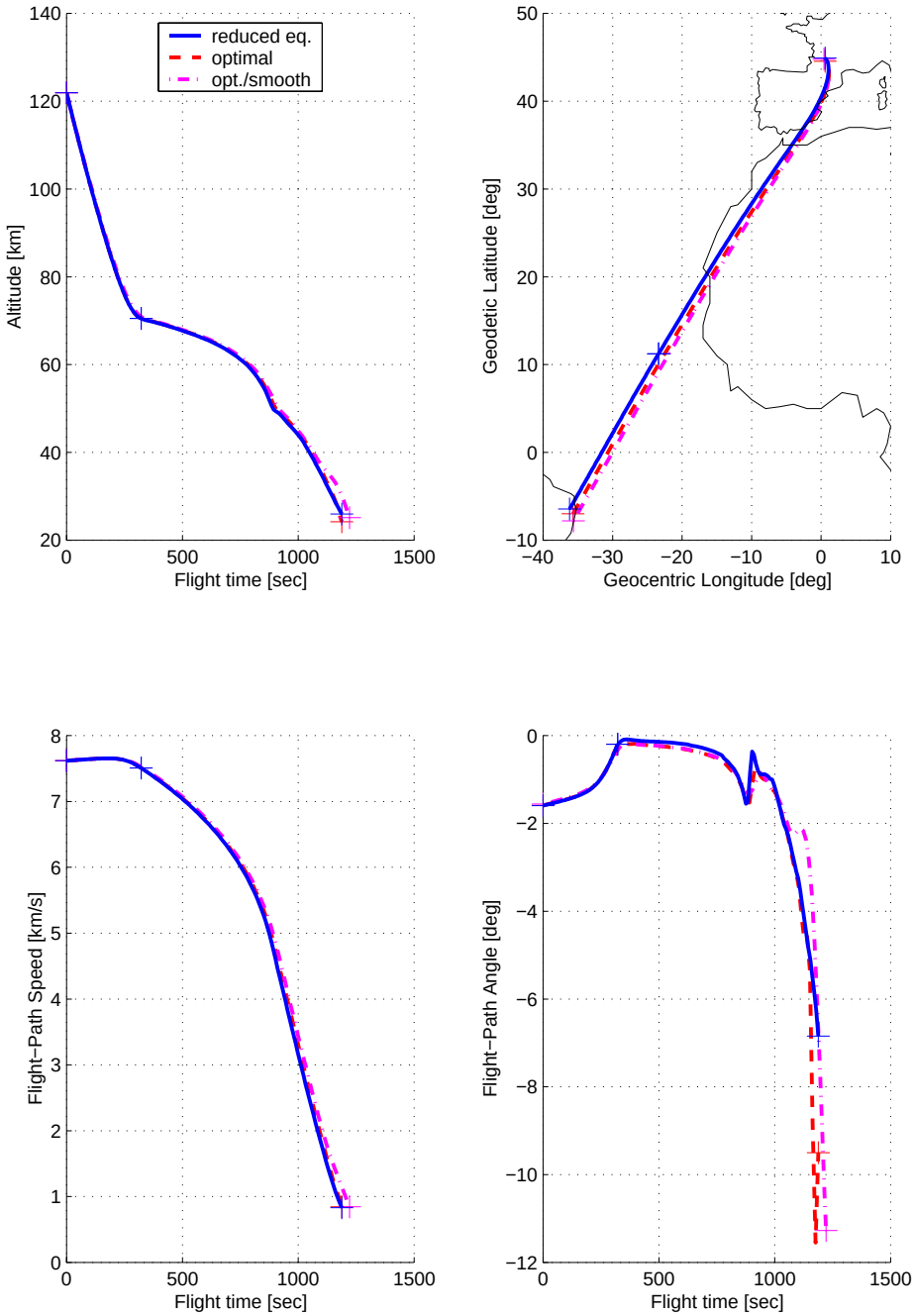

Fig. 5.4: Comparison of states for X-38 return to Captieux

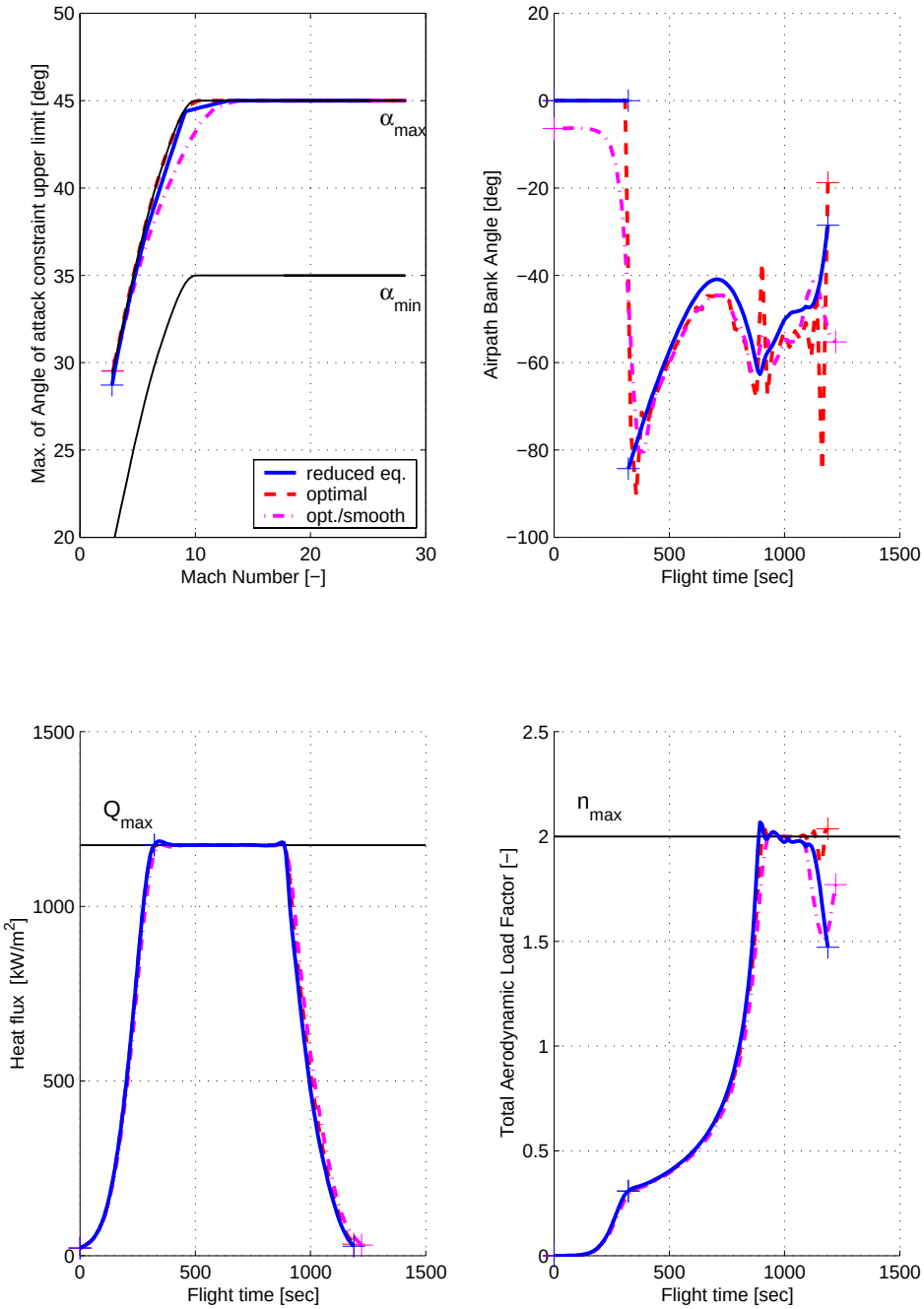

Fig. 5.5: Comparison of controls and constraints for X-38 return

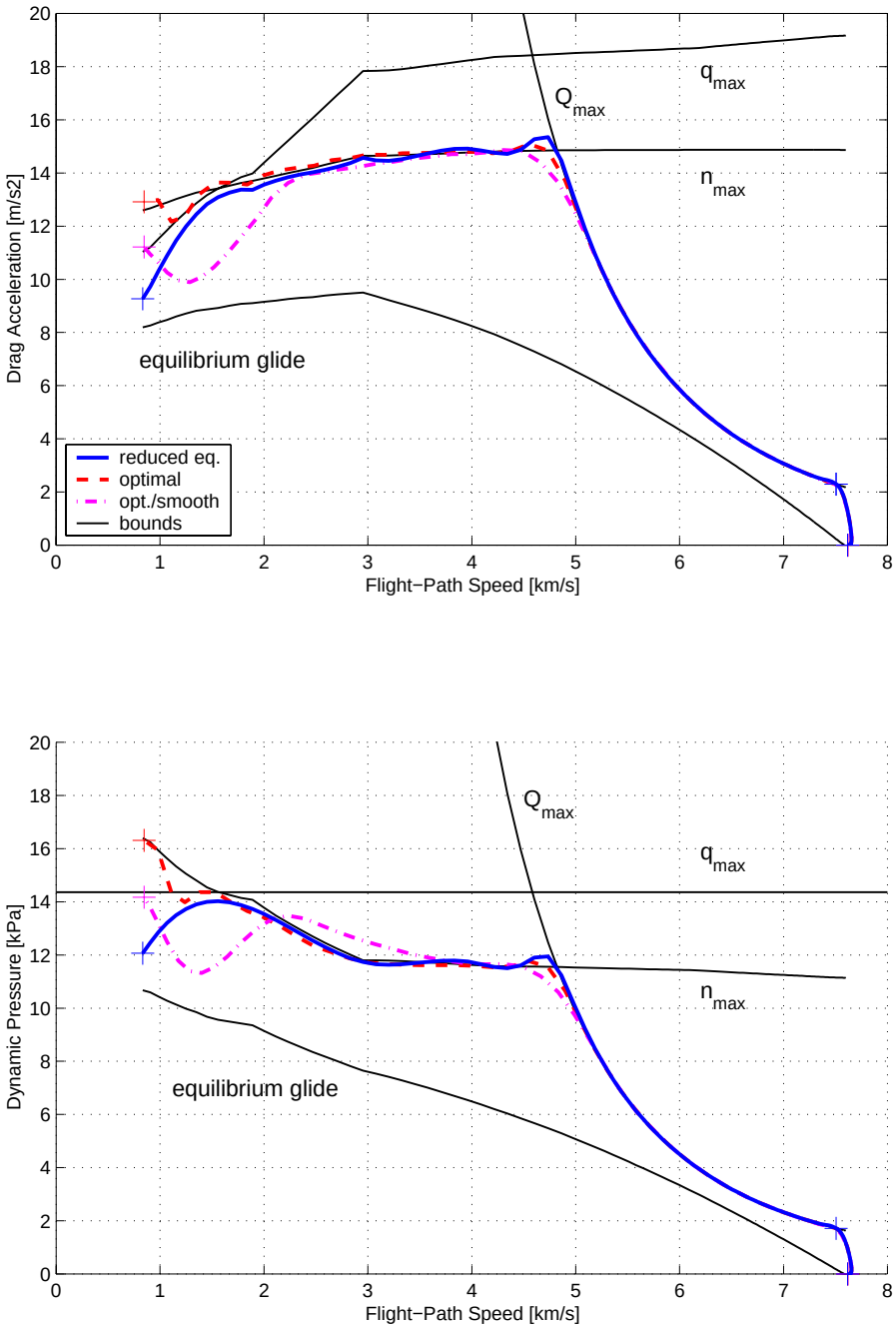

Fig. 5.6: Constraints in the drag and dynamic pressure diagram
Please note that the limits are computed for the reduced equation case, small deviations for the other cases are possible.

Note that only the velocity points must be given by the user. The grid can be rather sparse, but it should be more dense at the point, where the transition from the heat flux constraint to the dynamic pressure or normal load constraint takes place. The initial profile is estimated by using the maximum heat flux and the maximum dynamic pressure value supplied by the user. The upper and lower limits are obtained by multiplying this estimate by 0.5 or 1.1, respectively (see Table 5.22).

5.2.2 X-38 Return to Coober Pedy with Bank Reversals

Return to Coober Pedy (Australia) is the NASA benchmark mission. The applicable constraints are shown in Table 5.23. For guidance reasons, two distinct bank reversals (sign changes of the bank angle) are foreseen (a third one, as foreseen by NASA, is outside of the final time). Additional phases were introduced to model these control changes (see Table 5.24).

Table 5.23: Constraints of the X-38 return to Coober Pedy

Initial Boundary Constraints	**Path Constraints**	**Final Boundary Constraints**
initial orbit: $i = 51.6^o$ $r = 6838$ km entry altitude: $h = 121.9$ km	$\dot{Q} \le 1175\text{kW/m}^2$ $n_{max} \le 2$ $q \le 14364\text{Pa}$ $\gamma \le 0$ $\alpha_{min}(M) \le \alpha \le \alpha_{max}(M)$	$24.1\text{km} \le h \le 25.1\text{km}$ $645\text{m/s} \le v \le 845\text{m/s}$ Landing site: $\delta_T = -28.2402^o$ $\lambda_T = 134.9825^o$

Table 5.24: Phase structure of optimal solution

Phase	**Duration (seconds)**	**Differential Equations**	**Control Laws**
1	0 – 1015	flight-path equations	AoA: optimal bank angle: optimal, $\mu \ge 0$
2	1015 – 1150	flight-path equations	AoA: optimal bank angle: optimal, $\mu \le 0$
3	1150 – 1224.5	flight-path equations	AoA: optimal bank angle: optimal, $\mu \ge 0$

The additional phase boundaries, at fixed times, complicate the optimization process, especially, since the duration of the optimal flight is much smaller than the flight time of the nominal. The bank reversal times may have to be adjusted accordingly.

The optimal solution shows large oscillations of the bank angle, especially in the last phase. In addition, the optimization did not converge to the required precision. Therefore another optimization was done with a control smoothing term, using Promis in conjunction with the SLLSQP package (see Table 5.25).

Table 5.25: Comparison of execution times and results of X-38 return to Coober Pedy

	nominal	**optimal***	**optimal, smoothed**	**reduced ode**
Iteration		135	103	69
Execution time		25126 s	21727 s	928 s
Optimizer		Promis SNOPT	Promis SLLSQP	Tropic
Integ. heatload		976 MJ/m^2	964 MJ/m^2	996 MJ/m^2
Final velocity	645–845 m/s	845 m/s	845 m/s	713 m/s
Final altitude	24.1–25.1 km	25.1 km	25.1 km	-12.1 km
Target distance	< 30 km	30 km	30 km	13 km

* not converged; optimization ended with message “reached apparent stall”.

5.2.2.1 Reduced Order Solution

While the reference solution has fixed phase timing (except for the final time, which is optimizable), the reduced order solution needs variable timing (see Table 5.26). The dynamic pressure profile is based on velocity points and within each phase the sequence of these points, together with the initial velocity of the phase must be monotonically decreasing. Therefore a fixed phase would unduly restrict the optimization process.

The dynamic pressure profile is specified for each phase. Variables to connect the slope are introduced at each phase junction (see Table 5.27).

Table 5.26: Phase structure of reduced order solution

Phase	Duration (seconds)	Differential Equations	Control Laws
1	0 - 433	flight-path equations	AoA: optimal bank angle: vertical
2	433 - 944	reduced flight-path equations	AoA: optimal dynamic pressure profile, $\mu \geq 0$
3	944 - 1060	reduced flight-path equations	AoA: optimal dynamic pressure profile, $\mu \leq 0$
4	1150 - 1224.5	reduced flight-path equations	AoA: optimal dynamic pressure profile, $\mu \geq 0$

Table 5.27: Specification of dynamic pressure profile

P	Para-meter	at Velocity	Estimate*	Lower Bound*	Upper Bound*	Optimal Value
2	V_0	–	7526 m/s	3763 m/s	11289 m/s	7515 m/s
	q	V_0	1736 Pa	0 Pa	5359 Pa	1652Pa
	dq/dV	V_0	-1.11 sPa/m	-3.34 sPa/m	3.34 sPa/m	-2.00 sPa/m
	q_1	6000 m/s	4506 Pa	2253 Pa	4956 Pa	4511 Pa
	q_2	6500 m/s	3194 Pa	1597 Pa	3513 Pa	3149 Pa
	q_3	7000 m/s	2322 Pa	1161 Pa	2554 Pa	2322Pa
	q_4	7300 m/s	1939 Pa	969 Pa	2133 Pa	1938 Pa
3	V_0	–	5564 m/s	2782 m/s	8345 m/s	5650 m/s
	q	V_0	5748 Pa	0 Pa	17245 Pa	5558Pa
	dq/dV	V_0	-2.85 sPa/m	-8.54 sPa/m	8.54 sPa/m	-2.99 sPa/m
	q_1	5000 m/s	9868 Pa	4934 Pa	10855 Pa	9069 Pa
	q_2	5400 m/s	7088 Pa	3544 Pa	7797 Pa	7102 Pa
4	V_0	–	4218 m/s	2109 m/s	6326 m/s	4400 m/s
	q	V_0	14134 Pa	0 Pa	42403 Pa	11438 Pa
	dq/dV	V_0	-5.43 sPa/m	-16.3 sPa/m	16.3 sPa/m	-3.95 sPa/m
	q_1	1000 m/s	14364 Pa	7182 Pa	15800 Pa	14158 Pa
	q_2	2000 m/s	14364 Pa	7182 Pa	15800 Pa	12871Pa
	q_3	3000 m/s	14364 Pa	7182 Pa	15800 Pa	11169 Pa
	q_4	3800 m/s	14364 Pa	7182 Pa	15800 Pa	10947 Pa

* computed

5.2.3 Hermes Return to Kourou

Hermes was a project of the ESA. Launched on top of an Ariane 5, it was planned to be the European entry into manned space exploration. Due to international treaties on the usage of the future space station, the project was cancelled, however many results of the research are used in the X-38 and CRV project.

The major constraints can be seen in Table 5.28. For the optimal solution the flight-path velocity are used (see Section 3.1.2 on page 56). Due to thermodynamic reasons, the angle of attack follows a fixed profile as a function of the Mach number. Since speed brakes cannot be applied at high speeds, the bank angle is the only control left (see Table 5.29).

Table 5.28: Constraints of the Hermes return to Kourou

Initial Boundary Constraints	**Path Constraints**	**Final Boundary Constraints**
initial orbit: $i = 51.6^{o}$ $r = 6838$ km entry altitude: $h = 121.9$ km	$\dot{Q} \leq 440\,\mathrm{kW/m^2}$ $n_{max} \leq 2.5$ $q \leq 14400\,\mathrm{Pa}$ $\gamma \leq 0$	$30\,\mathrm{km} \leq h \leq 40\,\mathrm{km}$ $800\,\mathrm{m/s} \leq v \leq 1200\,\mathrm{m/s}$ Landing site: $\delta_T = 5.25^{o}$ $\lambda_T = -52.8^{o}$

Table 5.29: Phase structure of optimal solution

Phase	**Duration (seconds)**	**Differential Equations**	**Control Laws**
1	0 – 1196	flight-path equations	AoA: Mach profile bank angle: optimal

The results are shown in Table 5.30. Since the optimal solution shows some fluctuations of the bank angle, an second optimization with a control smoothing term is presented.

Table 5.30: Comparison of execution times and results of Hermes case

	nominal	**optimal**	**optimal, smoothed**	**reduced ode**
Iteration		32	44	13
Execution time		2848 s	4124 s	83 s
Optimizer		Promis SLLSQP		Tropic
Integ. heatload		360 MJ/m^2	353 MJ/m^2	347 MJ/m^2
Final velocity	0.8–1.2 km/s	1.2 km/s	1.2 km/s	1.19 km/s
Final altitude	30 – 40 km	32.61 km	32.57 km	32.5 km
Longitude	-52.8^o	-52.799^o	-52.9^o	-52.82^o
Latitude	5.25^o	5.2501^o	5.2499^o	5.205^o

5.2.3.1 Reduced Order Solution

The initial phase of the reentry is flown with a bank angle of zero. Using all available lift ensures that the initial flare is completed without violating the thermal constraint. When the dynamic pressure has reached a sufficient level, it is used as a control for the second phase. The final times of both phases are optimizable (see Table 5.31).

Table 5.31: Phase structure of optimal solution

Phase	**Duration (seconds)**	**Differential Equations**	**Control Laws**
1	0 – 243	flight-path equations	AoA: Mach profile bank angle: optimal
1	243 – 1092	reduced flight-path equations	AoA: optimal dynamic pressure profile, $\mu \leq 0$

In Table 5.32 the parameters describing the dynamic pressure profile are given. Note that during flight the velocity is steadily decreasing. Therefore the first data point encountered is $q(V_0)$, than q_{13} and so on. The point q_1 is actually outside the velocity range considered, therefore it has only a small influence.

Table 5.32: Specification of dynamic pressure profile

Parameter	at Velocity	Estimate*	Lower Bound*	Upper Bound*	Optimal Value
V_0	–	7573 m/s	3787 m/s	7573 m/s	7573 m/s
q	V_0	940 Pa	0 Pa	2819 Pa	980 Pa
dq/dV	V_0	-1.44 sPa/m	-4.30 sPa/m	4.30 sPa/m	-1.48 sPa/m
q_1	500 m/s	14400 Pa	7200 Pa	15840 Pa	7200 Pa
q_2	1000 m/s	14400 Pa	7200 Pa	15840 Pa	9705 Pa
q_3	2000 m/s	14400 Pa	7200 Pa	15840 Pa	9098 Pa
q_4	3000 m/s	14400 Pa	7200 Pa	15840 Pa	8008 Pa
q_5	4000 m/s	13940 Pa	6970 Pa	15333 Pa	7240 Pa
q_6	4500 m/s	8702 Pa	4351 Pa	9573 Pa	7291 Pa
q_7	4750 m/s	7010 Pa	3505 Pa	7711 Pa	6928 Pa
q_8	5000 m/s	5710 Pa	2855 Pa	6281 Pa	5771 Pa
q_9	5500 m/s	3900 Pa	1950 Pa	4290 Pa	3896 Pa
q_{10}	6000 m/s	2753 Pa	1377 Pa	3029 Pa	2754 Pa
q_{11}	7000 m/s	1486 Pa	743 Pa	1635 Pa	1486 Pa
q_{12}	7200 m/s	1328 Pa	664 Pa	1461 Pa	1330 Pa
q_{13}	7400 m/s	1190 Pa	595 Pa	1309 Pa	1185 Pa

* computed

5.3 Advanced Launcher

The concept of the Sänger vehicle is an advanced launcher. The lower stage is equipped with air-breathing engines, which offer a turbojet and a ram jet mode. The upper stage is powered by a rocket engine.

The base mission is, starting from a European site, to deliver the upper stage into a transfer orbit up to a low circular orbit. After release of the upper stage, the carrier returns to the launch site. However, the return is not modelled in the presented case. A fuel reserve for the return flight and for residual fuel that cannot be used is included in the structural mass. The optimization criterion was to minimize the fuel consumption of the lower stage.

In order to avoid the complex aerodynamics and thrust models for the transonic region, the optimization was started at a a velocity of 490 m/s and in an altitude of 12.6 km. An amount of 12,020 kg of fuel for the acceleration (estimated by preliminary simulations) is not included in the fuel consumed, as well as 8,500 kg for the return flight and 500 kg of residual fuel, which cannot be burned. (see Table 5.35).

The turbojet engine can be operated up to Mach 3.5, the ramjet starting form that Mach number. Therefore an equality constraint is set at the phase boundary when the engine type is switched. Both types of air-breathing engines can operate only in a region of dynamic pressure that is between 20 kPa and 50 kPa. A path constraint during the ramjet operation ensures that the Mach number remains below 7 (see Table 5.33).

While the turbojet engine can only be operated at full thrust level in supersonic flight, the ramjet can be operated with a varying degree of overfueling (using more hydrogen than needed for combustion). The throttle setting is always one for the turbojet, and in between zero (completely burned hydrogen) to one (maximum overfueling). However, the overfueling capability is hardly used, since the aim of the optimization is to minimize the fuel consumed by the lower stage.

The phase structure of the optimal solution is presented in Table 5.34. A trajectory smoothing term, which integrates the square of the derivative of the flight-path angle, was introduced. It is multiplied by an user supplied constant and added to the cost function. This term penalizes oscillations.

Table 5.33: Constraints of the Sänger ascent mission

Phase	Initial Boundary Constraints	Path Constraints	Final Boundary Constraints
1	$h = 12.6\text{km}$ $\lambda = 4.59^0$ $\delta = 42.59^0$ $v = 490\text{m/s}$ $\chi = 180^0$	$20\text{kPa} \le q \le 50\text{kPa}$ $0^0 \le \alpha \le 6^0$	$M = 3.5$
2		$20\text{kPa} \le q \le 50\text{kPa}$ $0^0 \le \alpha \le 6^0$ $M \le 7$	$M \le 7$
3		$a_x \le 34.5\text{m/s}$	$h_a = 70\text{km}$ $h_p = 450\text{km}$ $i = 28.5^0$

Table 5.34: Phase Structure of the Sänger ascent mission

	Duration (seconds)	Active Propulsion	Differential Equations	Control Laws
1	176 – 444	Turbojet	flight-path equations, trajectory smoothness	AoA: optimal bank angle: optimal
2	444 – 1346	Ramjet	flight-path equations, trajectory smoothness	AoA: optimal bank angle: optimal
3	1346 – 1640	Upper stage rocket engine	flight-path equations, trajectory smoothness	AoA: optimal bank angle: optimal

Table 5.35: Comparison of execution times and results for Sänger ascent mission

	nominal	**optimal**	**optimal**	**guidance law***
Iteration		149	142	26
Execution time		8116 s	1399 s	123 s
Optimizer		Promis/ SNOPT	Tropic	Tropic
Fuel consumption	143 600 kg	138 483 kg	140 928 kg	140 475 kg
Perigee altitude	70 km	70.0 km	70.0 km	70.0 km
Apogee altitude	450 km	446 km	450 km	447 km
Inclination	28.5^o	28.50^o	28.50^o	28.51^o

* reduced accuracy

5.3.1 Reduced Order Solution

The phase structure of the this solution is shown in Table 5.36. The end times of all phases are optimizable and differ slightly from those of the optimal solution. Even though during optimization the required constraint accuracy was relaxed, the solution satisfies the boundary conditions as well as the optimal one (see Table 5.35).

Table 5.36: Phase Structure of the reduced order solution

	Duration (seconds)	**Active Propulsion**	**Differential Equations**	**Control Laws**
1	176 – 435	Turbojet	reduced flight-path equations	n_h: optimal dynamic pressure q)
2	435 – 1329	Ramjet	reduced flight-path equations	n_h: optimal dynamic pressure $q(v)$
3	1329 – 1626	Upper stage rocket engine	flight-path equations	AoA: optimal bank angle: optimal

The parameter of the guidance laws used are depicted in Table 5.37. In the first phase a dynamic pressure profile as a function of the time is used. In

the second phase a profile as a function of the velocity, which is more flexible with respect to the variable phase times.

The reduced order solution is very close to the optimal one (see Figs. 5.7 and 5.8). Small deviations, f. i. at the end of the second phase can be attributed to the limited flexibility of the guidance law, when compared to the optimal solution. Note, that even the pull-up maneuver to achieve favorable conditions for delivering the upper stage can be modelled using the dynamic pressure profile.

Table 5.37: Specification of dynamic pressure profile

Parameter	**at Time / at Velocity**	**Estimate***	**Lower Bound***	**Upper Bound***	**Optimal Value**
t_0	–	*176 s*	*88 s*	*180 s*	180 s
q	t_0	*39.2 kPa*	20 kPa	50 kPa	39.4 kPa
dq/dt	t_0	*38.2 Pa/s*	*-115 Pa/s*	*115 Pa/s*	38.2 Pa/s
q_1	200 s	40 kPa			44.2 kPa
q_2	250 s	40 kPa			37.5 kPa
q_3	300 s	40 kPa	20 kPa	50 kPa	37.3 kPa
q_4	350 s	40 kPa			40.1 kPa
q_5	400 s	40 kPa			39.9 kPa
V_0	–	*1060 m/s*	*530 m/s*	*1060 m/s*	1029 m/s
q	V_0	*40 kPa*	20 kPa	50 kPa	40.0 kPa
dq/dV	V_0	*33.6 sPa/m*	*-101 sPa/m*	*101 sPa/m*	33.7 sPa/m
q_1	1200 m/s	40 kPa			40.9 kPa
q_2	1300 m/s	40 kPa			38.1 kPa
q_3	1400 m/s	40 kPa			35.9 kPa
q_4	1600 m/s	40 kPa			33.4 kPa
q_5	1800 m/s	40 kPa	20 kPa	50 kPa	29.8 kPa
q_6	2000 m/s	40 kPa			34.4 kPa
q_7	2050 m/s	40 kPa			39.6 kPa
q_8	2100 m/s	40 kPa			50.0 kPa
q_9	2150 m/s	40 kPa			28.9 kPa

* values in *italics* are computed automatically, all others are supplied by the user

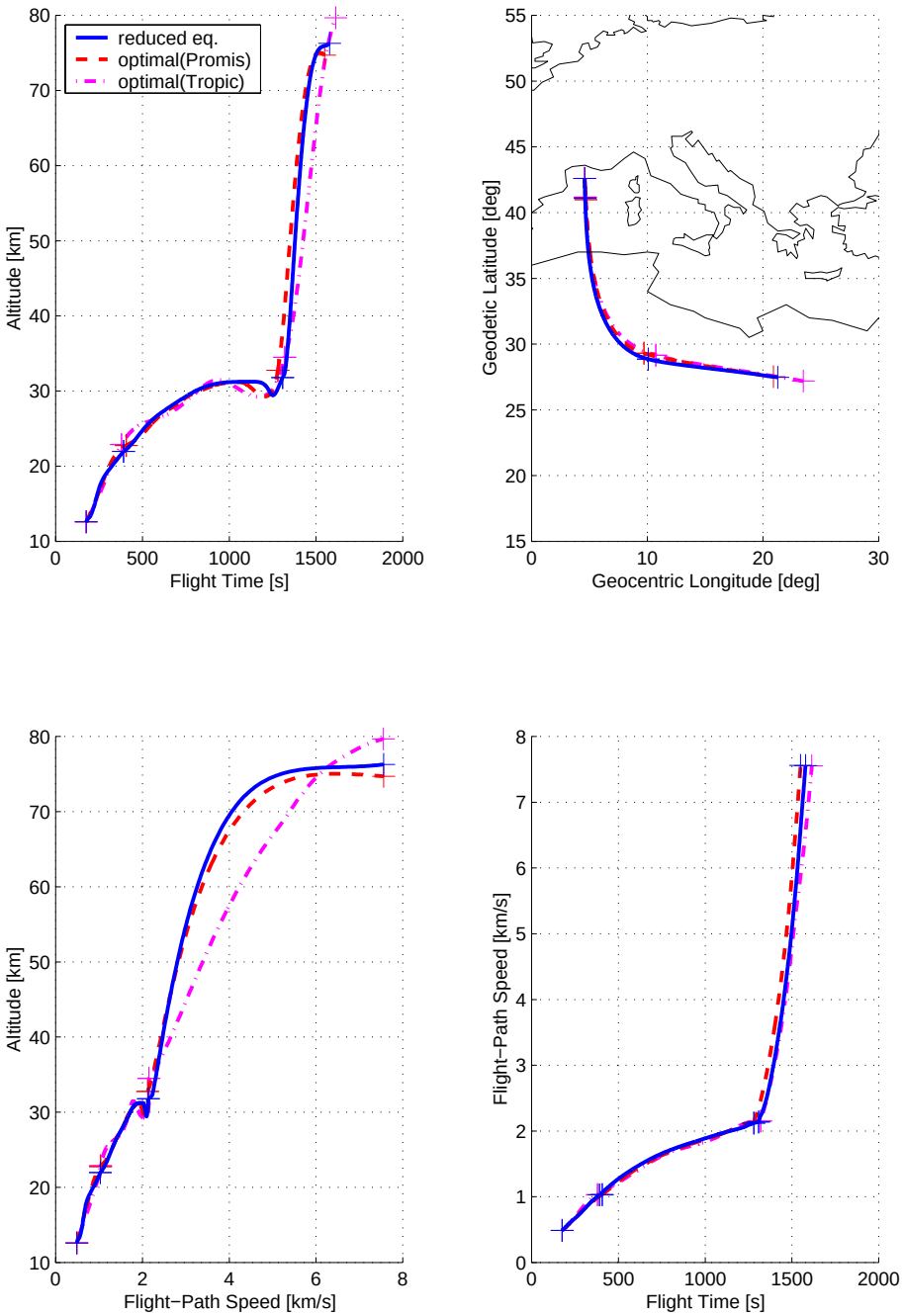

Fig. 5.7: Comparison of states for Sänger ascent

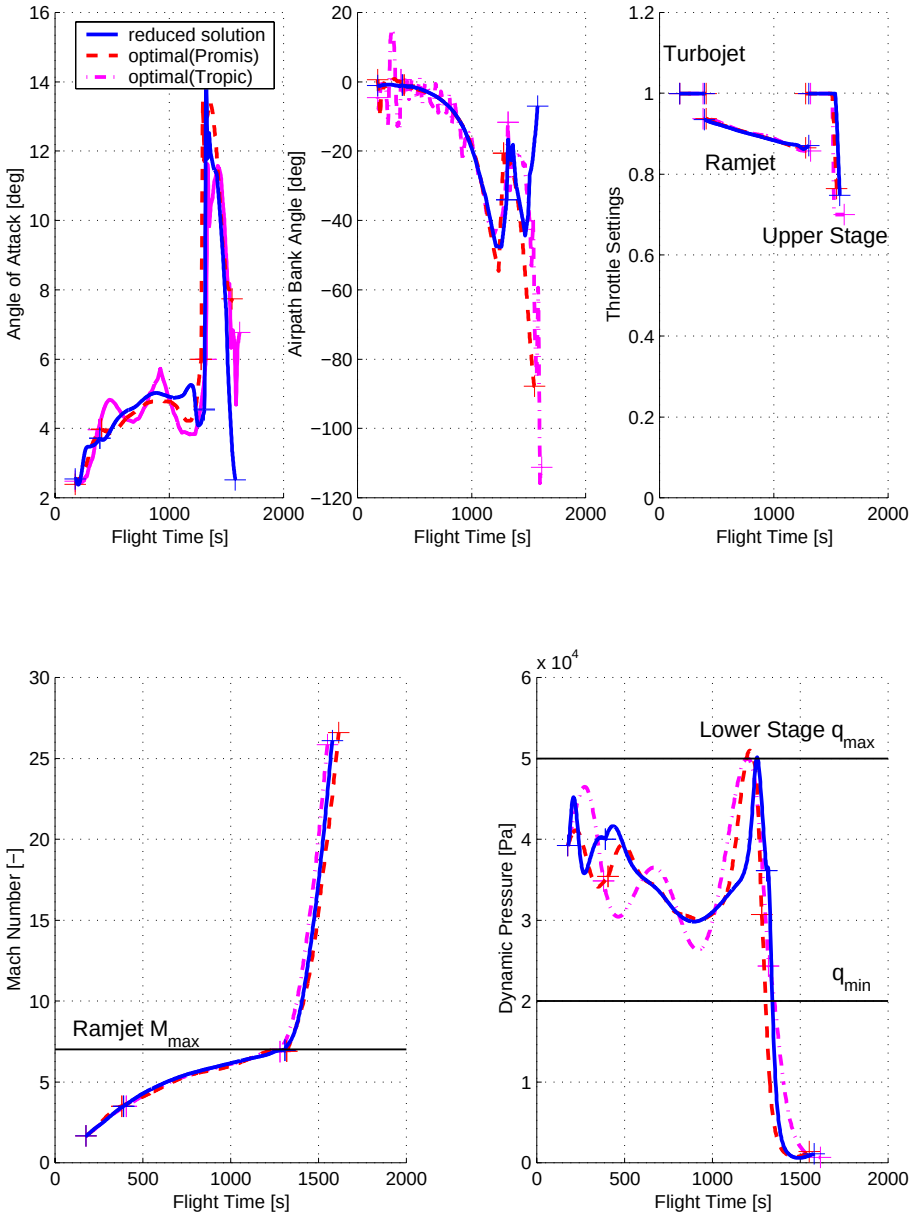

Fig. 5.8: Comparison of controls and constraints for Sänger ascent

6 Conclusion

Optimization is a valuable tool, especially for aerospace engineering. However, currently most programs need a kind of starting solution, an initial guess. One way to describe an initial guess is by specifying a guidance law: an algorithm which computes the value of a control depending on the state vector at each point.

This thesis presents guidance laws for three different kinds of aerospace vehicles: rocket launchers, air-breathing launchers and reentry vehicles. These guidance laws are characterized by a small number of free parameters, which are directly related to the trajectory problem and therefore can be easily estimated by the user.

Moreover, the guidance laws are constructed in a way that makes them suitable for optimization. The small number of parameters and the robust performance expedite the optimization process considerably.

In cases, when the optimum is relatively flat, direct optimization techniques often introduce crooked control histories: smoothness – beauty in the eyes of an engineer – is simply not part of the optimization criterion. The limited degree of freedom of the guidance laws does not allow the optimizer to introduce arbitrary movements in the control histories and therefore obviates the necessity for manual smoothing.

Conventional Launchers

Using the guidance law which describes the control time history with a small number of parameters can speed up the optimization time considerably (by a factor between two and four). However there is a penalty in the form of a smaller payload (on the average by 10% less).

The bi-linear tangent law in conjunction with an optimal lower stage guidance consistently shows an almost identical performance to an optimized control. It can be concluded that this guidance law is appropriate for the upper stage, however that the gravity turn and the yaw guidance options are often sub-optimal. More research should be devoted to find better control laws for the atmospheric phases of the trajectory.

Using the bi-linear tangent law as a pure (non-optimizing) initial guess generator, when compared to the required velocity guidance, has the advantage of giving a smooth control time history and also a better performance. This can be attributed to the fact that the bi-linear law is based on an optimum criterion, whereas the required velocity guidance is rather an engineering “rule of thumb” approach.

Reentry Vehicles

Using the reduced equations of motion for optimization does often result in tremendously reduced optimization times. This is mainly due to the fact, that the optimizer Tropic can be used, since the frequency content of the solution is reduced.

The accuracy of the solution obtained is very high, when compared to the optimal trajectory. As an additional benefit, control oscillations, which must be smoothed by using a penalty term, can hardly occur.

The guidance of reentry vehicles can be closely related to the dynamic pressure, since this quantity directly influences both the aerodynamic forces and the major constraints encountered along the trajectory. While altitude has been used widely as a pseudo-control in papers about singular perturbation theory, the dynamic pressure also includes the air density in the control, which simplifies the relation of the pseudo-control to the most important path constraints. The constraints formulae do contain the control directly, a fact which simplifies the optimization process.

Advanced Launchers

The dynamic pressure profile in conjunction with the reduced order differential equations proved to be effective also for advanced launchers. The result is very close to the optimal solution.

The optimization time is considerably less than the time needed for optimization with conventional controls. The size of the parameter vector is reduced, partly because of the smaller state vector, but also because of a smaller number of collocation points needed.

It should be noted, however, that the guidance law does not achieve the same accuracy during optimization. Since the controls are described by very few parameters only, it is more difficult to satisfy all path and boundary constraints. Still, when using collocation, the reduced order solution can be more precise in a simulation than the full order one. This is due to the fact, that the fast part of the state vector is not present and therefore larger intervals for the collocation are admissible.

As an additional benefit, the guidance law allows to model the dynamic pressure constraints as box constraints on the parameters which are treated much more efficiently by the optimizer. Since the second path constraint, the angle of attack range, is not active in the solution, this allows to set constraint evaluation points only at the end of the second phase, when the Mach number constraint becomes active. This reduction in evaluations speeds up each iteration of Tropic noticeable.

Future Work

Converting fast states into pseudo-controls using the singular perturbation approach can reduce the number of parameters used for the discretization of the optimization problem in two ways. The length of the state vector is reduced, without the penalty of additional control parameters since the pseudo-controls can replace some other controls, and second – in the case of a direct collocation method like Tropic – the number of discretization nodes can be reduced. When an adaptive integration scheme is used (f. i. as in Promis), getting rid of the fast manifold of the states vector will accelerate the integration, since the step size can be larger.

However, even fast states cannot vary instantaneously. Therefore the pseudo-control history must be continuous and smooth to a degree depending on the model reduction used. Since in the current version of GESOP con-

trols can only be piece wise constant or linear, the discussed implementation of the control laws uses an internal parameterization. This does not allow to use the advanced graphical features of the optimization environment.

For a future version of GESOP it would be a worthwhile improvement to implement a spline with a user definable degree as a control option. The spline must be differentiable all throughout a single phase and the derivatives must be available to the user for the right hand side equations and for the path constraints. Furthermore it should be possible to specify continuity conditions not only for the value of a control at the beginning of a phase, but also for its derivatives.

References

[1] *ALTOS Software User Manual*, SUM 4.2.1-1.0, Institute of Flight Mechanics and Control. University of Stuttgart, 2000.

[2] *ALTOS Conventional Launchers Application Manual*, CLA 4.2.1-1.0, Institute of Flight Mechanics and Control. University of Stuttgart, 2000.

[3] *ALTOS Advanced Launchers Application Manual*, ALTOS ALA 4.2.1-1.0, Institute of Flight Mechanics and Control. University of Stuttgart, 2000.

[4] *ALTOS Reentry Application Manual*, ALTOS RVA 4.2.1-1.0, Institute of Flight Mechanics and Control. University of Stuttgart, 2000.

[5] *ALTOS Model Library Reference Manual*, ALTOS MLR 4.2.1-1.0, Institute of Flight Mechanics and Control. University of Stuttgart, 2000.

[6] International Organization for Standardization. *Flight Dynamics – Concepts, Quantities and Symbols*, International Standard ISO 1151, 1988.

[7] American National Standards Institute. *Recommended Practice for Atmospheric and Space Flight Vehicle Coordinate Systems*, American National Standard ANSI/AIAA R-004-1992, Feb. 1992.

[8] J.P. Arrington, J.J. Jones. *Shuttle Performance: Lessons Learned*. NASA Langley Research Center, 1983.

[9] R.H. Battin. *Astronautical Guidance.* McGraw-Hill Electronic Science Series, New York 1964.

[10] M. Baunach. *Lenkgesetz für einen Initial Guess Generator am Beispiel eines Sänger Modells.* Intermediate thesis, IFR. University of Stuttgart, 1995.

[11] R. Bayer, G. Sachs. *Optimal return-to-base cruise of hypersonic carrier vehicles*. Zeitschrift für Flugwissenschaften und Weltraumforschung, Vol. 19, 1995.

[12] A.E. Bryson, Jr., and Y.-C. Ho. *Applied Optimal Control*, 2nd edition (revised). Hemisphere Publishing Corp., Washington D.C., 1975.

[13] W. Buhl, D. Paris. *Guidance and Control for Re-Entry Vehicles*. ESTEC internal paper. Noordwijk, 1991.

[14] W. Buhl, K. Ebert, H. Wolff. *ALTOS Technical Report 2: Modelization*. Messerschmitt-Bölkow-Blohm GmbH. Ottobrunn 1993.

[15] J. Burkhardt, U.M. Schöttle, E. Messerschmid. *Mission and System Design Aspects of a Semi-Ballistic Reentry Experiment Vehicle*. 48th International Astronautical Congress. Turin 1997.

[16] A.J. Calise and D.D. Moerder. *Singular pertubation for real-time aircraft trajectory optimization and control*. CR 3597, NASA, USA, 1982.

[17] W. Causey, V. Sohoni. *Reentry Guidance for Space Shuttle*. 5th IFAC Symposium on Automatic Control in Space. Genoa, 1973.

[18] J.-S. Chern, C.-Y. Yang, N.X. Vinh, J.M. Hanson. *Decelerationa and Heating Constrained Footprint of Shuttle Vehicles*. Acta Astronautica, Vol. 12, No. 10. Pergammon Press Ltd, 1985.

[19] J.-S. Chern, C.-Y. Yang, J.-J. Sheen. *Optimal Lift and Bank Modulation for Three-Dimensional Reentry Trajectories with Heat Constraint*. 37th Congress of the International Astronautical Federation. Innsbruck 1986.

[20] H.-C. Chou, M.D. Ardema, J.V. Bowles. *Near-Optimal Entry Trajectories for Reusable Launch Vehicles*. Journal of Guidance, Control, and Dynamics, Vol. 21, No. 6, November-December 1998.

[21] E.M. Cliff, K.H. Well. *Energy-Heading Transients in Atmospheric Flight Guidance for Airbreathing Hypersonic Vehicles*. AIAA 3rd International Aerospace Planes Conference. Orlando, 1991.

[22] J.E. Corban, A.J. Calise, G.A. Flandro. *Optimal Guidance and Propulsion Control for Transatmospheric Vehicles*. AIAA Guidance, Navigation, and Control Conference. Boston 1989.

[23] J.E. Corban, A.J. Calise, G.A. Flandro. *Rapid Near-Optimal Aerospace Plane Trajectory Generation and Guidance*. Journal of Guidance, Vol. 14, No. 6, December 1991.

[24] J.A. Fay and F.R. Riddel. *Theory of stagnation point heat transfer in dissociated air.* Journal of the Aeronautical Sciences, 25(2): 73–85, 121, February 1958.

[25] W. Frank. *Ein Reichweiten-Energie-Verfahren zur Lenkung von Wiedereintrittskapseln*. Intermediate thesis, IFR. University of Stuttgart, 1996.

[26] D.P. Fuhry. *Adaptive Atmospheric Reentry Guidance for the Kistler K-1 Orbital Vehicle*. AIAA Guidance, Navigation, and, Control Conference. Portland, 1999.

[27] P. Gath. *Improvements to a Hybrib Algorithm for Rapid Generation of 3-D Optimal Launch Vehicle Ascent Trajectories.* Master's Thesis, IFR. University of Stuttgart, 1998.

[28] W. Grimm, M. Hans. *Time-Optimal Turn to a Heading: An Improved Analytic Solution*. Journal of Guidance, Control, and Dynamics, Vol. 21, No. 6. November-December 1998.

[29] W.L. Hankey. *Re-Entry Aerodynamics*. AIAA education series. Washington D.C., 1988.

[30] J.C. Harpold, and C.A. Graves. *Shuttle Entry Guidance*. In 25th Anniversary Conference, pages 99–132. American Astronomical Society, 1978.

[31] Ph. Hattis, R. Bailey. *Overview of the Kistler K1 Guidance and Control System*. AIAA Guidance, Navigation, and, Control Conference. Portland, 1999.

[32] M. Hechler. *On Atmospheric Re-entry Trajectory Control Calculations*. MAS Working Paper No. 277. ESOC Darmstadt 1988.

[33] J.A. Hermann, D.K. Schmidt. *Fuel-Optimal SSTO Mission Analysis of a Generic Hypersonic Vehicle*. AIAA Guidance, Navigation, and Control Conference. Baltimore, 1995.

[34] S.J. Isakowitz, J. Samella. *International Reference Guide to Space Launch Systems*, 2nd ed. AIAA Space Transportation Technical Committee. Washington, 1991.

[35] Y. Ishijima, S. Matsumoto, K. Hayashi. *Re-Entry and terminal Guidance for Vertical-Landing TSTO (Two-Stage to Orbit)*. AIAA Guidance, Navigation, and Control Conference. Boston, 1998

[36] K. Ishizuka, K. Shimura, S. Ishimoto. *A Re-Entry Guidance Law Employing simple Real-Time Integration*. AIAA Guidance, Navigation, and Control Conference. Boston, 1998.

[37] C. Jänsch. Personal communication.

[38] C. Jänsch, A. Markl. *Trajectory Optimization and Guidance for a Hermes-Type Reentry Vehicle*. AIAA Guidance, Naviagtion, and Control Conference. New Orleans, 1991.

[39] C. Jänsch, K. Schnepper, K.H. Well. *Trajectory Optimization of a Transatmospheric Vehicle*. ACC, Boston, 1991.

[40] B.K. Joosten. *Descent Guidance and Mission Planning for Space Shuttle.* Houston, 1982.

[41] F. Jouhaud. *Closed Loop Reentry Guidance Law of a Space Plane. Application to Hermes*. 42nd IAF Congress. Montreal 1991.

[42] F. Kaiser. *Der Steigflug mit Strahlflugzeugen; Teilbericht 1: Bahngeschwindigkeit für bestes Steigen*. Versuchsbericht 262-02-144, Messerschmidt AG. Augsburg 1944. Translated to English as R.T.B./T.I.B., No. G.D.C./15/148T, Ministry of Supply (U.K.).

[43] G. Koppenwallner. *Aerothermodynamic — Ein Schlüssel zu neuen Transportgeräten der Luft- und Raumfahrt*. *Zeitschrift für Flugwissenschaft und Weltraumforschung*, 12(1):6-18, January 1988.

[44] J.P. Kremer, K.D. Mease. *Aerospace Plane Ascent Guidance Considering Aeropropulsive Interactions.* AIAA Guidance, Navigation, and Control Conference. Baltimore, 1995.

[45] B. Kugelmann. *Fast Computation of Feedback Controls for a Re-Entering Orbiter.* 8th IFAC Workshop. Paris, 1989.

[46] Ph. Landiech, C. Aumasson, J. Droz. *Airbreathing Launcher Trajectory Optimization*. 40th IAF Congress. Malaga, 1989.

[47] T.A. Lovell, D.K. Schmidt. *Mission Performance of Highly-Integrated Hypersonic Aircraft via Energy-State Analysis*. AIAA Guidance, Navigation, and, Control Conference. Portland, 1999.

[48] P. Lu, J.M. Hanson, G.A. Dukeman, S. Bhargava. *An Alternative Entry Guidance Scheme for the X-33*. AIAA Atmospheric Flight Mechanics Conference. Boston, 1998.

[49] F.J. Marcus, B.A. Kriegsman. *An Entry Guidance System for the Shuttle Vehicle*. MIT Charles Stark Draper Laboratory. Cambridge, Mass., 1972.

[50] K.D. Mease, J.P. Kremer. *Shuttle Entry Guidance Revisited*. AIAA Guidance, Navigation, and Control Conference. Hilton Head Island, 1992.

[51] K.D. Mease, P. Teufel, H. Schöneneberger, D.T. Chen, S. Bharadwaj. *Re-Entry Trajectory Planning for a Reusable Launch Vehicle*. AIAA Atmospheric Flight Mechanics Conference. Portland, 1999.

[52] E. Messerschmid. *Grundlagen der Raumfahrtsysteme*. Institute of Space Systems. University of Stuttgart.

[53] T. Metzler. *Entwicklung und Untersuchung analytischer Lenkungskonzepte für Wiedereintrittsfahrzeuge mit geringem Auftrieb.* Master's Thesis, IFR, Universität Stuttgart, Stuttgart 1995.

[54] N.N. *Pegasus User's Guide*. Orbital Science Corp. 1998 (on-line version available at [87]).

[55] B.N. Pamadi. *An Adaptive Guidance Law for Single Stage to Low Earth Orbit*. AIAA Guidance, Navigation, and Control Conference. Boston, 1989.

[56] M. Paus, K.H. Well. *Optimal Ascent Guidance for a Hypersonic Vehicle*. AIAA Guidance, Navigation, and Control Conference. San Diego 1996.

[57] H.J. Pesch. *Optimal Re-Entry Guidance for Space Vehicles under Control and State Variable Inequality Constraints*. 8th IFAC Workshop. Paris, 1989.

[58] G. Pignie, P. Delpy, J.C. Carmona. *GNC for Advanced Launch Vehicles*. Final Report ESA Contract 9734/91/NL/JG.

[59] A Pohl. *Lenkgesetz für konventionelle Träger mittels Required-Velocity-Konzepts*. Master's thesis, IFR. University of Stuttgart, 1996.

[60] P. Riatti. *Optimal Control and Near-Optimal Guidance for the Ascent of ARIANE 5*. Master's Thesis, IFR. University of Stuttgart, 1997.

[61] C.J. Riley, F.R. DeJearnette. *Engineering Aerodynamic Heating Method for Hypersonic Flow.* Journal of Spacecraft and Rockets, Vol. 29, No. 3, May-June 1992.

[62] A.J. Roenneke, A. Markl. *Reentry Control to a Drag vs. Energy Profile*. AIAA Guidance, Navigation, and Control Conference. Monterey 1993.

[63] G. Sachs, M. Dinkelmann. *Trajectory Optimization for Reducing Coolant Fuel Losses of Aerospace Planes.* AIAA Guidance Navigationa and Control Conference. Baltimore, 1995.

[64] K. Schnepper. *Mehrzielige Aufstiegsbahnoptimierung eines zweistufigen Raumtransportsystems mit luftatmenden Triebwerken*. Ph.D. thesis. IFR, University of Stuttgart, 1999.

[65] U.M. Schöttle, J. Burkhardt, F. Zimmermann. *Optimal Flight of a Reentry Capsule with Consideration of Mission Constraints*. AIAA Guidance, Navigation, and Control Conference. New Orleans, 1997

[66] R.L. Schultz, M.J. Hoffman, A.M. Case, S.I. Sheikh. *Navigation, Guidance, and Trajectory Optimization for Hypersonic Vehicles*. Preprint, Honeywell Systems and Research Center. Minneapolis, ca. 1987.

[67] H. Seywald, E.M. Cliff, K.H. Well. *Range Optimization for a Supersonic Aircraft*. AIAA Guidance, Navigation, and Control Conference. New Orleans, 1991

[68] J. Shinar, K.H. Well, B. Järmark. *Near-Optimal Feedback Control for Three-Dimensional Interceptions*. 15th ICAS Congress. London 1986.

[69] L. Skalecki, M. Martin. *General Adaptive Guidance Using Nonlinear Programming Constraint Solving Methods (FAST)*. AIAA Guidance, Naviagtion, and Control Conference. New Orleans, 1991.

[70] P. Staufer. *Lenkung der Sänger-Oberstufe mit verschiedenen Varianten der Q-Guidance*. Intermediate thesis, IFR. University of Stuttgart, 1995.

[71] J. Stoer and R. Bulirsch. *Einführung in die numerische Mathematik II*. Springer Verlag, Berlin–Heidelberg–New York, 1978.

[72] P. Strohmaier, A. Kiefer, D. Burkhardt, K. Horn. *Reentry Trajectory Optimization and Control.* AGARD conference on Space Vehicles Flight Dynamics. Luxembourg 1989 (proceedings published 1990).

[73] L.E. Tannas Jr. *Re-Entry Guidance through Closed-Form Equations*. AIAA Journal, Vol. 5, Nr. 6, June 1967.

[74] M.E. Taubner, G.P. Meenes, and H.G. Adelmann. *Aerothermodynamics of transatmospheric vehicles*. Journal of Aircraft, 24(9):594–602, September 1987.

[75] P. Teufel. *Re-Entry Trajectory Planning for a Reusable Launch Vehicle*. Master's thesis. University of California, Irvine 1996.

[76] N.X. Vinh. Studies in Astronautics – *Optimal Trajectories in Atmospheric Flight*. Elsevier Scientific Publishing Company. Amsterdam, Oxford, New York, 1981.

[77] K.H. Well. *Flugmechanik.* Lecture notes, IFR. University of Stuttgart.

[78] K.H. Well. *Lenkverfahren*. Lecture notes, IFR. University of Stuttgart.

[79] K.H. Well, A. Markl, K. Mehlem. *ALTOS – A Trajectory Analysis and Optimization Software for Launch and Reentry Vehicles*. 48th International Astronautical Congress. Turin 1997.

[80] A. Wiegand, A. Markl, K.H. Well, K. Mehlem, G. Ortega, M. Steinkopf. *ALTOS – ESA's Trajectory Optimization Tool Applied to Reentry Vehicle Trajectory Design.* 50th International Astronautical Congress, Amsterdam 1999.

[81] R. Windhorst, M. Ardema, J. Bowles. *Minimum Heating Entry Trajectories for Reusable Launch Vehicles*. Journal of Spacecraft and Rockets, Vol. 35, No. 5, September-October 1998.

[82] R.C. Wingrove. *A Survey of Atmosphere Reentry Guidance and Control Methods*. IAS Paper No 63-86, 1963.

[83] T. Wolf, A. Daum, A. Markl. *Bahnoptimierung und Lenkung für den Wiedereintritt eines VTOVL-Fahrzeugs*. DGLR Jahrbuch 1994, Band I.

[84] F. Zimmermann, J. Burkhardt, U.M. Schöttle. *Comparison of Guidance Concepts for a Semi-Ballistic Reentry Capsule*. AIAA Guidance, Navigation, and Control Conference. San Diego, 1996

Internet web sites:

[85] The Boeing Company: http://www.boeing.com

[86] Kistler Aerospace Corp.: http://www.kistleraerospace.com

[87] Orbital Science Corp.: http://www.orbital.com

[88] Sea-Launch Ltd.: http://www.sea-launch.com

[89] British Aerospace (BAE): http://www.bae.co.uk

[90] NASA: http://www.nasa.gov

A Coordinate Systems

The description of the axis systems is taken, with minor omissions, from [5]. All designations are from [7], except when noted otherwise.

A.1 Planet-Relative Systems

A.1.1 Planet-Fixed Geocentric System E

The origin of the planet-fixed geocentric axis system is the planet's geometric center, which is assumed to be at rest (see Fig. A.1). The *z*-axis is parallel to the planet's angular momentum vector, the *x*-*y* axes span the equatorial plane. The *x*-axis is the intersection of the reference meridian and the equatorial plane. The axis system rotates with the planet as time progresses.

A.2 Vehicle-Carried Axis Systems

The following axis systems are used to specify position and velocity of the vehicle's center of gravity with respect to the planet. Their origins are attached to the vehicle (see Fig. A.1).

For the sake of simplicity, the influence of wind is neglected. For the vehicles treated, the velocity is very much higher than the expected wind velocity during most of the trajectory.

A.2.1 Local Horizontal System L and Vertical System V

The definition of the local vertical axis system conforms to the normal earth-axis system defined in flight mechanics [6]. The *z*-axis points downward to the center of the planet. The *x*-*y* axes span the local horizontal plane, the *x*-axis pointing north along the local meridian and the *y*-axis pointing east along the local parallel (see Fig. A.1).

The east longitude λ is measured from the Greenwich meridian to the vehicle's current meridian going east. The declination δ is the angle between the vehicle's radius vector and the equatorial plane. The transformation from planet-fixed geocentric coordinates to the local vertical axis system is given by

$$\mathbf{T}_E^V = \mathbf{T}_2\left(-\frac{\pi}{2}-\delta\right)\mathbf{T}_3(\lambda)\,. \tag{A.1}$$

The local horizontal system L differs from the vertical system just by the sequence (and direction) of the axis (see Fig. A.1).

A.2.2 Velocity-Carried Axis Systems

A.2.3 Trajectory System T

As depicted in Fig. A.2, the trajectory axis system is aligned with the plane spanned by the vehicle's flight-path velocity and the geocentric position vector. The *x*-axis is parallel to the velocity vector. The *z*-axis points downward and is contained in the local vertical plane. The *y*-axis is contained in the local horizontal plane.

The flight-path inclination angle γ indicates ascent or descent with respect to the local horizontal plane. The flight-path azimuth χ is the heading angle measured clockwise from north. The transformation from the local vertical system to the trajectory axis system is given by

$$\mathbf{T}_V^T = \mathbf{T}_2(\gamma)\mathbf{T}_3(\chi)\,. \tag{A.2}$$

A.2.4 Air-Path System A

The vertical air-path axis system AV is similar to the trajectory system, however, the *x*-axis is parallel to the air-path velocity, not the flight-path velocity (see Fig. A.3). The *y* and *z* axes are contained in the horizontal and vertical plane, respectively.

Corresponding to the flight-path angles, the air-path inclination γ_a and the air-path azimuth χ_a denote climb and heading of the air-path velocity, respectively. The air-path flight-path angle γ_a is formed by the air-path velocity vector and the local horizon and is positive for ascent. The air-path heading angle χ_a lies in the local horizontal plane and is measured clockwise from north. In the absence of wind, the trajectory axis system and the vertical air-path axis system are identical and $\gamma_a=\gamma$, $\chi_a=\chi$.

The air-path axis system differs from the vertical air-path system in that the *z*-axis is contained in the vehicle's *x*-*z* plane of symmetry, not the local vertical (see Fig. A.4). The air-path bank angle μ_a results from a rotation about the air-path velocity vector and is formed by the *y* axis and the local horizontal plane.

The transformation from local vertical coordinates to the air-path axis system is given by

$$\mathbf{T}_V^A = \mathbf{T}_1(\mu_a)\mathbf{T}_2(\gamma_a)\mathbf{T}_3(\chi_a)\,. \tag{A.3}$$

Fig. A.5 shows the direction of the aerodynamic lift *L* and drag *D* as well as the lateral, or cross-stream, force Y_a along the air-path axis system. Aerospace standards define positive lift acting in the negative *z*-axis direction, drag as being positive along the negative *x*-axis, and the lateral force as acting in the positive *y*-direction. In components of the air-path system the aerodynamic force vector is given by:

$$\vec{F}_{\text{aero}} = \begin{bmatrix} -D \\ Y_a \\ -L \end{bmatrix}_A . \tag{A.4}$$

A.3 Body-Axis Systems

The body-fixed axis system and the total angle-of-attack system are defined by aerospace standards [7]. The total force system has been added by the A. Roenneke.

A.3.1 Body-Fixed System B

The body-fixed axis system is shown in Fig. A.5. It is rigidly attached to the vehicle's geometry. The *x*-*z* axes span the vehicle's plane of symmetry, the *x*-axis pointing forward, the *z*-axis downward. The *y*-axis is pointing starboard and is perpendicular to the vehicle's plane of symmetry.

The angle-of-attack α and the sideslip angle β determine the orientation of the vehicle's forward axis with respect to the air-path velocity (see Fig. A.5). The mapping from the air-path axis system to body-fixed coordinates is given by

$$\mathbf{T}_A^B = \mathbf{T}_2(\alpha)\mathbf{T}_3(-\beta)\,. \tag{A.5}$$

The yaw angle Ψ, the pitch angle Θ, and the roll angle Φ determine the vehicle's orientation with respect to the vehicle-carried axis systems (see Fig. A.6). The transformation matrix from the local vertical system (index V) to body-fixed coordinates (index B) is given by

$$\mathbf{T}_V^B = \mathbf{T}_1(\Phi)\mathbf{T}_2(\Theta)\mathbf{T}_3(\Psi)\,. \tag{A.6}$$

Fig. A.5 shows the direction of the aerodynamic forces when decomposed along the body-fixed axis system. Analogous to drag and lift, aerospace standards define the axial force A to be positive in the negative x_B-direction, the normal force N to be positive in the negative z_B-direction, and the side force Y to be positive in the positive y_B-direction. Written in components along the body-fixed axis system, the aerodynamic force vector is given by

$$\vec{F}_{\text{aero}} = \begin{bmatrix} -A \\ Y \\ -N \end{bmatrix}_B . \tag{A.7}$$

A.3.2 Total Angle-of-Attack System TA

The total angle-of-attack, or aeroballistic, axis system is an aerodynamic reference frame applied to space flight vehicles whose forward axis is an axis of rotational symmetry. The *x-z* plane of such a vehicle is an arbitrary definition of the designer. Consequently, for a vehicle of rotational symmetry the distinction between angle of attack and sideslip is deliberate. The aerodynamic forces and moments acting on the vehicle only depend on the total angle of attack α_t between the body-fixed forward axis and the air-path velocity (see Fig. A.7).

The *x-z* axes of the total angle-of-attack system span exactly this total angle-of-attack plane, the x_{TA}-axis being parallel to the *body* x_B-axis. The y_{TA}-axis points starboard and is perpendicular to this plane. The z_{TA}-axis points downward completing a right-handed system.

In a 6-degree-of-freedom simulation, given the angle of attack and the sideslip angle, the total angle-of-attack α_t can be computed from:

$$\alpha_t = \operatorname{acos}(\cos\alpha\cos\beta)\,. \tag{A.8}$$

This expressions holds for $-\pi \leq \alpha, \beta \leq \pi$; the total angle of attack is always positive.

The angle formed by the y_{TA}-axis and the *body-fixed* y_B-axis is defined as the aerodynamic roll angle ϕ' given by

$$\sin\phi' = \frac{\sin\beta}{\sin\alpha_t} \qquad \cos\phi' = \frac{\sin\alpha\cos\beta}{\sin\alpha_t}. \tag{A.9}$$

The mapping from the total angle-of-attack axis system to body-fixed coordinates is given by

$$\mathbf{T}_{TA}^{B} = \mathbf{T}_1(\phi'). \tag{A.10}$$

The total axial force A_t is defined positive in the negative x_{TA}-direction, and the normal force N_t is positive in the negative z_{TA}-direction. By definition, no side force exists in the total angle-of-attack system. The total force vector is given by

$$\vec{F}_{\text{aero}} = \begin{bmatrix} -A_t \\ 0 \\ -N_t \end{bmatrix}_{TA}. \tag{A.11}$$

A.3.3 Total Force System TF

The total force axis system is an aerodynamic reference frame aligned with the total aerodynamic *lift and drag* acting on a vehicle of rotational symmetry. The magnitude of the total lift and drag are functions of the total angle-of-attack α_t.

As shown in Fig. A.7 the y_{TF}-axis is a normal vector on the total angle-of-attack plane and identical with the y_{TA}-axis of the total angle-of-attack system. The x_{TF}-axis is parallel to the air-path velocity.

The angle formed by the y_{TF}-axis and the y_A-axis is not defined by aerospace standards. It is denoted here as the aerodynamic bank angle μ_t given by

$$\sin\mu_t = \frac{\cos\alpha\sin\beta}{\sin\alpha_t} \qquad \cos\mu_t = \frac{\sin\alpha}{\sin\alpha_t}. \tag{A.12}$$

The mapping from the total force frame to air-path coordinates is given by

$$\mathbf{T}_{TF}^{A} = \mathbf{T}_1(\mu_t). \tag{A.13}$$

The mapping from the total force frame to the total angle-of-attack frame is given by

$$\mathbf{T}_{TF}^{TA} = \mathbf{T}_2(\alpha_t)\,. \tag{A.14}$$

The total drag D_t is defined to be positive along *the negative* x_{TF}-axis, and the total lift L_t opposes the z_{TF}-axis. By definition, no lateral force exists in the total force frame. The total force vector is given by

$$\vec{F}_{\text{aero}} = \begin{bmatrix} -D_t \\ 0 \\ -L_t \end{bmatrix}_{TF}\,. \tag{A.15}$$

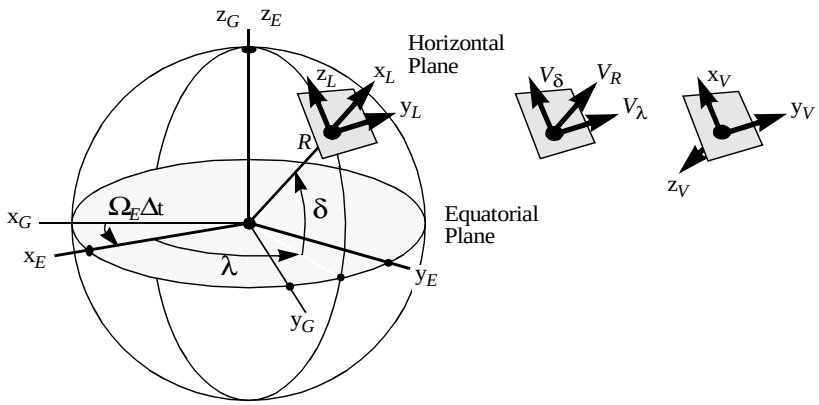

Fig. A.1: Planet-centered and vehicle-carried axis systems.

The *z* axis of the rotating planet-fixed axis system E coincides with the planet's axis of rotation. The local horizontal axis system L and the vertical axis system V are attached to the vehicle's center of mass.

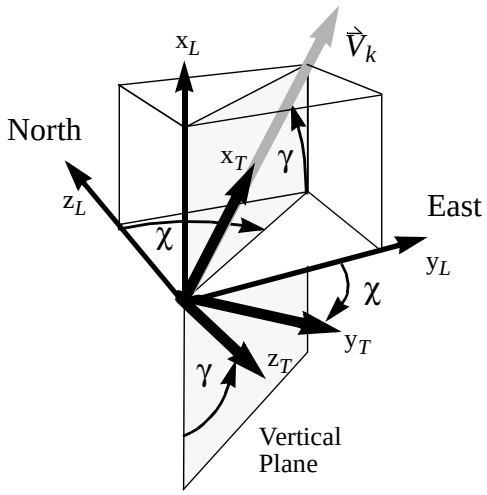

Fig. A.2: The trajectory axis system (index T).

The x_T and z_T axes are contained in the local vertical plane. The x_T-axis is parallel to the planet-relative velocity vector. The flight-path angle γ is formed by the velocity vector and the local horizon and is positive for ascent. The heading angle χ lies in the local horizontal plane and is measured clockwise from north.

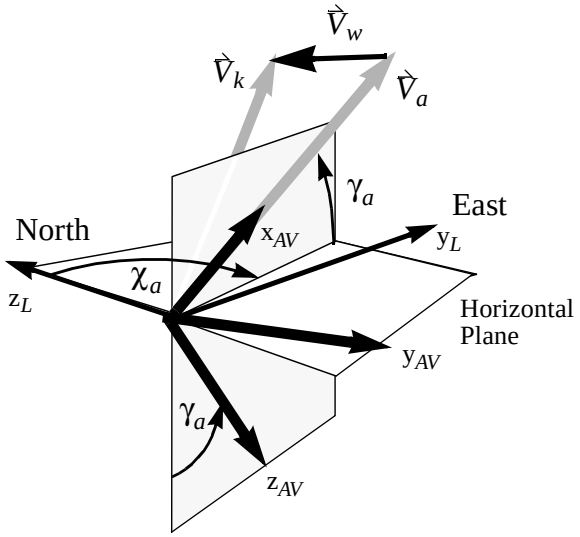

Fig. A.3: The vertical air-path axis system (index AV).

The x_{AV} and z_{AV} axes are contained in the local vertical plane. Note the presence of wind $\vec{V}_w$. The x_{AV} is parallel to the air velocity.

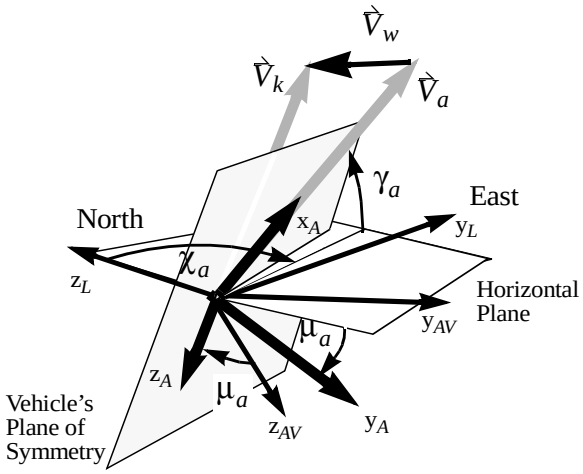

Fig. A.4: Definition of the air-path axis system (index A).

The x_A and z_A axes span the vehicle's plane of symmetry. The air-path bank angle μ_a results from a rotation around the air-path velocity vector.

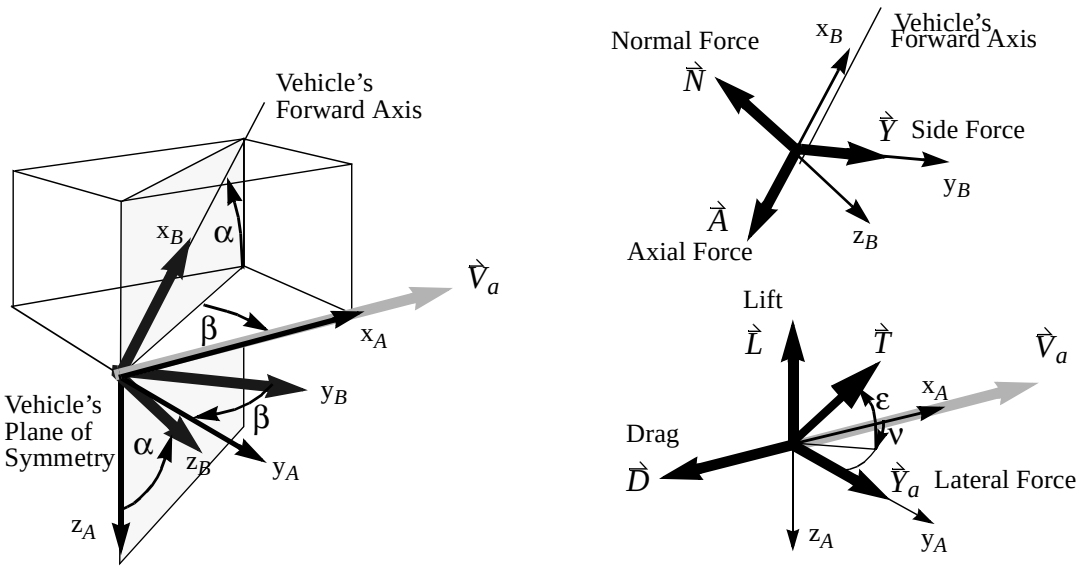

Fig. A.5: Definition of the body-fixed system (index B) and aerodynamic angles.

The normal, axial and side force are defined to be parallel to the body axes, whereas the triple lift, drag and lateral force is along the air-path velocity axes.

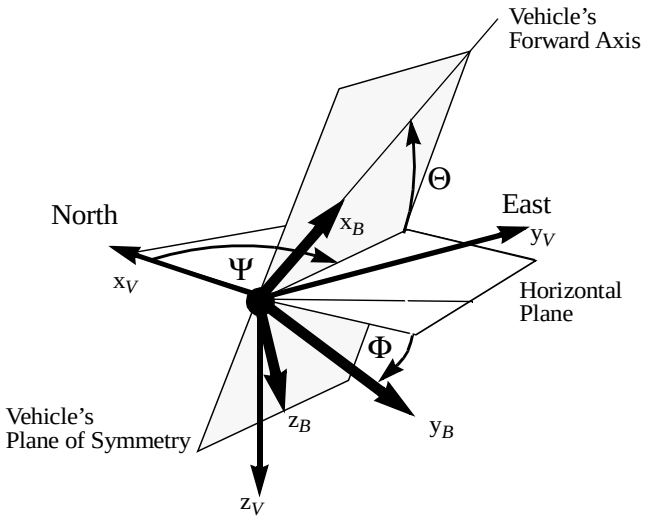

Fig. A.6: Definition of the Euler angles.

Transition from the vehicle-carried vertical system (index V) to the body-fixed axis system (index B)

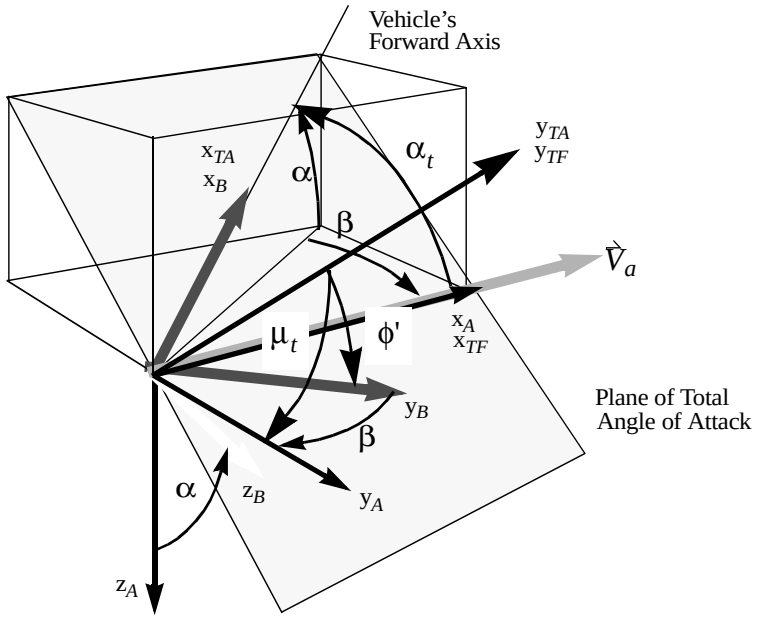

Fig. A.7: Definition of the total angle-of-attack axis system (index TA).

The total angle of attack is formed by the vehicle's forward axis and the air-path velocity vector. The total force axis system (index TF) is aligned with the air-path x_A axis, but rotated by the angle μ_t, so that z_A axis is along the total lift (the combination of lift and lateral force).

B Mathematical Appendix

B.1 The Bi-Linear Tangent Law

The differential equations for the optimization problem described in Section 4.1.5 are very simple:

$$\dot{x} = u;\ \dot{y} = v;\ \dot{u} = a\cos\beta;\ \dot{v} = a\sin\beta - g\,. \tag{B.1}$$

For motion in the horizontal plane, the gravitational acceleration g is set to zero.

For a cost function that only depends on the final state and/or on the final time, the Hamiltonian can be written as:

$$H = \lambda_u a\cos\beta + \lambda_v(a\sin\beta - g) + \lambda_x u + \lambda_y v\,. \tag{B.2}$$

The differential equations of the adjoints are derived from $\dot{\lambda} = -\delta H/\delta x$:

$$\dot{\lambda}_u = -\lambda_x;\ \dot{\lambda}_v = -\lambda_y;\ \dot{\lambda}_x = 0;\ \dot{\lambda}_y = 0\,. \tag{B.3}$$

Evidently the adjoint variables are of the form

$$\lambda_x = -c_1;\ \lambda_y = -c_2;\ \lambda_u = c_1 t + c_3;\ \lambda_v = c_2 t + c_4 \tag{B.4}$$

with constant c_i (the choice of the signs is for convenience only). Therefore the optimal control is found by

$$\delta H/\delta\beta = 0 = -(c_1 t + c_3)a\sin\beta + (c_2 t + c_4)a\cos\beta \tag{B.5}$$

or (as long as $c_1 t + c_3 \neq 0$ and $a \neq 0$):

$$\tan\beta = \frac{c_2 t + c_4}{c_1 t + c_3}\,. \tag{B.6}$$

This is called “bi-linear tangent law”, since the tangent of the control angle is the ratio of two linear functions. The coefficients must be chosen in order to satisfy the end conditions.

For the problem of maximizing the final horizontal velocity, any $\beta > \pi/2$ and $\beta < -\pi/2$ can be ruled out, since a thrust component in negative *x*-direction will only decrease the horizontal velocity.

Properties of the Bi-Linear Function

When the denominator vanishes (and when numerator and denominator are linearly independent), the function shows a pole. The function value switches from minus infinity to plus infinity or vice versa. This corresponds to a jump from $-\pi/2$ to $\pi/2$ (or vice versa) for the control angle. This jump has no physical meaning and therefore should be avoided.

When no pole exists within a time range, the function is strictly monotonic (except for the case, when it is constant). Therefore the inequalities hold for $t_0 < t_1 < t_2 < t_f$:

$$\begin{aligned}
&\Theta_0 < \Theta_f \Rightarrow \Theta_0 < \Theta(t_1) < \Theta(t_2) < \Theta_f \\
&\Theta_0 = \Theta_f \Rightarrow \Theta_0 = \Theta(t_1) = \Theta(t_2) = \Theta_f \\
&\Theta_0 > \Theta_f \Rightarrow \Theta_0 > \Theta(t_1) > \Theta(t_2) > \Theta_f \ .
\end{aligned} \tag{B.7}$$

B.2 Cubic Spline with Prescribed End Slopes

When given a set of function values for a series of monotonous abscissa values, there are many ways to define an interpolating function. It can be shown, f.i. by a mechanical analog, that a natural cubic spline will have the least bending energy, that is the integral of the square of the second derivative will be the least.

A cubic spline consists of a set of cubic polynomials, one per consecutive interval of the abscissa values. It has the properties that it is continuous and even two times continuously differentiable. For (n+1) points this means that there are n intervals and 4n coefficients. Each cubic must satisfy the function values at both sides, this results in 2n conditions. Also at the n-1 intermediate points the first and the second derivative must be continues, from which 2(n-1) are derived.

This leaves two more conditions, which can be arbitrarily chosen. A common case is the “natural” spline, for which the curvature at the two outermost points is set to zero. Another possibility is to specify the slope at both sides.

As described in detail in [71], the spline coefficients can be computed using a matrix equation of the form

$$\begin{bmatrix} 2 & \lambda_0 & & & & \\ \mu_1 & 2 & \lambda_1 & & & \\ & \mu_2 & 2 & \lambda_2 & & \\ & & . & . & . & \\ & & & \mu_{n-1} & 2 & \lambda_{n-1} \\ & & & & \mu_n & 2 \end{bmatrix} \begin{bmatrix} M_0 \\ M_1 \\ . \\ . \\ . \\ M_n \end{bmatrix} = \begin{bmatrix} d_0 \\ d_1 \\ . \\ . \\ . \\ d_n \end{bmatrix} \tag{B.8}$$

with the “moments” M_i being the second derivatives of the spline at the support points and the abbreviations and with

$$\lambda_i = \frac{x_{j+1} - x_j}{x_{j+1} - x_{j-1}} \; ; \; \mu_i = 1 - \lambda_i = \frac{x_j - x_{j-1}}{x_{j+1} - x_{j-1}} \; ; \; \text{i=2, ..., n-1} \tag{B.9}$$

and

$$d_i = \frac{6}{x_{j+1} - x_{j-1}} \left\{ \frac{y_{j+1} - y_j}{x_{j+1} - x_j} - \frac{y_j - y_{j-1}}{x_j - x_{j-1}} \right\} \; ; \; \text{i=2, ..., n-1 .} \tag{B.10}$$

[71] discusses three cases: natural spline (the curvature at both sides is zero), prescribed slope at both sides and cyclical spline (when the conditions at the end of the interval match those at the very beginning). The latter case is of no interest here and is discarded.

The first conditions can be accommodated by setting

$$\lambda_0 = 0 \; , \; d_0 = 0 , \tag{B.11}$$

$$\mu_n = 0 \; , \; d_n = 0 , \tag{B.12}$$

while the second set of conditions will give

$$\lambda_0 = 1 \; , \; d_0 = \frac{6}{x_1 - x_0} \left(\frac{y_1 - y_0}{x_1 - x_0} - y_0' \right) , \tag{B.13}$$

$$\mu_n = 1 \; , \; d_n = \frac{6}{x_n - x_{n-1}} \left(y_n' - \frac{y_n - y_{n-1}}{x_n - x_{n-1}} \right) . \tag{B.14}$$

However, both can be combined as well (eqns. (B.11) and (B.14), f.i.), giving a spline with prescribed slope at one side and a vanishing curvature at the other.

B.3 Estimation of the Flight-Path Angle

B.3.1 Dynamic Pressure as a Function of the Time

Given a profile for the dynamic pressure as a function of the flight-path velocity $q(V)$, we can derive an estimate for the flight-path angle needed to follow this profile.

By definition, dynamic pressure is:

$$q = \frac{1}{2}\rho V^2. \tag{B.15}$$

The time derivative results to:

$$\dot{q} = \frac{1}{2}\dot{\rho} V^2 + \rho V \dot{V}. \tag{B.16}$$

Given a locally exponential atmosphere with the scale height h_S:

$$\rho \approx \rho_0 e^{-h/h_S} \tag{B.17}$$

it follows that

$$\dot{\rho} = \rho_0 e^{-h/h_S}\left(-\frac{\dot{h}}{h_S}\right) = -\rho\frac{\dot{h}}{h_S} \tag{B.18}$$

and thus

$$\dot{q} = \frac{1}{2}\left(-\rho\frac{\dot{h}}{h_S}\right) + \rho V\dot{V} = -\frac{\dot{h}}{h_S}q + 2\frac{\dot{V}}{V}q \tag{B.19}$$

with the differential equation for radius (and also altitude) Eq. (3.11) we obtain:

$$\frac{\dot{q}}{q} = 2\frac{\dot{V}}{V} - \frac{V\sin\gamma}{h_S} \tag{B.20}$$

or

$$\sin\gamma = \frac{h_S}{V}\left(2\frac{\dot{V}}{V} - \frac{\dot{q}}{q}\right). \tag{B.21}$$

With the differential equation of the velocity (Eq. (3.16), but for simplicity without the centrifugal term of the earth rotation and the – rather small – lateral part of the gravity), we get:

$$\sin\gamma = \frac{h_S}{V}\left[\frac{2}{V}\left(\frac{T-D}{m} - g\sin\gamma\right) - \frac{\dot{q}}{q}\right]. \tag{B.22}$$

and thus

$$\sin\gamma = \frac{h_S}{V^2 + 2gh_S}\left(2\frac{T-D}{m} - \frac{\dot{q}V}{q}\right). \tag{B.23}$$

In order to match the initial boundary of the dynamic pressure profile, it is necessary to compute the derivative of the dynamic pressure for a given velocity and flight-path angle:

$$\dot{q} = \frac{q}{V}\left(2\frac{T-D}{m} - \frac{V^2 + 2gh_S}{h_S}\sin\gamma\right). \tag{B.24}$$

B.3.2 Dynamic Pressure as a Function of Velocity

Often it is convenient to specify the dynamic pressure as a function of the air path velocity, f.i. some path constraints can be expressed easily in terms of velocity and dynamic pressure.

Since the profile is given as a function of velocity, the derivative of q with respect to the time can be replaced by one with respect to the velocity (denoted here by an apostrophe):

$$\dot{q} = \frac{dq}{dt} = \frac{dq}{dV}\frac{dV}{dt} = q'\dot{V}, \tag{B.25}$$

therefore (B.21) becomes:

$$\sin\gamma = \frac{h_S \dot{V}}{V}\left(\frac{2}{V} - \frac{q'}{q}\right). \tag{B.26}$$

With the differential equation of the velocity (Eq. (3.14) simplified), we get:

$$\sin\gamma = \frac{h_S}{V}\left(\frac{2}{V} - \frac{q'}{q}\right)\left(\frac{T-D}{m} - g\sin\gamma\right). \tag{B.27}$$

For small flight-path angle, the gravity acceleration can be neglected compared to the one from thrust and drag, thus

$$\sin\gamma = \frac{h_S}{V}\left(\frac{2}{V} - \frac{q'}{q}\right)\frac{T-D}{m} \tag{B.28}$$

otherwise we have to use

$$\sin\gamma = \frac{h_S(2 - Vq'/q)}{V^2 + gh_S(2 - Vq'/q)}\frac{T-D}{m}\ . \tag{B.29}$$

In order to compute the derivative of the dynamic pressure for given V and γ

$$q' = q\left(\frac{2}{V} - \frac{Vm\sin\gamma}{h_S(T - D - gm\sin\gamma)}\right) \tag{B.30}$$

can be used.

B.4 Estimation of the Bank Angle

Differentiating Eq. (B.21) with respect to time, we obtain:

$$\dot{\gamma}\cos\gamma = h_S\left[2\frac{\ddot{V}V^2 - \dot{V}2V\dot{V}}{V^4} - \frac{\ddot{q}Vq - \dot{q}(\dot{q}V + \dot{V}q)}{V^2q^2}\right] \tag{B.31}$$

or

$$\dot{\gamma}\cos\gamma = \frac{h_S}{V^2}\left[2\ddot{V} - 4\frac{\dot{V}^2}{V} - \frac{\ddot{q}V}{q} + \frac{V\dot{q}^2}{q^2} + \frac{\dot{q}\dot{V}}{q}\right]. \tag{B.32}$$

Combining this with Eq. (3.38) gives an estimate for the required vertical lift acceleration:

$$\begin{aligned}\frac{h_S}{V^2\cos\gamma}&\left[2\ddot{V} - 4\frac{\dot{V}^2}{V} - \frac{\ddot{q}V}{q} + \frac{V\dot{q}^2}{q^2} + \frac{\dot{q}\dot{V}}{q}\right] = \\ &-g\cos\gamma - g_\delta\cos\chi\sin\gamma + \frac{V^2}{R}\cos\gamma + \frac{Y\sin\mu_a + L\cos\mu_a}{m} \\ &+ 2\omega_E V\sin\chi\cos\delta + R\omega_E^2\cos\delta(\sin\delta\sin\gamma\cos\chi + \cos\delta\cos\gamma)\end{aligned} \tag{B.33}$$

or (neglecting g_δ and the side force):

$$\begin{aligned}\frac{L\cos\mu_a}{m} = &\left(g - \frac{V^2}{R}\right)\cos\gamma + \frac{h_S}{V^2\cos\gamma}\left[2\ddot{V} - 4\frac{\dot{V}^2}{V} - \frac{\ddot{q}V}{q} + \frac{V\dot{q}^2}{q^2} + \frac{\dot{q}\dot{V}}{q}\right] \\ &-2\omega_E V\sin\chi\cos\delta - R\omega_E^2\cos\delta(\sin\delta\sin\gamma\cos\chi + \cos\delta\cos\gamma)\end{aligned}. \tag{B.34}$$

B.4.1 Dynamic Pressure as a Function of Velocity

When we differentiate Eq. (B.28) once more (neglecting variations of the scale height), a formula for $\dot{\gamma}$ can be obtained:

$$\dot{\gamma}\cos\gamma = h_S\left[2\frac{\ddot{V}V - 2\dot{V}^2}{V^3} - \frac{q''\dot{V}^2 + q'\ddot{V}}{qV} + \frac{\dot{V}^2Vq'^2 + q'q\dot{V}^2}{q^2V^2}\right]. \tag{B.35}$$

When we assume that the acceleration changes slowly (in other words, the second derivative of the velocity is close to zero), the formula reduces to:

$$\dot{\gamma} = \left[-\frac{4q}{V^2} - q'' + \frac{Vq'^2 + q'q}{qV}\right]\frac{\dot{V}^2 h_S}{qV\cos\gamma} \tag{B.36}$$

and, in the special case of a constant dynamic pressure profile, to:

$$\dot{\gamma} = -4\frac{\dot{V}^2}{V^3}\frac{h_S}{\cos\gamma}. \tag{B.37}$$

Note that this is always negative, i.e. the curvature of the *h(v)* is always in the same direction for constant dynamic pressure.

Combining this with Eq. (3.38) gives an estimate for the required vertical lift acceleration:

$$\begin{aligned}\left[-\frac{4q}{V^2} - q'' + \frac{Vq'^2 + q'q}{qV}\right]\frac{\dot{V}^2}{q}\frac{h_S}{\cos\gamma} &= \\ -g\cos\gamma - g_\delta\cos\chi\sin\gamma + \frac{V^2}{R}\cos\gamma + \frac{Y\sin\mu_a + L\cos\mu_a}{m} & \\ + 2\omega_E V\sin\chi\cos\delta + R\omega_E^2\cos\delta(\sin\delta\sin\gamma\cos\chi + \cos\delta\cos\gamma) & \end{aligned} \tag{B.38}$$

or (neglecting g_δ and the side force):

$$\begin{aligned}\frac{L\cos\mu_a}{m} = \left(g - \frac{V^2}{R}\right)\cos\gamma + \frac{\dot{V}^2 h_S}{\cos\gamma}\left[-\frac{4}{V^2} - \frac{q''}{q} + \frac{Vq'^2 + q'q}{q^2V}\right] & \\ -2\omega_E V\sin\chi\cos\delta - R\omega_E^2\cos\delta(\sin\delta\sin\gamma\cos\chi + \cos\delta\cos\gamma) \quad . & \end{aligned} \tag{B.39}$$

B.5 Estimate of the Reentry Conditions

While for the launcher applications usually the launch conditions are fixed, like f.i. the location, and the final conditions are given by some non-linear equations, for the reentry case this is just the other way round. The landing site is fixed in most cases, but the starting point is optimizable. This makes it necessary to estimate the starting point of the trajectory.

We can distinguish three kinds of initial conditions. The most simple, form the modeling point of view, is the prescriptions of the radius and the velocity vector. This form does not require any additional computations. It is also called “atmospheric condition”.

An other condition is described by the elements of a transfer orbit. Of this set, usually one or two parameters are considered optimizable (and therefore must be estimated), whereas the others are given by the mission.

The computation of the de-orbit parameters is left to the third option. These parameters consist of the velocity change in three directions: opposite the velocity vector at the point of de-orbit, parallel to the radius vector and a third component, normal to these. However in order to lessen the user calculations, the altitude of the peri-apsis can be specified. This is value which is quite characteristic for a each combination of vehicle and a planet's atmosphere and makes the data specification independent from the kind of initial orbit used.

Atmospheric Conditions

This initial state consists of a position and a velocity vector. Both can be given, independently, in inertial or planet relative coordinates.

This kind of specification is used to describe a fixed initial situation, therefore no parameters are optimizable per se, however after an initial guess is obtained, each state can be made optimizable manually. In this case also non-linear initial conditions can be enforced.

Transfer Orbit

This situation arises when a de-orbit maneuver has already taken place and the vehicle is on its transfer orbit. An other possibility is that the de-orbit impulse was given by other considerations and only some parameters can still be adapted.

Note that all elements of the Orbit record can take a bounded value, i.e each can be composed of a value, an unit and, optionally a lower and/or an upper bound. When one bound is not given, the value is assumed for it. When both bounds coincide (which includes the case when no bound is given at all), then the parameter will be fixed and not optimizable during iterations.

Although this option can be applied to any of the orbital elements, it is probably only sensible for the true anomaly at the time of de-orbit and for the right ascension of the ascending node. While the former is variable for almost any kind of conceivable mission, adjusting the latter can be done during early phases of mission planning.

The eccentricity and the argument of the perigee are optional and will be set to the values shown (which correspond to a circular orbit), when not specified by the user.

De-Orbit State

When also the de-orbit impulse shall be optimized, this option can be used. The parameters are the same as for the transfer orbit, with the addition of a record of velocity changes.

The orbit specification is the one of the initial orbit, before the de-orbit maneuver takes place. Whereas the tangential impulse is opposite the velocity vector and actually means a velocity decrement, the two other impulses are in the direction of the corresponding axes.

All values can be bounded as described above. The default value for the radial and normal velocity increment is zero.

Reentry State

More comfort for the user is achieved by using the reentry state. Instead of the de-orbit impulse, data of a target orbit is entered. This relieves the user from computing the de-orbit impulse which depends on the initial orbit as well as on the planet properties. Also in this case the part of the trajectory between the de-orbit and the entry into the atmosphere is approximated by a Keplerian arc.

The perigee altitude is the lowest point of the transfer orbit. It is a measure how deep the vehicle will enter into the atmosphere before it can be flared.

The reentry altitude is an altitude where atmospheric effects are assumed to be negligible. For the Earth it is traditionally set to 400,000 feet, or about 121.9 km.

Target longitude and latitude correspond to the landing site or to the interface to the terminal energy management area. The estimate of the downrange depends mostly on the vehicle. These parameters are used to estimate the true anomaly and the right ascension of the de-orbit point, when they can be varied.

Setting the ascending branch flag to true will set the target site on the northbound part of the trajectory. This has only an effect when the modulus of the latitude of the landing site is less than the inclination of the initial orbit.

Finally, when the ascending node passage is not set fixed, the initial guess will find a node passage which is close the landing site, even though this may take several revolutions.

B.6 Estimation of the De-Orbit parameters

The reentry state (see previous section) relieves the user from some tedious calculations. Some heuristic is used to chose suitable orbit parameters. This is described step by step in the follow-

ing. Note that for all quantities that will be optimized, upper and lower bounds as well as a nominal value must be computed.

Entry Radius

The entry altitude is an arbitrarily border of the atmosphere. It is chosen in a way that the atmosphere will have still negligible influence. For the computation of the initial boundary constraint actually the radius is used.

Due to the oblateness of the earth, it will vary with latitude. Therefore the nominal value is computed with a mean planet radius, whereas the upper and lower bounds are computed with the equatorial and the polar radii, respectively.

Transfer Orbit Perigee

For convenience the user has to enter the altitude of the transfer orbit instead of the radius. For the estimate of the radius, the radius of the landing site is used and the altitude is added.

$$R_{Tp}^{+} = h_p^{+} + R_{LS} \; , \; R_{Tp}^{o} = h_p^{o} + R_{LS} \; , \; R_{Tp}^{-} = h_p^{-} + R_{LS} \, . \tag{B.40}$$

The indices “$^{+}$”, “^{o}” and “$^{-}$” denote upper bound, nominal value and lower bound, respectively. The subscripts “$_{T}$” stands for transfer orbit, “$_{p}$” for perigee.

Velocity Decrement

Since again the bounds must be computed, two extreme combinations of the radii of the transfer orbit are used, as well as a mean one (see Table B.1). From this radii the semi major axis of the transfer orbit and its eccentricity are calculated:

Table B.1: Combinations of radii

Velocity decrement	Transfer orbit perigee	Transfer orbit apogee
ΔV^{+}	$R_{Ta} = R_{Ip}$	$R_{Tp} = R_{Tp}^{-}$
ΔV^{o}	$R_{Ta} = R_{Ip}$	$R_{Tp} = R_{Tp}^{o}$
ΔV^{-}	$R_{Ta} = R_{Ia}$	$R_{Tp} = R_{Tp}^{+}$

$$a_T = \frac{R_{Ta} + R_{Tp}}{2}; e = \frac{R_{Ta}}{a} - 1 \tag{B.41}$$

and the momentum

$$M_T = \sqrt{\mu a(1 - e^2)} \tag{B.42}$$

and, with the momentum of the initial orbit

$$\Delta v = \frac{M_T - M_I}{R_{Ta}}. \tag{B.43}$$

Note that this will be negative. It is assumed that de-orbit point is the apogee of the transfer orbit and therefore the velocity is perpendicular to the radius vector.

Right Ascension and Argument of the Perigee

For the following computations it is assumed, that the right ascension of the ascending node and the true anomaly of the de-orbit point are not limited by any bounds. If such bounds exist and the value obtained is outside, it will be set to the border closest to the computed value. This includes the case, where the borders coincide and there is no liberty for variations at all.

In the first step the node and the argument of the perigee of a transfer orbit is computed, whose perigee is exactly over the landing site. In the case the landing site is North or South of the inclination band, the positive or negative inclination is used as a pseudo target. The argument of the perigee of this orbit depends also on the “Ascending_Branch” flag.

The increment of the ascending node $\Delta\Omega$ in Table B.2 is computed as:

$$\Delta\Omega = \operatorname{acos}\frac{\cos\Delta\omega}{\cos\delta_T}. \tag{B.44}$$

Since by virtue of the formula used the modulus of the perigee argument is always in between zero and $\pi/2$, also $\Delta\Omega$ will fall into this range. Both formulas can be easily derived by using spherical geometry.

Table B.2: Deriving Argument of the Perigee and Node

Case	Target Declination	Pseudo Target Declination δ_T	Perigee Argument Modulus $\Delta\omega$	Perigee Argument ω_{LS}	Earth relative Node Ω_{LS}
North of inclination	$i \le \delta$	i	$\frac{\pi}{2}$	$\frac{\pi}{2}$	$\lambda_T - \frac{\pi}{2}$
North of Equator (ascending)	$0 < \delta < i$	δ	$\text{asin}\frac{\sin\delta}{\sin i}$	$\Delta\omega$	$\lambda_T - \Delta\Omega$
North of Equator (descending)				$\pi + \Delta\omega$	$\lambda_T - (\pi - \Delta\Omega)$
Equator	$\delta = 0$	$\delta = 0$	0	0	λ_T
South of Equator (ascending)	$-i < \delta < 0$	δ,	$\text{asin}\frac{-\sin\delta}{\sin i}$	$2\pi - \Delta\omega$	$\lambda_T - (2\pi - \Delta\Omega)$
South of Equator (descending)				$\pi + \Delta\omega$	$\lambda_T - (\pi + \Delta\Omega)$
South of inclination	$-i \le \delta$	-i	$-\frac{\pi}{2}$	$\frac{3\pi}{2}$	$\lambda_T - \frac{3\pi}{2}$

True Anomaly from De-Orbit down to the Entry Interface

The formula is akin to the one for true anomaly, just that the angle from the apogee onward is used:

$$\nu_T = \pi - \arccos\frac{A(1-e^2) - r_e^o}{e r_e^o}. \tag{B.45}$$

Argument of the Perigee of the Transfer Orbit

With the angles obtained so far, and with the user supplied estimate for the downrange, we can obtain

$$\omega_{Tp} = \left(\pi - \frac{S}{r_{equ}} - \nu_T + \omega_{LS}\right) \bmod 2\pi \tag{B.46}$$

and the true anomaly of the de-orbit point in terms of the initial orbit:

$$\nu_{Ta} = (\pi + \omega_{Tp} - \omega_I) \bmod 2\pi\,. \tag{B.47}$$

When this value is outside the user supplied bounds, it is set to the nearest boundary.

Inertial Ascending Node

With the total time of flight, form de-orbit until the end of the supersonic phase, the angle from the vernal equinox to the ascending node can be given:

$$\Omega = (\Omega_{rel} + \lambda_0 + \omega_E T) \bmod 2\pi \tag{B.48}$$

with the hour angle of the zero meridian λ_0 and the earth rotation. The angle is set to be within the user bounds.